

Effect of *N*-Oxide Incorporation on Thiazole-Containing Conjugated Polymers

by

Robert Claridge

A thesis

presented to the University of Waterloo

in fulfillment of the

thesis requirement for the degree of

Master of Science

in

Chemistry

Waterloo, Ontario, Canada, 2018

©Robert Claridge 2018

Author's Declaration

I hereby declare that I am the sole author of this thesis. This is a true copy of the thesis, including any required final revisions, as accepted by my examiners.

I understand that my thesis may be made electronically available to the public.

Abstract

The use of conjugated polymers (CPs) in organic electronics has been an area of continued interest over the last several years due to many advantages over their inorganic counterparts. Due to the nature of CPs, devices can be made flexible, light weight and are easy to fabricate and process in comparison to devices fabricated with inorganic materials. Due to the continued interest, developing high performance materials is essential, and therefore, developing methods for fine-tuning the optoelectronic properties of said materials becomes imperative. Tuning the electronic properties of materials allows one to mold a compound to a desired application. We introduce a new method for tuning the energy levels of thiazole containing materials through the incorporation of oxidized functional groups. Increasing the number of *N*-oxide moieties within the materials leads to a reduction in the HOMO-LUMO gap, due to a rise in the energy level of the HOMO as well as a lowering of the LUMO level. This phenomenon arises from a non-covalent interaction between the lone pairs of the oxygen of one thiazole- *N*-oxide and the σ^* orbital of the S-C bond of an adjacent thiazole ring. Due to this interaction, the planarity of the system is increased, leading to a reduction in the HOMO-LUMO gap up to 0.45 eV. This effect on the planarity of the conjugated molecules can be observed through UV-Vis spectroscopy, voltammetry and computational calculations. This method establishes viable means for fine tuning thiazole-containing conjugated materials.

Acknowledgements

First of all, I would like to thank my supervisor, Prof. Derek Schipper for allowing me to pursue a Master's degree in his lab, in addition to all of the help and support he has provided throughout my time here. I would also like to thank Prof. Graham Murphy and Prof. Mario Gautier for taking their time to act as my committee, as well as any input they provided me with during my time as a Master's student.

Fellow members of the Schipper Group have made my time here as enjoyable as possible in addition to providing support when needed. I would specifically like to thank our former undergraduate students Alma Maqbool and Meixin Cheng for their help in the completion of this project as well as former graduate student Luke Vanderzwet for guidance as well as collaboration of ideas and compounds used throughout this project.

TABLE OF CONTENTS

Author's Declaration	ii
Abstract	iii
Acknowledgments	iv
List of Figures	vi
List of Schemes	viii
List of Tables	x
Abbreviations	xi
1.0 Introduction to Conjugated Materials and their Development	1
1. 1 Conjugated Materials	1
1. 2 Band Gap.....	2
1.2.1 Band Gap Engineering Strategies	5
1.3 Chalcogen Bonding.....	12
1.4 Methods for Estimating HOMO-LUMO Gap.....	16
1.5 Synthesis of Conjugated Materials	18
1.6 Direct Arylation	21
1.6.1 Dehydration Reaction.....	23
2.0 Oxidation of Thiazole-Containing Conjugated Materials.....	25
2.1 Thesis Proposal.....	25
2.2 Controlled Oxidation of Thiazole Containing Conjugated Polymers	26
2.3 Properties of Thiazole-N-Oxide-Containing Materials.....	36
2.3.1 Optical Electronic Effects on Small Molecules	36
2.3.2 Computational Studies.....	43
2.3.3 Longer Chain Small Molecules.....	48
2.3.4 Thiazole Containing Conjugated Polymers.....	51
2.4 Device Testing	64
Conclusions.....	65
Supporting Information.....	67
References.....	108

List of Figures

Figure 1. Delocalization of electrons through polymer backbone of polythiophene	1
Figure 2. Difference between band gap in the solid-state and HOMO-LUMO gap in molecular systems.....	4
Figure 3. Conceptual image of the band gap in electronic materials	5
Figure 4. Orbital mixing in push-pull motif.....	8
Figure 5. UV-Vis spectra seen from Campos showing the effect of increasing oxidation of thiophene containing conjugated polymers.....	9
Figure 6. Intramolecular non-covalent interactions seen in the literature that are believed to facilitate planarization	11
Figure 7. Molecular balances used to exhibit the chalcogen-chalcogen interaction.....	12
Figure 8. Dithienothiophene derivatives used as anion transporters.....	13
Figure 9. S-O interaction seen in the crystal structures of various antagonist molecules.....	14
Figure 10. Examples of molecules studied for effects rigidification due to interactions with the C-S σ^* antibonding orbital	15
Figure 11. Creation of an electron-hole pair through photoelectric absorption.....	16
Figure 12. Cyclic voltammogram.....	17
Figure 13. Repeating unit of proposed thiazole-containing conjugated polymers.....	30
Figure 14. UV-Vis spectra of poly(4,4'-dinonyl-5-thienyl-2,2'-bithiazole).....	33
Figure 15. UV-Vis spectra of the 4-4'-dimethyl-2,2'-bithiazole compounds.....	39
Figure 16. UV-Vis spectra of 4-methylthiazole and 4-methylthiazole <i>N</i> -oxide.....	40
Figure 17. UV-Vis spectra of the two 5-(5-hexylthienyl)-4-methylthiazole- <i>N</i> -oxide compounds.....	43
Figure 18. Single point energies of bithiazole and bithiazole- <i>N</i> -Oxides for conformations from 90-180° (N-C-C-N bond) in 10° intervals.....	44
Figure 19. Optimized geometry of 2,2'-bithiazole- <i>N,N'</i> -dioxide from Gaussian DFT calculation.....	45
Figure 20. Rotational Energies of Conjugated Systems.....	46
Figure 21. S-O interactions as determined through Gaussian NBO calculations	47
Figure 22. Molecular geometry obtained for 4,4',5,5'-tetramethyl-2,2'-bithiazole-3,3'-bis(olate) through single crystal X-ray crystallography.....	47
Figure 23. UV-vis and fluorescence spectra for the 5,5'-(5-hexylthienyl)- 4-4'-dimethyl-2,2'-bithiazole compounds.....	49

Figure 24. Thiophene series of thiazole containing polymers	52
Figure 25. UV-Vis and fluorescence spectra of fluorene polymer series.....	54
Figure 26. UV-Vis and fluorescence spectra of thiophene polymer series.....	55
Figure 27. Linear sweep voltammograms of polymers.....	58
Figure 28. Frontier orbital energies and electrochemical HOMO-LUMO gaps of the fluorine series of polymers.....	61
Figure 29. Frontier orbital energies and electrochemical HOMO-LUMO gaps of the thiophene series of polymers.....	62
Figure 30. Solvatochromism study for the di-N-oxide fluorene series polymer.....	63
Figure S1. Optimized Molecular Geometries.....	81
Figures S2-S21. NMR Spectra.....	83-102
Figures S22-S26. GPC Traces.....	103-107

List of Schemes

Scheme 1. HOMO-LUMO gap engineering strategies.....	7
Scheme 2. Schematic difference of increasing rigidity of aromatic materials by conformational locking through covalent and non-covalent bonding	10
Scheme 3. Oxidative polymerization of poly(3-alkylthiophenes).....	18
Scheme 4. Cross coupling of 3-alkylthiophenes utilizing a) Kumada cross coupling (McCullough's method) and b) Negishi cross coupling (Rieke's method).....	19
Scheme 5. Examples of conjugated polymer synthesis through the use of a) Stille ³³ and b) Suzuki cross-coupling methods	20
Scheme 6. Catalytic cycle of a general Stille coupling method.....	21
Scheme 7. Conceptual scheme highlighting the fact that direct arylation effectively streamlines the synthesis of conjugated materials.....	22
Scheme 8. Dehydration reaction between of 3,4-dimethylthiazole <i>N</i> -oxide.....	23
Scheme 9. Proposed mechanism of <i>N</i> -oxide dehydration reaction.....	24
Scheme 10. Dehydration polymerization of a di- <i>N</i> -oxide containing monomer.....	24
Scheme 11. Conceptual scheme of post-polymerization alterations versus altering monomers to produce different polymers.....	27
Scheme 12. Method for the synthesis of poly(3-alkylthiophenes) with varying degrees of oxidation (TDO moieties).....	28
Scheme 13. Initial proposal for the synthesis of thiazole-containing conjugated polymers	29
Scheme 14. Synthesis of 4,4'-dinonyl-2,2'-bithiazole.....	30
Scheme 15. Synthesis of poly(5,5'-thieryl-4,4'-dinonyl-2,2'-bithiazole).....	31
Scheme 16. Synthesis of 4,4'-dinonyl-2,2'-bithiazole containing polymers.....	34
Scheme 17. Failed oxidation of 4,4'-dinonyl-2,2'-bithiazole containing polymers.....	35
Scheme 18. Conceptual scheme of utilizing non-covalent interactions for rigidification of conjugated systems	36
Scheme 19. Synthesis of bithiazole small molecules	38
Scheme 20. The difference in systems where there can be no S-O interactions upon oxidation versus a system that contains at least one S-O interaction.....	40
Scheme 21. Synthesis of 5-(5-hexylthieno)-4-methylthiazole(5) and <i>N</i> -oxide.....	41

Scheme 22. Synthesis of the 5,5'-(5-hexylthienyl)-4,4'-dimethyl-2,2'-bithiazole compounds.....	48
Scheme 23. Synthesis of the fluorene polymer series.....	51

List of Tables

Table 1. Molecular weight and dispersity of polymers P2-P4.....	34
Table 2. Stokes shift of small molecules with extended conjugation.....	50
Table 3. Molecular weights of the fluorene and thiophene polymer series.....	53
Table 4. Stokes shift of fluorene and thiophene polymer series.....	56
Table 5. Optical and electronic data for both polymer series.....	60
Table 6. Solvent polarity.....	64
Table S1. Single Point Energies.....	82
Table S2. Second Order Perturbation Interaction Energies.....	82

Abbreviations

Ar	Aryl
Bu	Butyl
CP	Conjugated polymer
DAr	Direct arylation
DArP	Direct arylation polymerization
DCM	Dichloromethane
DFT	Density functional theory
HOMO	Highest occupied molecular orbital
LDA	Lithium diisopropyl amide
LUMO	Lowest unoccupied molecular orbital
mCPBA	<i>meta</i> -Chloroperoxybenzoic acid
MeCN	Acetonitrile
MMPP	Magnesium monoperoxyphthalate
M_n	Number-average molecular weight
MTO	Methyltrioxorhenium
M_w	Weight-average molecular weight
MS	Mass spectrometry
NBO	Natural bond order
NMR	Nuclear magnetic resonance
OFET	Organic field effect transistor
OLED	Organic light emitting diode
OPV	Organic photovoltaic
OSC	Organic semi-conductor
OTFT	Organic Thin-Film Transistor
PDI	Polydispersity index
Ph	Phenyl
PT	Poly(thiophene)
SEC	Size exclusion chromatography
THF	Tetrahydrofuran
UHP	Urea-hydrogen peroxide

Chapter 1.

1.0 Introduction to Conjugated Materials and their Development

1.1 Conjugated Materials

Conjugated materials are at the forefront of electronics research due to the interesting and useful optical and electronic properties they possess, such as, high extinction coefficients, high quantum yields and semi-conducting abilities.¹ Conjugated polymers can therefore be used for applications such as organic photovoltaics (OPV),² organic field effect transistors (OFET),³ organic light emitting diodes (OLED)⁴ and chemical sensors. The functional properties required for these devices stem from the fully conjugated backbone of the conjugated system. This extended conjugation allows for delocalization of electrons through the entirety of the molecule or polymer chain which allows for effective charge-carrier mobility, whether that be an electron or a 'hole'. This idea can be observed in Figure 1 where the π -electrons in polythiophene are shown to delocalize throughout the polymer backbone, facilitating charge transfer throughout the system.⁵

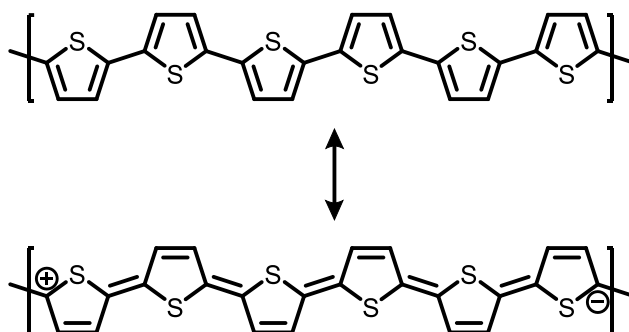


Figure 1: Delocalization of electrons through polymer backbone of polythiophene.

The use of conjugated polymers (CP) in organic electronics has been an area of continued interest in recent years due to the many advantages that these materials have over their traditional inorganic counterparts. Devices that are constructed using these materials have advantages that include, flexibility, light weight and ease of fabrication/processing. However, conjugated polymers also suffer from significant drawbacks that currently limit their use in many applications.⁶ One disadvantage of conjugated polymers is that organic compounds tend to degrade much faster than inorganic compounds, thereby shortening the lifetime of the device.⁷ In addition, crystalline silicon devices often have a higher performance than organic-based devices, in parameters such as power conversion efficiency in photovoltaics and charge mobility in transistor applications. While organic-based devices may never reach the efficiency that inorganic materials currently possess, they still have the potential to be used as cost-efficient alternatives and can potentially be used in areas and applications where heavy silicon devices cannot. Additionally, since there are an unlimited amount of organic materials that can be synthesized, this area of research has an unending amount of possibilities.

1. 2 Band Gap

While there are several characteristics that conjugated materials must possess in order to be ideal candidates for organic electronic applications, certain characteristics may be valued to differing degrees depending on the application in question. Typically, materials used for OLEDs, OFETs and OPVs require a high level of charge transport, strong absorption and/or emission, acceptable HOMO-LUMO levels as well as being able to form well-behaving thin films.⁸ Most importantly, these materials also require a suitable band gap based on the application in

question. The band gap of electronic materials is important when it comes to device performance, however there are other contributing factors such as electron or hole mobility and extinction coefficient. For example, the optimal band gap for conjugated polymers in photovoltaic application is $\sim 1-1.5$ eV with a broad absorption spectrum but there have been examples of materials that possess band gaps in excess of 2 eV and still have good power conversion efficiencies (PCE) of 8% or greater due to high electron mobility.⁹

The band gap is the difference in energy between the valence band and the conduction band in solid-state materials. The valence band and conduction band refer to the bands of orbitals closest to the Fermi level, both higher in energy (conduction band) and lower in energy (valence band).¹⁰ This energy gap is the amount of energy that is required to promote an electron into the conduction band so that it can move freely throughout the system, or create an electrical current. This is related to the HOMO-LUMO gap, which is defined as the energy it takes to promote an electron from the HOMO to LUMO in organic compounds. The difference is that the HOMO and LUMO are energetically defined molecular orbitals, whereas the valence and conduction bands are energy ranges of multiple orbitals in a solid-state material (Figure 2).

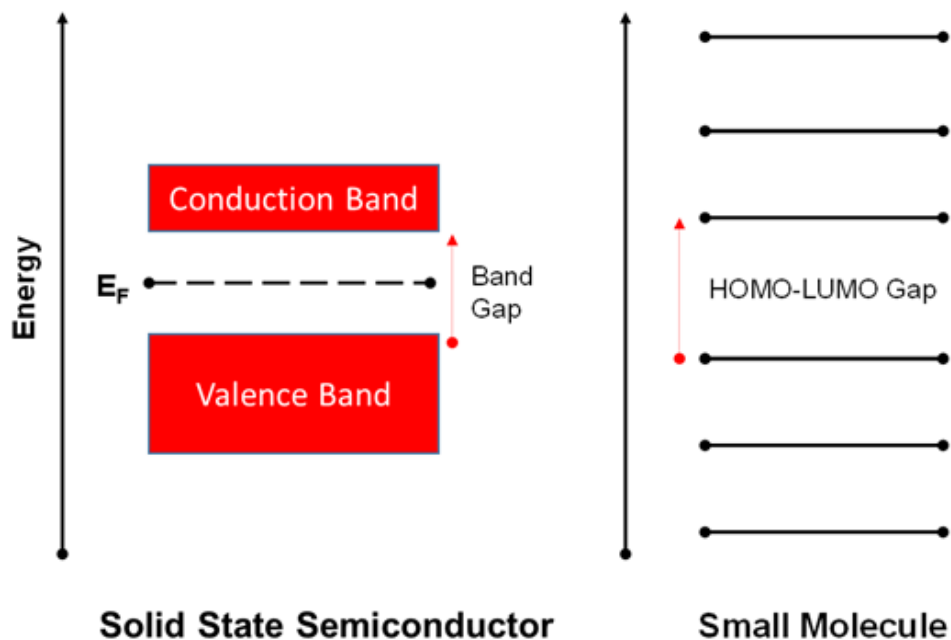


Figure 2: Difference between band gap in solid-state systems and HOMO-LUMO gap in molecular systems.

Electronic materials can be divided into three categories that are dependent upon the band gap: insulators, semi-conductors and conductors (Figure 3). Insulators have high band gaps and are unable to carry any charge without an excessive amount of energy input to the system, such as rubbers and plastics. Conductors, such as copper and gold, do not have a band gap as the valence and conduction bands are overlapping, allowing for free charge transport through the material. Semi-conductors, however, can act as either insulators or conductors depending upon the energy input on the system.¹¹ This property is what makes semi-conducting materials so desirable in electronics and computing. A semi-conducting material has the ability to ‘turn on’ in the presence of an external energy source, thereby acting as a conductor, whereas in the absence of an energy source, the material acts as an insulator. This therefore gives semi-conducting materials the ability to be utilized in a plethora of applications including electronic switches and chemical sensors.¹²

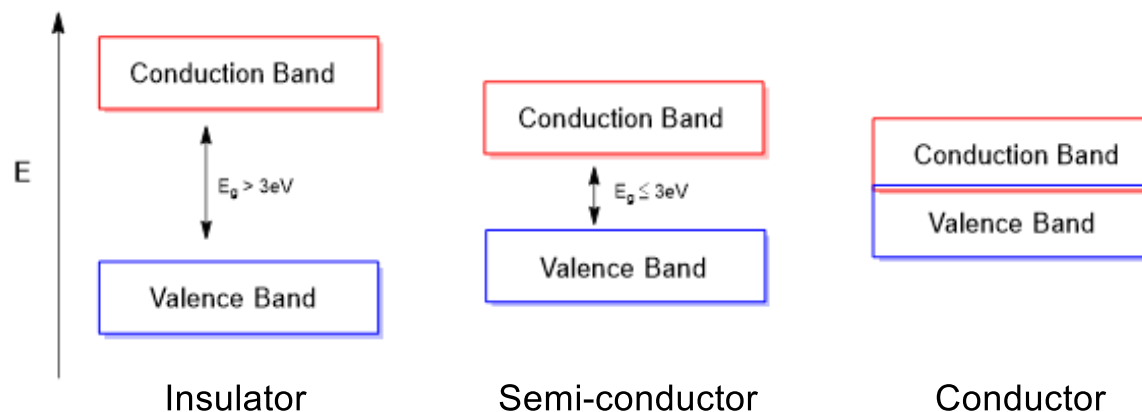


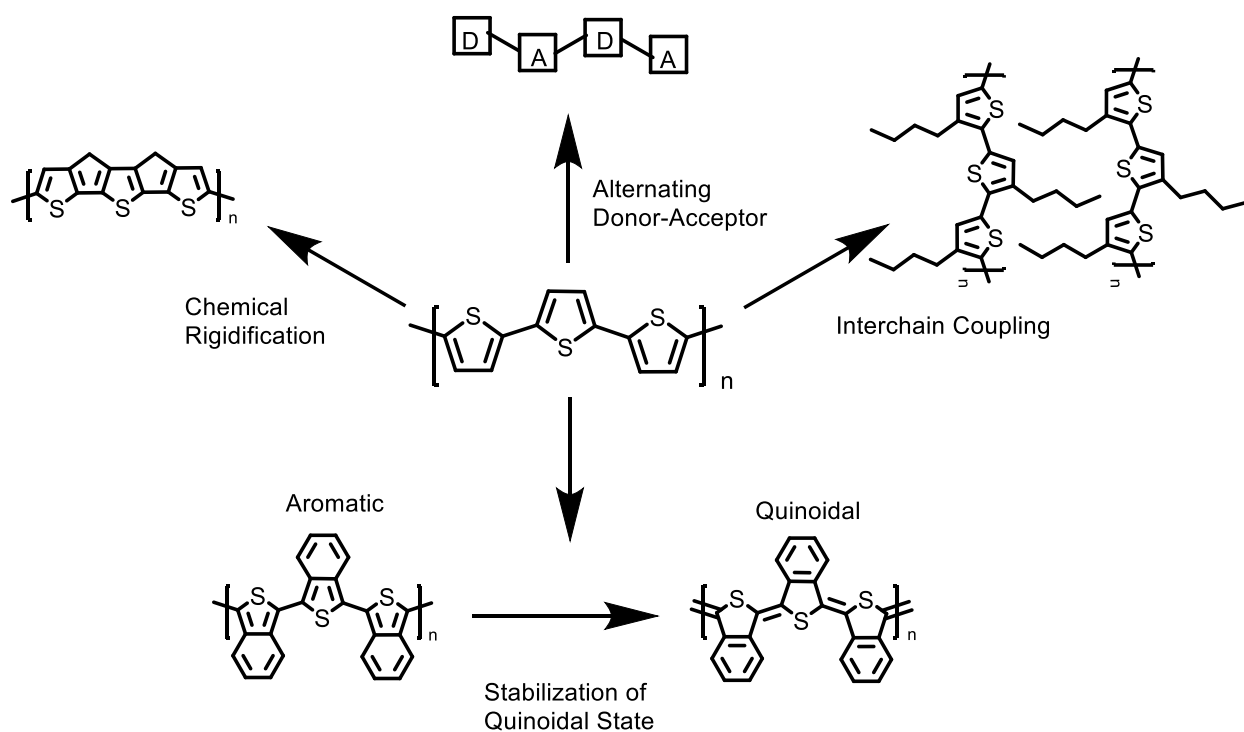
Figure 3: Conceptual image of the band gap in electronic materials.

The size of the band gap and the position of the frontier orbitals are the most important factors determining the optical and electronic properties of conjugated materials which can greatly affect the performance of a device.¹³ For example, in OPV's, ideal materials absorb photons in the red/near IR of the spectrum because the highest output from the sun is in this region. Therefore, the band gap of compounds used in photovoltaic devices generally fall in the area of 1.1 eV and contain a broad absorption spectrum.¹⁴ In contrast, in OLED devices, a wide range of band gaps may be required to achieve various colours in the display. Due to the wide range of band gaps used in organic electronics, it is imperative to be able to effectively and efficiently tune the energy levels in order to manipulate the band gap of the system to the desired level, as this is extremely important to the device performance.

1.2.1 Band Gap Engineering Strategies

Due to the large effect of the band gap on a materials performance and properties, there currently exist many band gap engineering strategies for conjugated materials. These strategies include: chemical rigidification, increasing aromaticity, intramolecular charge transfer, inductive

or mesomeric effects and interchain coupling (Scheme 1).⁸ Rigidification of the conjugated system extends the effective conjugation length and therefore increases π -orbital overlap, reducing the band gap of the system. The effective conjugated length is defined as the length of repeating units that are planar and therefore facilitates conductivity.¹⁴ Stabilizing the excited, or quinoidal state by the introduction of aromaticity reduces the energy of the excited state which in turn decreases the band gap of the compound. The inclusion of electron donating groups or electron withdrawing groups directly onto a polymer backbone can instill electronic effects (via inductive or mesomeric effects) that can alter the molecular orbitals in the polymer. In general, the incorporation of electron-donating groups will raise the HOMO (to a greater extent than the LUMO) as it adds electron density to the conjugated system. This is in contrast to the addition of electron-withdrawing groups, which lowers the LUMO to a greater extent than the HOMO of the polymer due to removal of electron density from the system. Both of these methods result in a decrease in the energy of the band gap.¹⁵



Scheme 1: HOMO-LUMO gap engineering strategies.

While these methods are all used extensively to tune the properties of conjugated materials, perhaps the most popular method is the addition of alternating conjugated electron-rich donor and electron-poor acceptor moieties into the polymer backbone, which is known as a push-pull motif. This motif assists the delocalization of electrons and the formation of a quinoidal excited state. The high lying HOMO of the electron-rich donor and the low lying LUMO of the electron-poor acceptor results in a photoinduced intramolecular charge transfer that accounts for the large decrease in optical band gap. This idea can be simplified by viewing the system as a hybridization between the frontier orbitals of the donor and acceptor moieties (Figure 4).¹⁶

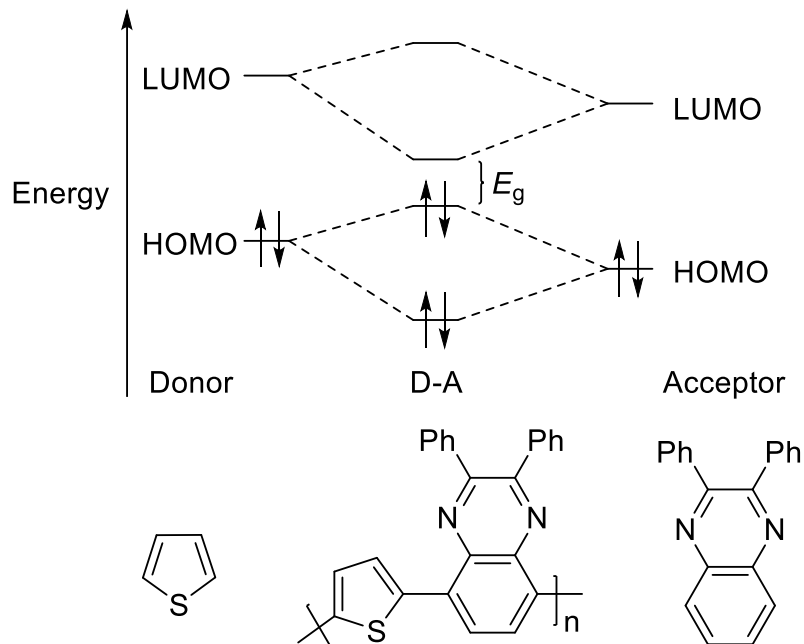


Figure 4: Orbital mixing in a push-pull motif.

Two extensions of the previous band gap tuning strategies that have recently gained a lot of interest are the controlled oxidation of conjugated materials and conformational locking through non-covalent interactions. Controlled oxidation is a process in which the degree of oxidation can be varied in a controlled manner in order to obtain desired levels of oxidation in the system. In a recent paper by Campos et al. the controlled oxidation of poly(3-alkylthiophene) was investigated.¹⁷ They observed that upon successive oxidations to the corresponding thiophene-S,S-dioxide moieties there was a significant bathochromic (or red) shift observed in the UV-Vis absorbance corresponding to successive reductions in the band gap of the system, as seen in Figure 5. This large shift in the band gap occurs due to the breaking of aromaticity of thiophene upon oxidation to TDO. The result is that the TDO moieties act similar to a diene system, and therefore require less energy in order to reach the excited state because it does not

require a break of aromaticity. While this method produced very promising results that could further be explored for use in conjugated materials, the use of Rozen's reagent ($\text{HOF}\cdot\text{CH}_3\text{CN}$) for thiophene oxidation is impractical for most laboratories. This process utilizes fluorine gas to produce HOF *in situ*, which is a highly toxic and reactive chemical that requires specific safety and ventilation measures.

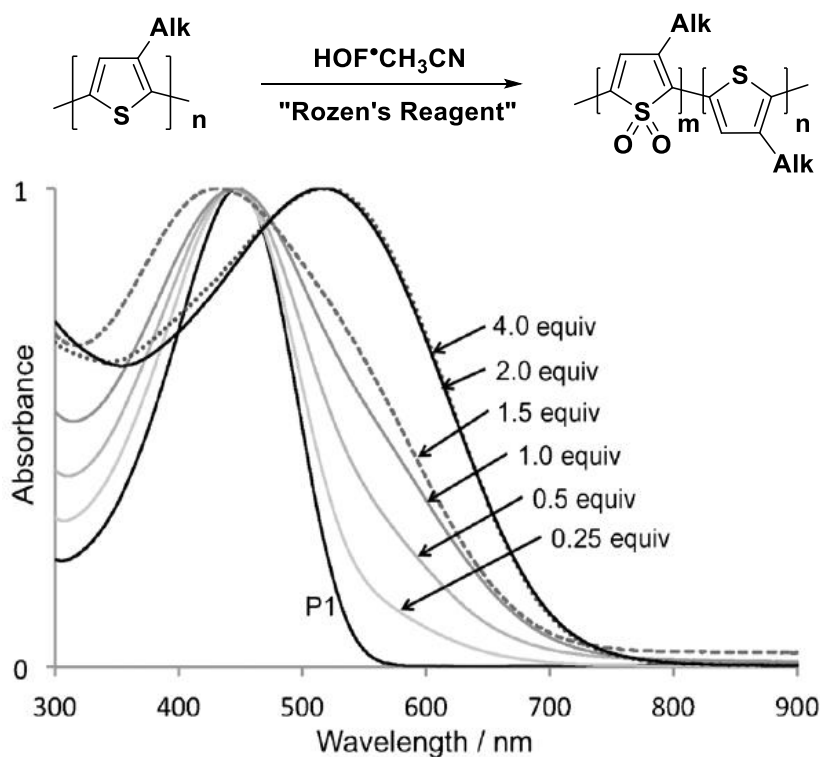
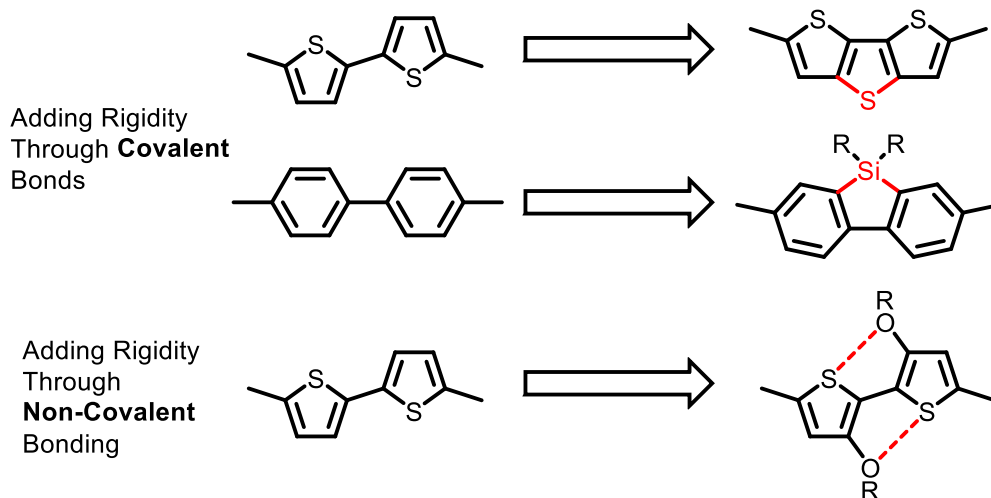


Figure 5: UV-Vis spectra seen from Campos showing the effect of increasing oxidation of thiophene containing conjugated polymers. Reproduced with the permission of Angewante Chemie International Edition.¹⁷

Conformational locking, on the other hand, is used to increase the π -orbital overlap throughout the backbone of the conjugated polymer and can be performed through rigidification of the polymer via one of two distinctive methods. The classical method is to form covalent bonds, usually through the formation of a fused aromatic system in the backbone of the

conjugated material. A common example of such a method is to replace bithiophene units with dithienothiophene (Scheme 2). This can be synthetically demanding, and often fusing rings



Scheme 2: Schematic difference of increasing rigidity of aromatic materials by conformational locking through covalent and non-covalent bonding.

requires an sp^3 atom in the bridging position, which, in the case of CR_2 and SiR_2 groups, can have negative effects on intermolecular interactions. The second method utilizes the idea of locking the conformation of the system through non-covalent interactions, such as, S-O, S-N interactions, or hydrogen bonding. This method is more appealing, as it can also produce a rigidification effect, and therefore a reduction in the band gap, but through less synthetically demanding means. As opposed to covalently bonding or fusing ring structures together, one can incorporate side chains or heteroaromatic rings in order to obtain these non-covalent interactions, as seen in Figure 6.^{9,18,19} Upon introduction of non-covalent interactions, all of the compounds in Figure 6 displayed bathochromic shifts in the UV-Vis spectrum which results in a closing of the electrochemical band gap and increases device performance in OFET and OSC's.^{9, 18,19}

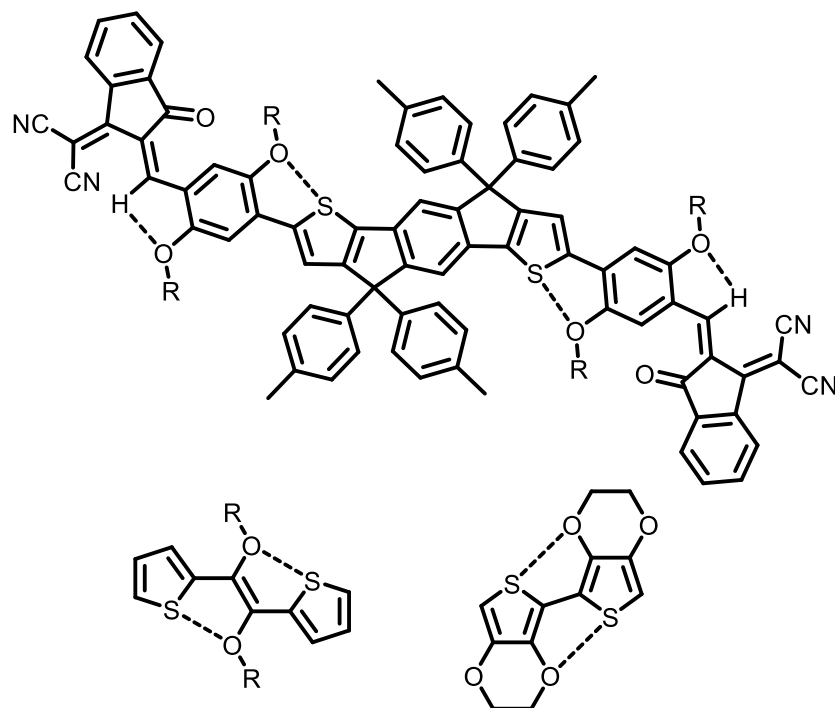


Figure 6: Intramolecular non-covalent interactions seen in the literature that are believed to facilitate planarization.^{9, 18, 19}

By locking the conformation of a polymer in a planar structure through non-covalent interactions, one increases the effective conjugated length. This effect allows for better overlap of π -orbitals and therefore reduces the band gap of the polymer, as seen in both computational and experimental studies. Due to the difficulty in untangling the strong electronic component of adding electron-donating oxygens from the effect of the intermolecular interactions, the experimental studies currently found in the literature often fall short of the proof that it is in fact the rigidification, and not the electronic component that contributes to the HOMO-LUMO gap reduction.²⁰

1.3 Chalcogen Bonding

Typically, sulfur is not viewed as an electron accepting atom, however it has been seen in the literature that the σ^* orbital of chalcogen bonds (excluding oxygen) in electron-deficient systems can in fact act as an electron acceptor. It has recently been shown that the lone pair of a chalcogen atom (O, S) can delocalize electron density into the empty σ^* orbital of an adjacent chalcogen atom (S, Se).²¹ This was shown utilizing molecular balances to probe the conformational equilibrium, since the position of said equilibrium depends on all of the intermolecular interactions as well as solvent effects (Figure 7). The closed conformation was in fact more favourable than the open conformation, pointing to an interaction between the chalcogen atoms. Contributions from electrostatic, solvophobic, van der Waals dispersion and orbital effects were examined. Interestingly, the magnitude of the interaction was largely independent of the solvent being used. In addition, it was found that electrostatic and van der Waals dispersion contribution were minimal. It was found through NBO, single point energy and geometry calculations, that orbital delocalization from the lone pair into the S-C σ^* bond was the driving force behind this interaction.²¹

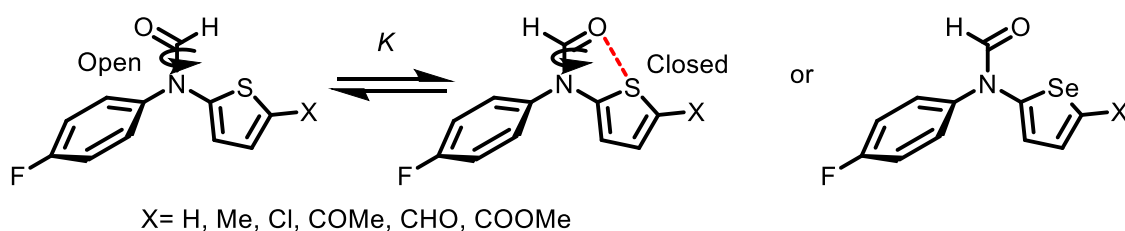


Figure 7: Molecular balances used to exhibit the chalcogen-chalcogen interaction. If the interaction is more favourable, it will conform to the 'closed' structure more often than the 'open' conformation.²¹

In a 2016 paper by Benz et al., it was shown that dithienothiophene derivatives could utilize sulfur-anion interactions to complex with a variety of anions for transport purposes (Figure 8).²²

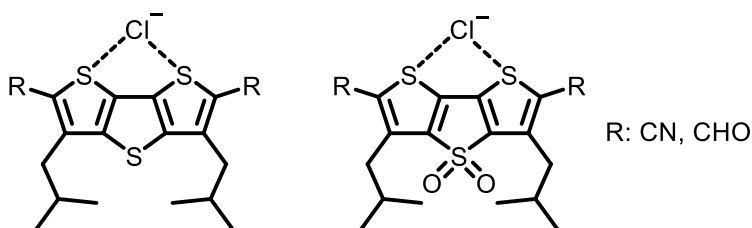


Figure 8. Dithienothiophene derivatives used as anion transporters through the interaction of chalcogen σ^* antibonding orbitals.²² Similar behaviour, seen in Figure 6, involves the antibonding orbital of the C-S bond accepting electron density from neighbouring oxygen atoms.²²

In addition to the use in anion transporters, these chalcogen bond interactions were also seen to effectively rigidify the structure of (acylamino)thiadiazoline in a series of antagonist molecules (Figure 9).²³ The crystal structures of these systems show a clear non-covalent interaction between the sulfur atom and the adjacent carbonyl oxygen. The distance between the two atoms in all three antagonist molecules is substantially lower than the sum of the van der Waals radii of sulfur and oxygen (3.25 Å), showing a significant interaction leading to a planarization effect on the molecules. Although these interactions where sulfur acts as an electron acceptor are not regularly utilized in biological systems, they can be seen biological anion transporters such as prodigiosin and synthetic mimics.²²

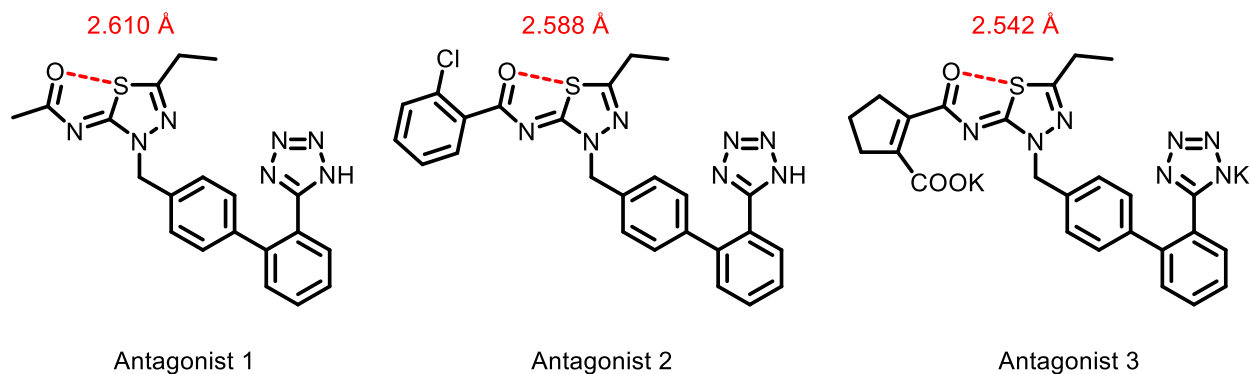


Figure 9: S-O interaction seen in the crystal structures of various antagonist molecules.²³

Due to the significant interactions between these C-S σ^* anti-bonding orbital and electron rich atoms, it was hypothesized that these interactions could act as a new method for the rigidification of conjugated materials. By incorporating side chains that had the ability to form these non-covalent interactions, planarization of these systems would be substantially less synthetically demanding than fusing or bridging aromatic rings. Due to the appeal of this method, there have been some computational and experimental studies performed to probe the effect of this interaction on conjugated small molecules and polymers (Figure 10).^{9,24} These studies include probing the effect of different electronegative atoms interacting with the C-S σ^* orbital; oxygen, nitrogen and fluorine. The addition of these interactions into molecular systems has been shown to have positive implications on the optical and electronic properties. For example, when replacing the alkyl chains (Figure 10:A) with the alkoxy chains (Figure 10:B), the optical band gap underwent a bathochromic shift of 0.3 eV. In addition, polymer B also possessed a mobility ($\mu_{u/h}$) of $3 \times 10^{-6} \text{ cm}^2/\text{Vs}$, whereas the polymer without any S-O interactions was inactive.⁹ In Figure 10 C and D, computational studies were performed and rotational barriers in excess of 20 kcal/mol

were commonly observed in instances where such an interaction was present, though this could also be affected by steric interactions from the bulky aromatic systems.²⁴

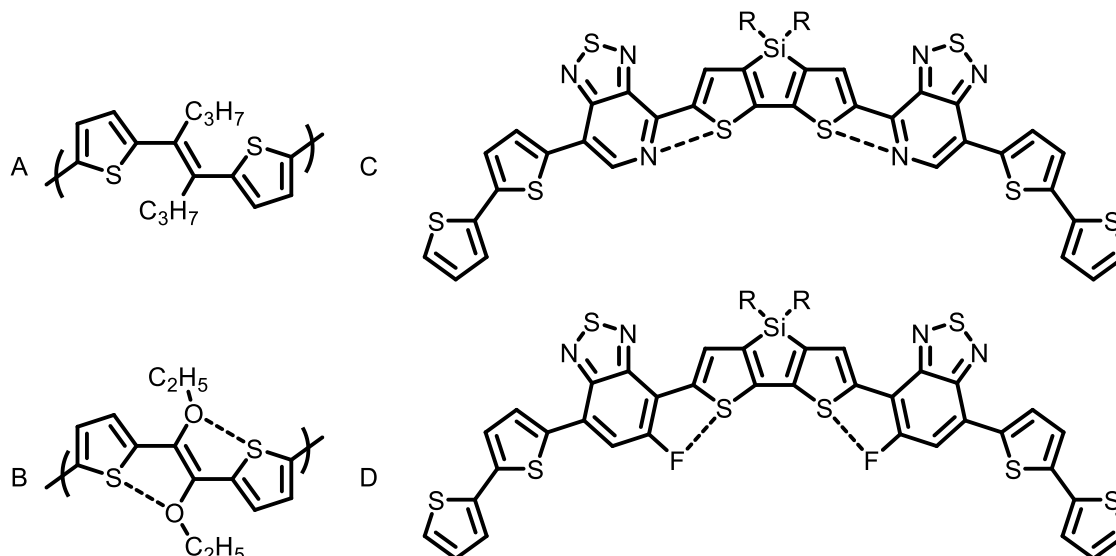


Figure 10: Examples of molecules studied for effects of rigidity due to interactions with the C-S σ^* antibonding orbital.^{9,24}

In addition to their uses as anion transporters, the interaction between oxygen lone pairs and this C-S antibonding orbital has been hypothesized in the literature to act as a method for rigidity of conjugated materials.^{19,20,22} While there is a lack of evidence for this effect in terms of a rigidity technique, Jackson et al.²⁵ performed a comprehensive computational study exploring the rotational barriers of a variety of compounds, showing some relatively large rotational barriers (~ 8 kcal/mol) in systems with these non-covalent bonds.

1.4 Methods of Estimating the HOMO-LUMO Gap

Obtaining accurate estimations of the HOMO-LUMO gap in electronic materials is imperative in determining the viability of testing said materials in electronic devices. The two most common methods for making these measurements are UV/Vis spectrometry (commonly denoted as $E_{g(\text{opt})}$) and various types of voltammetry (commonly denoted as $E_{g(\text{ec})}$), including, cyclic, linear sweep, differential scanning and square wave.

When utilizing the UV/Vis method, electrons are excited to the conduction band with light of sufficient energy, a bound electron-hole pair (exciton) is formed (Figure 11). Due to this bound pair, the recorded optical band gap is lower than the true band gap of the material. In spite of this, optical band gap is a commonly recorded value in the area of conjugated materials and is equal to the energy of the onset of absorption.

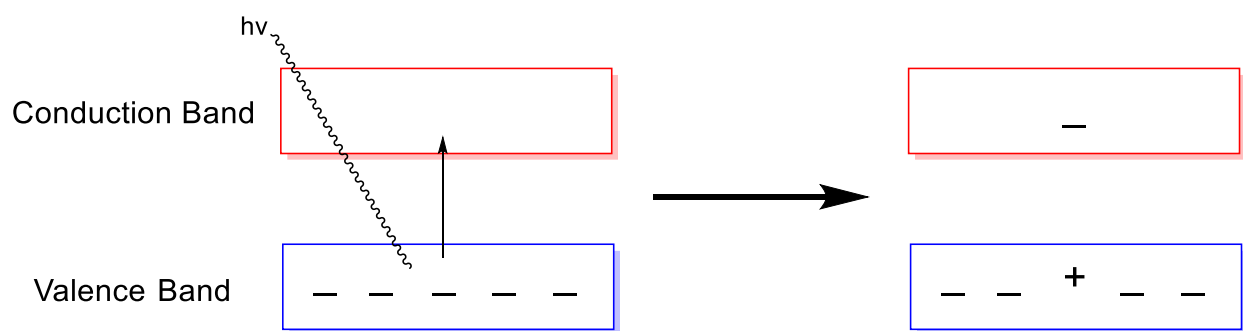


Figure 11. Creation of an electron-hole pair through photoelectric absorption.

Voltammetry, contrary to UV/Vis spectrometry, is a method used to estimate the band gap of materials through electrochemical means. There are many types of voltammetry used to determine the energy levels of solid-state and molecular systems but most of these methods rely upon sweeping the voltage from positive to negative (or vice-versa) and recording current

as an output. This method tends to be more accurate as no bound electron-hole pair is formed. The output is typically referenced using an Ag/AgCl cell or by using ferrocene as an internal reference.

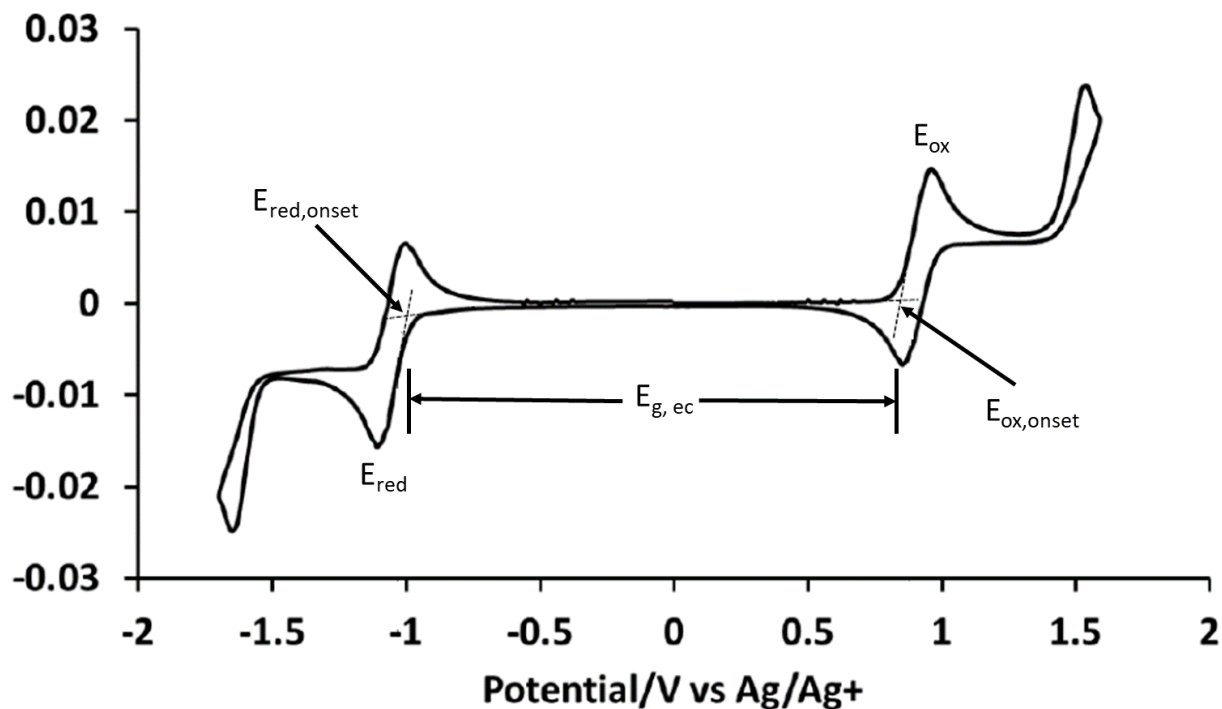


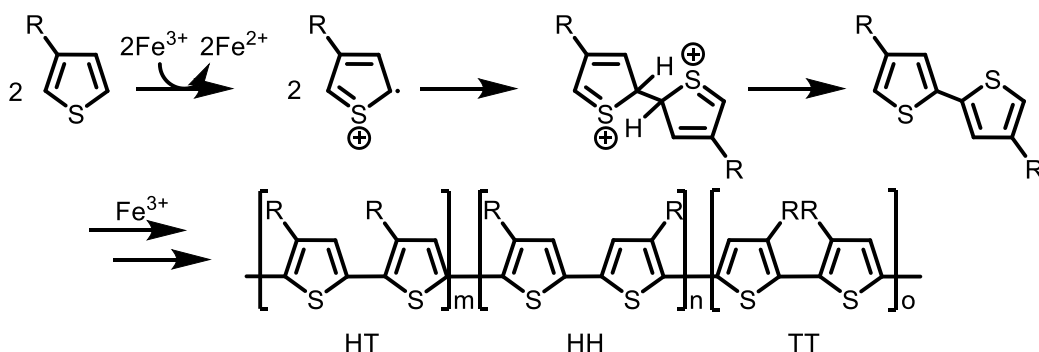
Figure 12: Cyclic voltammogram.

A voltammogram is outlined in Figure 12 above. As the voltage is swept from left to right, an oxidation occurs, where an electron is removed from the HOMO of the material. This can be seen in the above figure by the large peak E_{ox} and the onset of this peak ($E_{ox,onset}$) corresponds to the energy of the HOMO. The onset of the peak is determined by the extrapolation of the baseline and the slope of the peak. The intersection of these lines corresponds to the energy of the HOMO. As the voltage is swept in the opposite direction, a reduction occurs (E_{red}), where an electron is added to the LUMO of the material. The onset of

this peak ($E_{\text{red, onset}}$) corresponds to the LUMO and therefore the value of $E_{\text{LUMO}} - E_{\text{HOMO}}$ (or $E_{\text{red, onset}} - E_{\text{ox, onset}}$) equal to the electrochemical HOMO-LUMO gap ($E_{\text{g, ec}}$).

1.5 Synthesis of Conjugated Materials

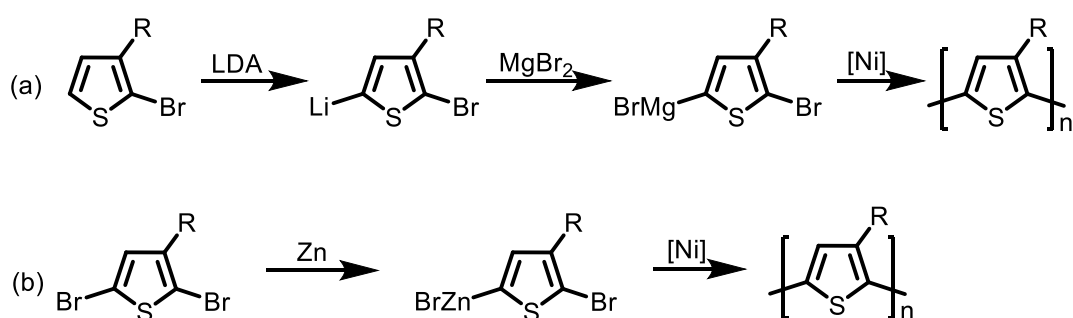
Conjugated small molecules and polymers have become very important in the realm of various dye and organic electronic applications. Due to a large supply of monomers and endless possible variations in organic molecules, there is an abundance of methods by which to synthesize these materials. The incorporation of heteroaromatic moieties in these materials has become almost essential due to the high performance associated with them.



Scheme 3: Oxidative polymerization of poly(3-alkylthiophenes).²⁷

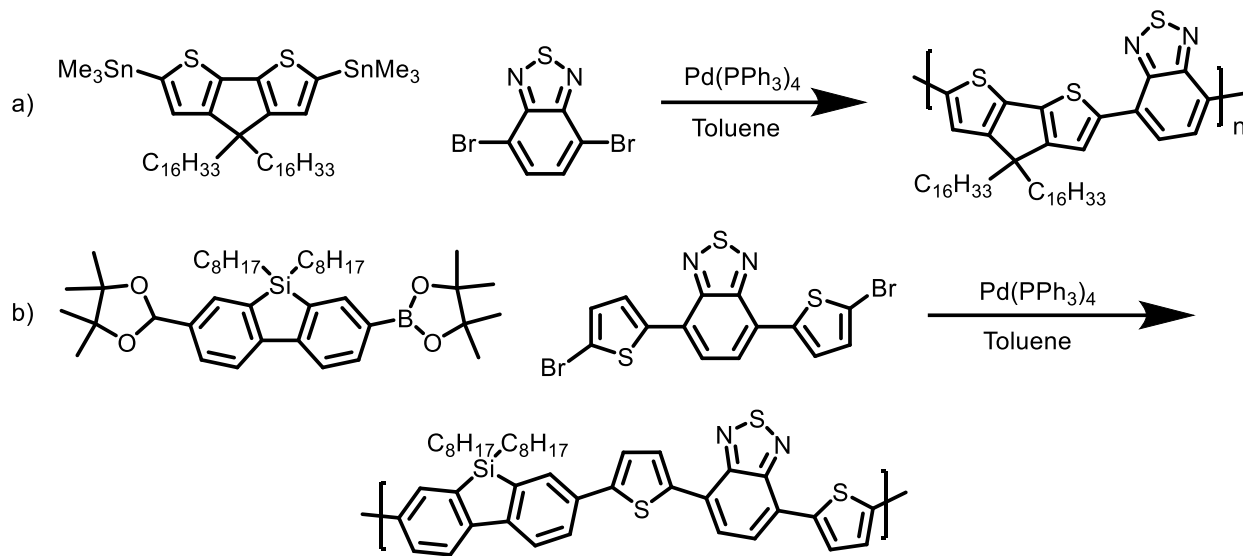
The synthesis of heteroaromatic polymer systems has been traditionally performed utilizing electrochemical and oxidative methods.²⁶ These methods were often applied in the polymerization of thiophenes, and more importantly poly(3-alkylthiophenes) due to the solubility issues associated with polythiophene. The issue with these methods stems from the fact that there is a lack of regioselective control during the polymerization, which results in head-to-tail, head-to-head and tail-to-tail linkages throughout the polymer backbone (Scheme 3). This

lack of regioregularity can have negative effects on the properties of the polymer such as inconsistent (and larger) optical and electronic band gaps.²⁷ Alternatively, using Kumada cross coupling methods, treating 2-bromo-5-alkylthiophene with LDA can yield very high regioregularity in these systems (Scheme 4).²⁸ The same result can also be achieved by performing alternate cross-coupling methods such as Negishi cross-coupling with an organozinc monomer.²⁹



Scheme 4: Cross coupling of 3-alkylthiophenes utilizing a) Kumada cross coupling (McCullough's method) and b) Negishi cross coupling (Rieke's method).^{28, 29}

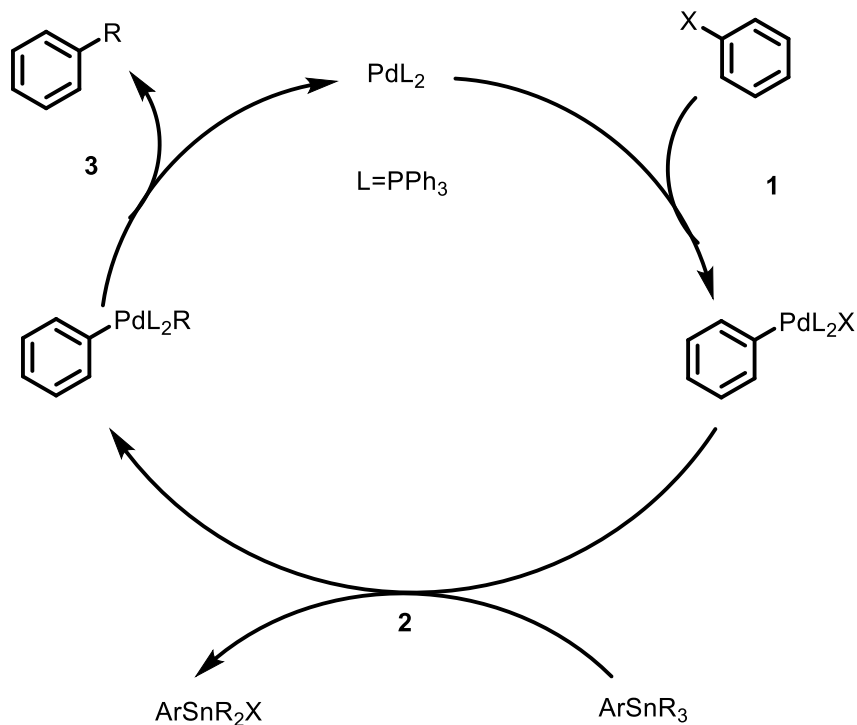
In more recent years, palladium-catalyzed cross-coupling reactions have become the standard for synthesizing conjugated polymers with great selectivity, yield and molecular weights.³⁰ The most common reactions for creating poly(hetero)arene systems are Stille and Suzuki coupling methods (Scheme 5), which utilize a palladium catalyst.³¹ These methods are very useful in synthesizing many families of conjugated materials, however they require preactivation of C-H bonds prior to coupling, which can be both synthetically complex and increase cost.³²



Scheme 5. Examples of conjugated polymer synthesis through the use of a) Stille³³ and b) Suzuki cross-coupling methods.³⁴

Stille coupling requires the use of aryl stannanes and aryl halides, whereas in the Suzuki method boronic esters are used in place of the organotin monomers. In addition to being quite efficient, these methods also tolerate a wide variety of functional groups. Despite these reactions working very well for the synthesis of conjugated materials, they do have drawbacks. In addition to the added synthetic complexity of converting an aryl compound into pre-activated organotin or organoboron monomers, other disadvantages include, toxic organotin by-products that are produced in the Stille reaction³⁵ and by-products that can be hard to separate from the product in Suzuki reactions, which can cause problems due to the fact that device fabrication requires very pure electronic materials.³⁶ Both Stille and Suzuki coupling follow a typical organometallic cross-coupling mechanism (Scheme 6),³⁷ that is, the cycle begins with oxidative addition (Scheme 6:1) of the aryl halide to the metal centre. This is followed by transmetalation (Scheme 6:2) where a second C-Pd bond is formed, the result being a syn-addition of the aryl starting materials.

Finally, reductive elimination (Scheme 6:3) occurs to yield the coupled product in addition to regeneration of the palladium catalyst.

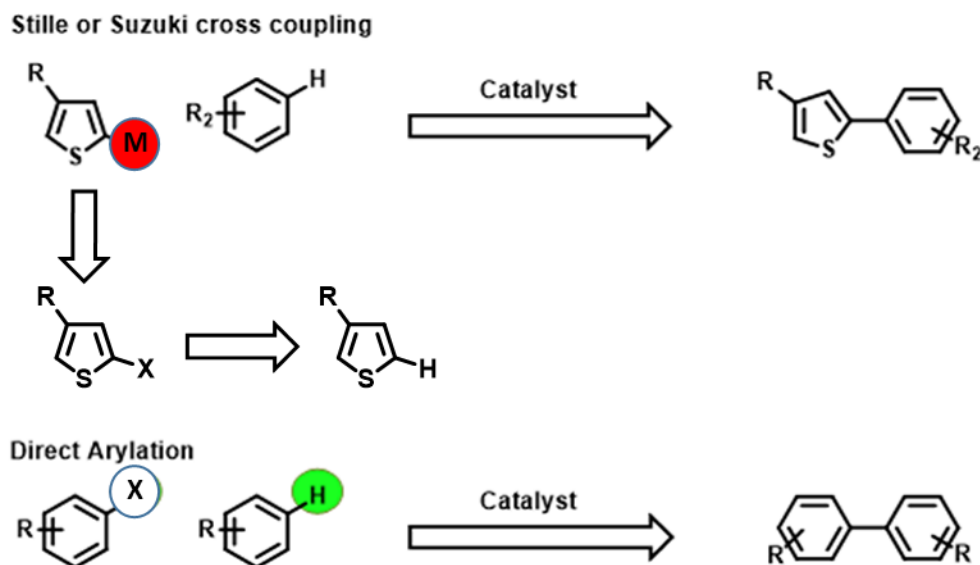


Scheme 6. Catalytic cycle of a general Stille coupling method.

1.6 Direct Arylation

When evaluating the strength of a synthetic route, efficiency and number of steps are key parameters for organic chemists. As such, C-H bond activation methods such as direct arylation (DAr) are currently of high interest.³⁸ As opposed to using organometallic monomers, as is the case in Stille and Suzuki methods, direct arylation effectively streamlines the synthesis by allowing the coupling of aryl halides directly to a C-H bond of the aryl precursor (Scheme 7). Due to the reduction of synthetic steps in the synthesis of the monomers, DAr is relatively inexpensive and does not have the drawbacks of toxic or hard to separate by-products. This method has

shown to be as effective as traditional approaches in many coupling and polymerization reactions, however, direct arylation remains less tolerant of some functional groups as compared to Stille and Suzuki couplings.³⁹



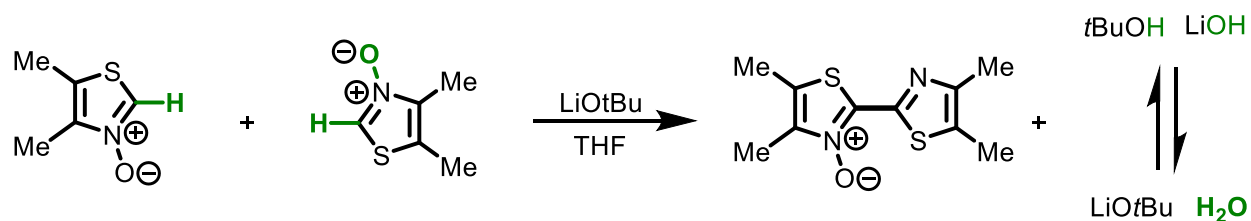
Scheme 7. Conceptual scheme highlighting the fact that direct arylation effectively streamlines the synthesis of conjugated materials without the need for an organometallic monomer.

Due to the fact that the monomers are not pre-activated (as in previous organometallic cross-coupling methods) direct arylation proceeds through a different mechanism that requires a step in which a C-H bond is activated in order to form the intermediate Pd-C bond.⁴⁰ The mechanism once again begins with an oxidative addition of the aryl halide to the metal centre. The next step of the mechanism is a concerted metalation-deprotonation (CMD), which has been studied heavily in recent years, including by Fagnou and co-workers.⁴¹ In this step, a base (typically a carbonate ion or acetate derivative) coordinated to the palladium is able to

additionally coordinate to and deprotonate the aryl group, allowing for the formation of a new C-Pd bond. This complex can then undergo reductive elimination to yield the coupled product.

1.6.2 Dehydration Reaction

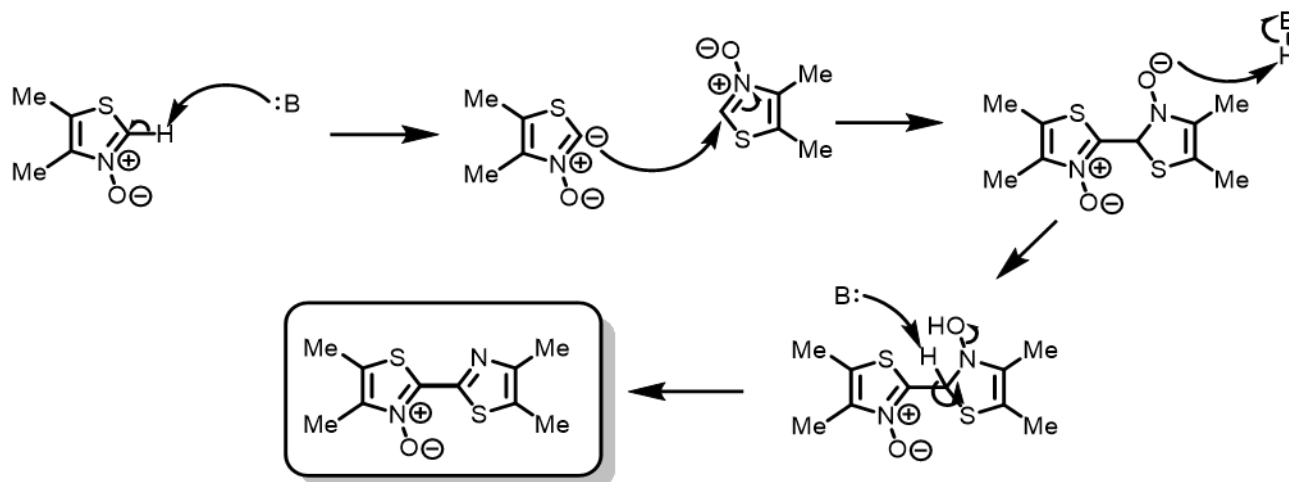
Direct arylation and other methods that utilize C-H activation are a step in the right direction in terms of reducing the number of synthetic steps needed to produce conjugated materials, which ultimately makes the synthesis of these materials more commercially viable. These techniques, however, still require the use of transition metal catalysts, ligands and additives. Recently, a new dehydration reaction has been developed by Schipper et al. that efficiently couples thiazole *N*-oxides to yield a dimer with the reduction of a single *N*-oxide moiety (Scheme 8).⁴² This reaction is performed with only the use of strong base (LiOtBu) in tetrahydrofuran (THF) and affords a formal loss of water, resulting in an efficient method for the coupling of thiazole *N*-oxides.



Scheme 8. Dehydration reaction between two equivalents of 3,4-dimethylthiazole *N*-oxide.⁴²

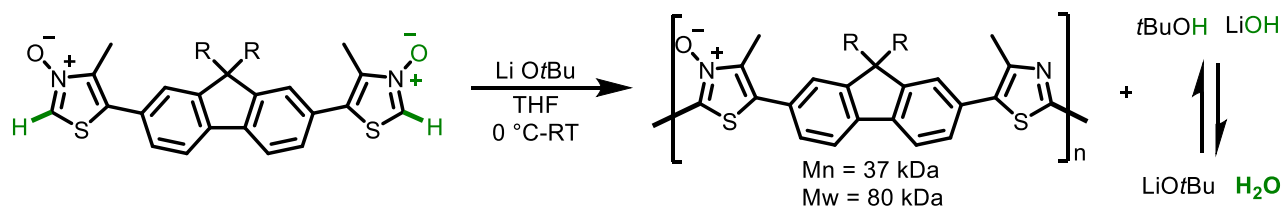
The proposed mechanism begins with deprotonation at the 2-position of the first equivalent thiazole *N*-oxide. The carbanion then is able to perform a nucleophilic attack the 2-position of the second equivalent of thiazole *N*-oxide. Next, the negatively charged oxygen atom

of the same thiazole is protonated, which ultimately allows for the elimination of hydroxide to produce the dimerized product (Scheme 9).⁴²



Scheme 9: Proposed mechanism of *N*-oxide dehydration reaction.

This reaction was then optimized for the use in conjugated polymer synthesis utilizing di-*N*-oxide monomers in a homopolymerization (Scheme 10).⁴² This was again performed through only the use of a strong base in THF and was able to produce high molecular weight polymers efficiently, with no more purification than precipitation in methanol. Conjugated polymers of this nature are very rigid. This rigidity results in an overestimation of the molecular weight when calculating from polystyrene standards. However, this is still the common practice for the characterization of conjugated polymer molecular weights.



Scheme 10. Dehydration polymerization of a di-*N*-oxide containing monomer.⁴²

Chapter 2

2.0 Oxidation of Thiazole-Containing Conjugated Materials

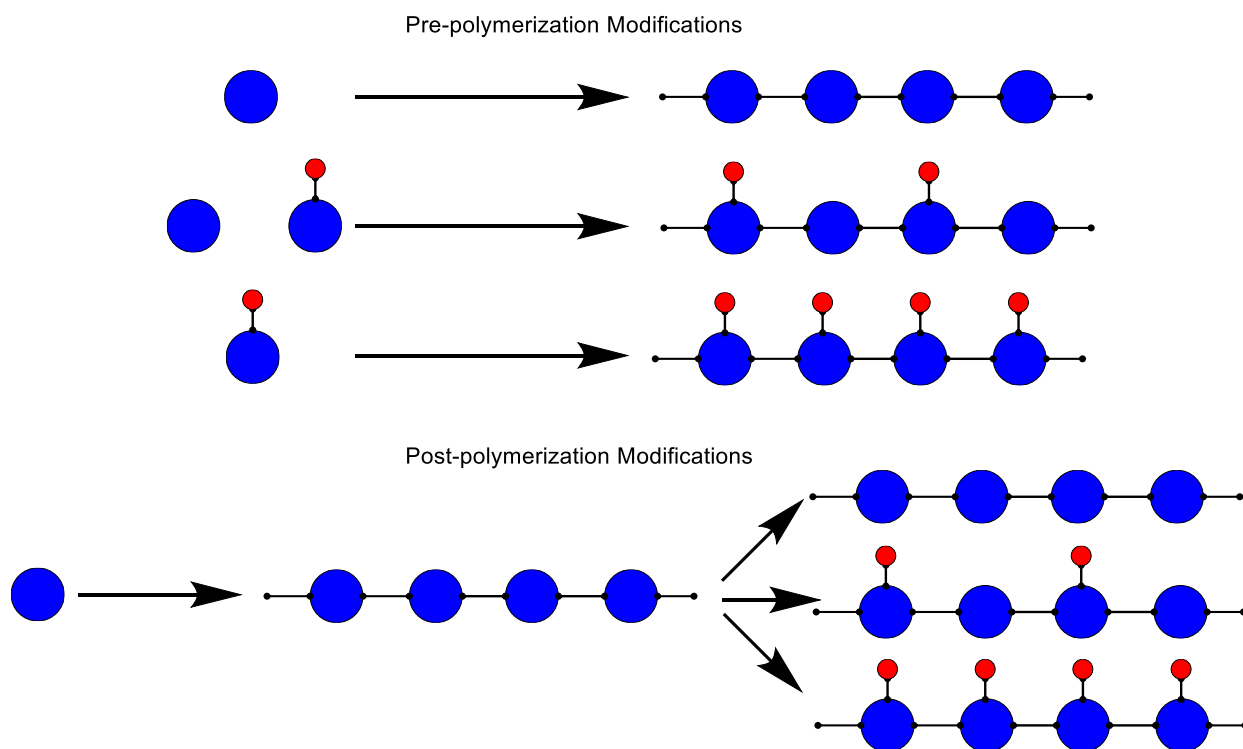
2.1 Thesis Proposal

Thiazoles have been used extensively in conjugated polymer research due to their high potential in device applications such as OPV's and OFET's.⁴³ In comparison to thiophene, an extensively used motif for CP's, the 3-position carbon is replaced with a nitrogen, which relieves some of the steric hindrance from the C-H bond at the 3-position of thiophene, resulting in a planar thiazole structure.⁴⁴ Due to this planarity, thiazole-based polymers tend to have high interchain interactions as well as intermolecular S-N and S-S interactions, which can lead to enhanced electronic properties.⁴⁵ Systems containing thiazole rings are therefore heavily studied and provide a good system for studying the tuning of optical and electronic properties. While thiazoles and their benefits have been heavily studied in conjugated polymers, extensive work has been done in the Schipper laboratory on the less studied use of thiazole *N*-oxides in conjugated small molecules and polymers.

The goal of this project was to develop a new method for tuning the optical and electronic properties of conjugated materials, specifically through the controlled oxidation of thiazole-containing systems. The further objective was to be able to perform these thiazole oxidations post-polymerization, thereby eliminating the synthetic complexity of altering monomers to successfully tune conjugated systems.

2.2 Controlled Oxidation of Thiazole Containing Conjugated Polymers

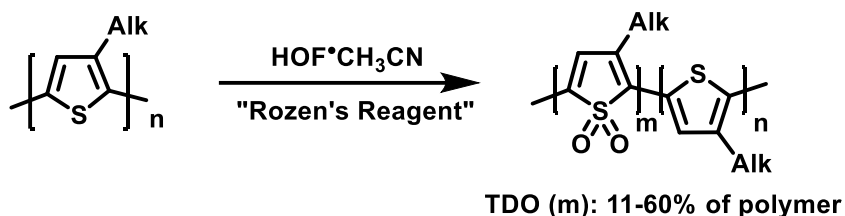
The tunability of conjugated materials is what makes them so interesting for use in organic electronic devices. However, many of the methods required for tuning the properties of these materials rely heavily on synthetic organic chemistry techniques. In most cases this requires altering the starting materials (monomers), which can make it more challenging to achieve a successful polymerization. While the potential advantage of organic molecules is the reduced cost compared to inorganic materials, finding methods that are less synthetically demanding is desirable. One such way is to synthesize polymers that can be altered to varying degrees post-polymerization in order to tune the optical and electronic properties. As seen in Scheme 11, synthesizing a base polymer which can then be altered post-polymerization to create a family of polymer materials with differing optical and electronic properties can be a much more efficient process.



Scheme 11. Conceptual scheme of post-polymerization alterations versus altering monomers to produce different polymers.

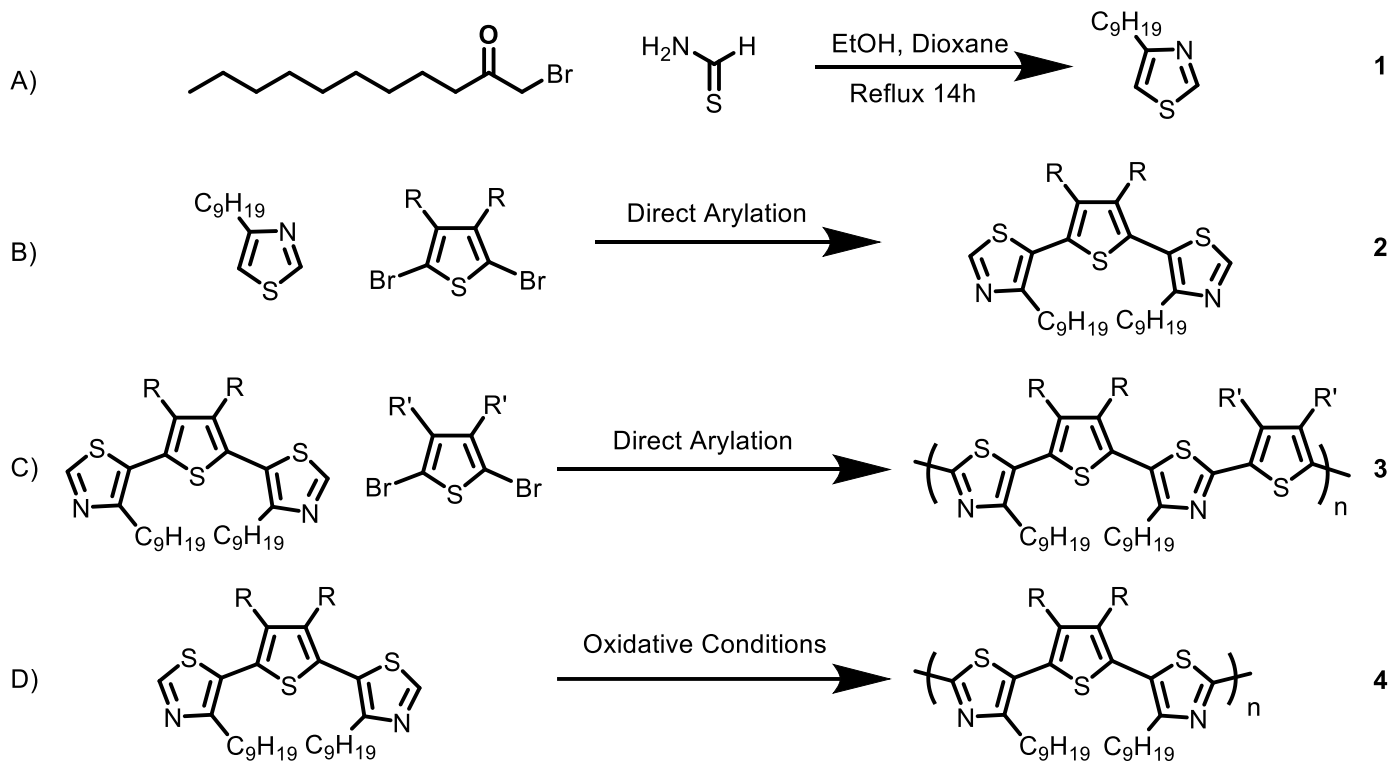
One method that utilizes this post polymerization approach has been discussed earlier, in which poly(3-alkylthiophenes) were oxidized to varying degrees, through increasing the number of equivalents of oxidizing agent used in order to tune the properties (Scheme 12).¹⁷ While this method produced high yields of oxidized polymers, it required the use of fluorine gas to prepare HOF *in situ*. These oxidation conditions are very efficient but they require resources and safety considerations that are not practical in general laboratory use. It is therefore proposed that a similar method could be used on thiazole-containing conjugated polymers in which they could be oxidized to varying degrees, to hopefully observe the same tunability of the optical and electronic properties. The reason why this is an attractive pathway is that it is much easier to

oxidize the nitrogen of thiazoles to thiazole *N*-oxides than thiophene can be oxidized to the S,S-dioxide. This is due to the fact that oxidizing thiophene to thiophene-S-oxide requires breaking the aromaticity of the system, whereas oxidizing thiazole to the thiazole *N*-oxide does not.⁴⁶ This enables the use of much milder oxidation conditions, such as the use of *meta*-chloroperbenzoic acid (*m*CPBA) as the oxidant.



Scheme 12: Method for the synthesis of poly(3-alkylthiophenes) with varying degrees of oxidation (TDO moieties).¹⁷

It was originally envisioned that molecules based on a framework of alternating thiazole and thiophene (or other aryl unit) moieties could be developed to observe this effect. The bithiazole monomer (**2**) bridged by an aryl linker could then be polymerized (**3,4**). The hope was that this compound could be polymerized utilizing direct arylation or copper-catalyzed oxidative conditions, due to the inherent low cost and chemical efficiency (Scheme 13). It has been shown in literature that various aromatic compounds, including thiazole and thiophene systems, can be efficiently coupled through a copper catalyzed reaction. Not only can these reactions be used to couple C-H/C-H bonds in aromatic systems but the reactions are also performed in the presence of air, as the oxygen acts as the oxidant. This is very appealing as typical cross-coupling reactions are performed under inert conditions.⁴⁷

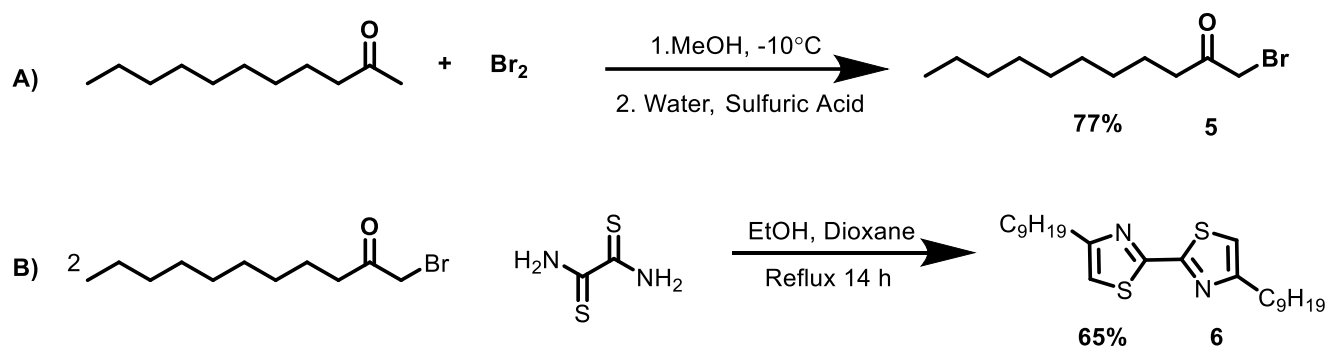


Scheme 13. Initial proposal for the synthesis of thiazole-containing conjugated polymers.

Upon attempting this synthesis, it was found that not only was synthesizing thioformamide *in situ* unpleasant, as it and the starting material gave off foul odors, but the product, 4-nonylthiazole (**1**), was also difficult to isolate. Following a literature procedure⁴⁸ for the synthesis of **1** resulted in yields of approximately 25%. Following this, it was found that performing washes with copious amounts of HCl allowed the extraction of the product much more easily and resulted in yields over 50% (Scheme 13:A).

The direct arylation of 4-nonylthiazole and 2,5-dibromothiophene proceeded well with yields of 70% or greater of the bithiazole monomer (Scheme 13:B), however the polymerization did not proceed as planned. Under direct arylation polymerization conditions there was no monomer conversion detected. Similarly, when oxidative conditions were implemented no

polymerization was observed. This lack of reactivity can be attributed to the reactivity of the thiazole ring itself. The free 2 positions of the thiazole are electrophilic in nature and not well suited towards direct arylation (Scheme 13:C). Synthesis of a monomer with an unreacted 5 position could prove beneficial to the polymerization conditions being utilized.



Scheme 14. Synthesis of 4,4'-dino-2,2'-bithiazole.

Due to the reactivity issues observed in the original model, we next envisioned a bithiazole monomer (**6**) that retained the unreacted 5 positions (Scheme 14). With this model, the bithiazole moieties are arranged in such a way that polymerization through direct arylation conditions would be able to proceed. This would allow for the formation of polymers with the framework seen in Figure 13, where the repeating unit contains two 4-nonylthiazole units as opposed to the alternating framework attempted in the previous model.

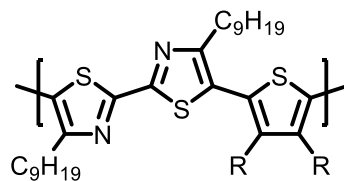
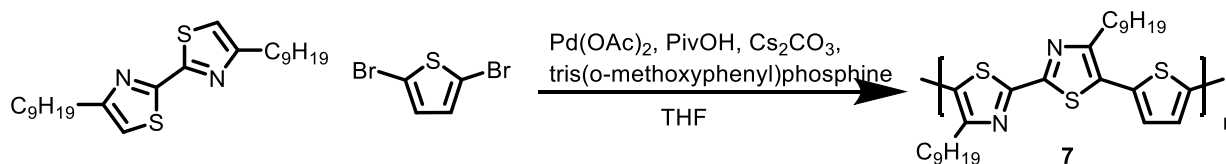


Figure 13: Repeating unit of proposed thiazole-containing conjugated polymers.

This synthesis began with the terminal bromination of 2-undecanone with bromine (Scheme 14:A). The long nonyl chain was incorporated to act as a solubilizing chain in the conjugated polymer system. The 4,4'-dinonyl-2,2'-bithiazole monomer was then produced through a double Hensch thiazole synthesis in 65% yield (Scheme 14:B). With the monomer in hand, the next step was to polymerize with an aryl dihalide co-monomer, for which we chose 2,5-dibromothiophene (Scheme 15). The thiophene linker was selected as it is a very common substituent in conjugated polymers due to its very desirable optical and electronic properties, as well as the fact that thiophene polymers tend to be quite planar. Unfortunately, this system was not soluble enough to undergo a direct arylation polymerization as the polymer (**7**) would become insoluble in solution below 5 kD with a substantial amount of unreacted monomer still remaining in the reaction mixture. This is not very desirable as the very low solubility of the polymer affects the processability and mechanical properties, which is one of the appealing factors of conjugated polymers. Despite the low solubility, the oligomer chains formed had an optical band gap of 2.27 eV stemming from a UV-Vis onset of 545 nm. This was a promising start as electronic materials with optical band gaps in the same range have been used to fabricate devices with good performance.^{2,9}



Scheme 15. Synthesis of poly(5,5'-thienyl-4,4'-dinonyl-2,2'-bithiazole)

In order to avoid solubility issues of our conjugated polymer, we instead devoted our attention to synthesizing polymers containing aromatic spacers that also contained solubilizing chains, namely, 3,4-dihexylthiophene, dioctylfluorene, and 1,4-dodecyloxybenzene. These

polymers would then act as models for post-polymerization alterations and would allow us to observe the effect of a controlled oxidation on different aromatic systems. Polymers **8-10** were prepared via direct arylation polymerization of the bithiazole and the corresponding dihalogenated arene (Scheme 16). The solubility of these polymers was no longer an issue and they possessed respectable molecular weights (Table 1) as well as optical properties as seen by the UV-Vis spectrum (Figure 14). Although the molecular weights of the polymers were calculated to be high (from polystyrene standards), the values are not absolute. This is due to the conjugated polymers resembling more rigid, rod-like conformations, which results in an inflated molecular weight. The dispersity (PDI) of the polymers is also respectable and consistent with what should be expected in a step-growth polymerization according to the Carothers equation, $PDI = 1 + p$, where p is the fraction of monomer conversion. If all monomer is converted the PDI according to this equation should be equal to 2.

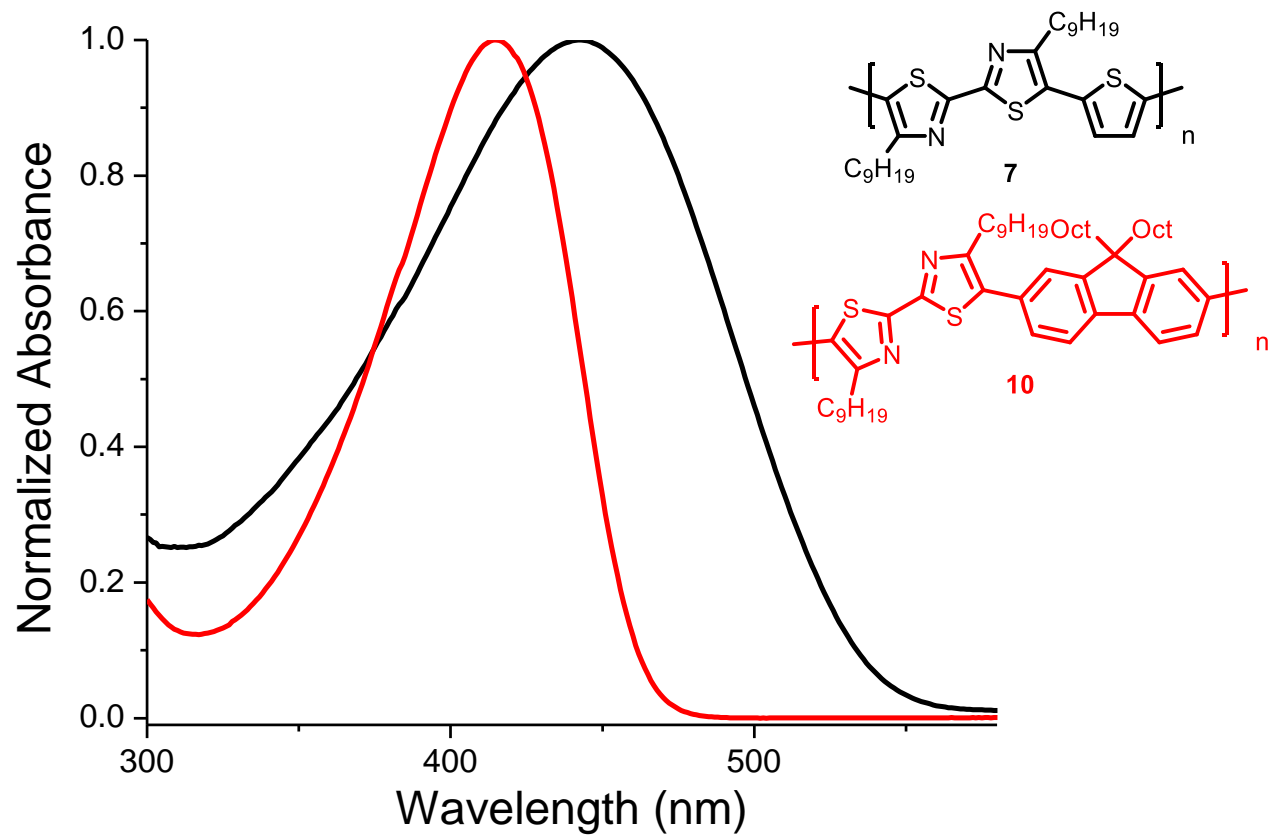
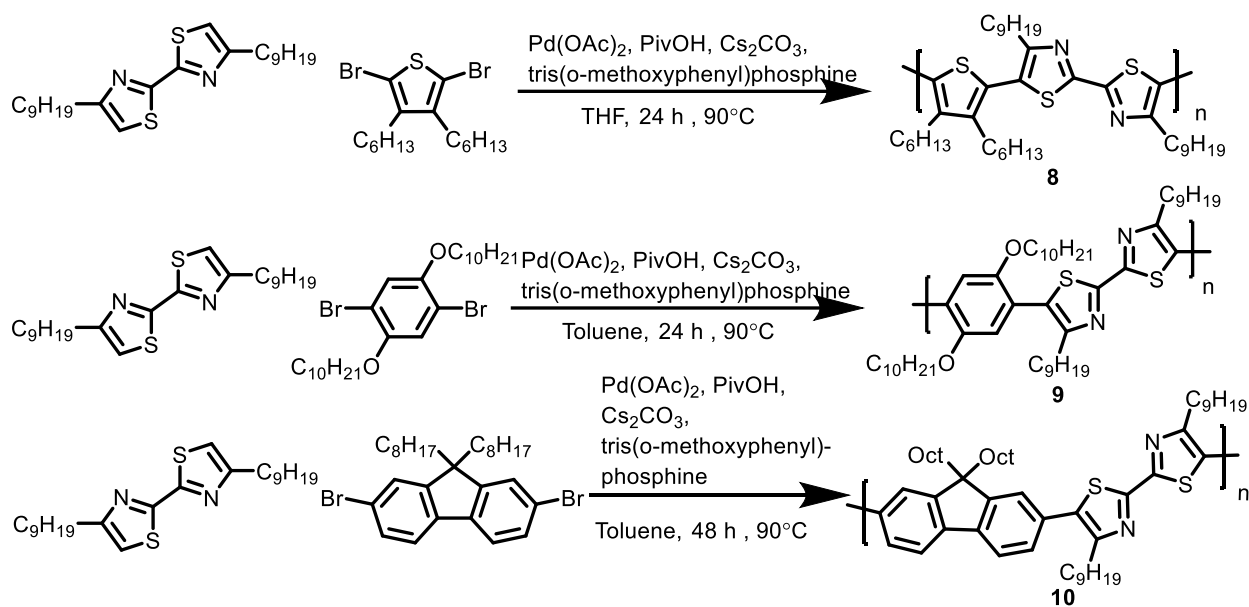


Figure 14. UV-Vis spectrum of poly(5-thienyl-4,4'-dinonyl-2,2'-bithiazole).



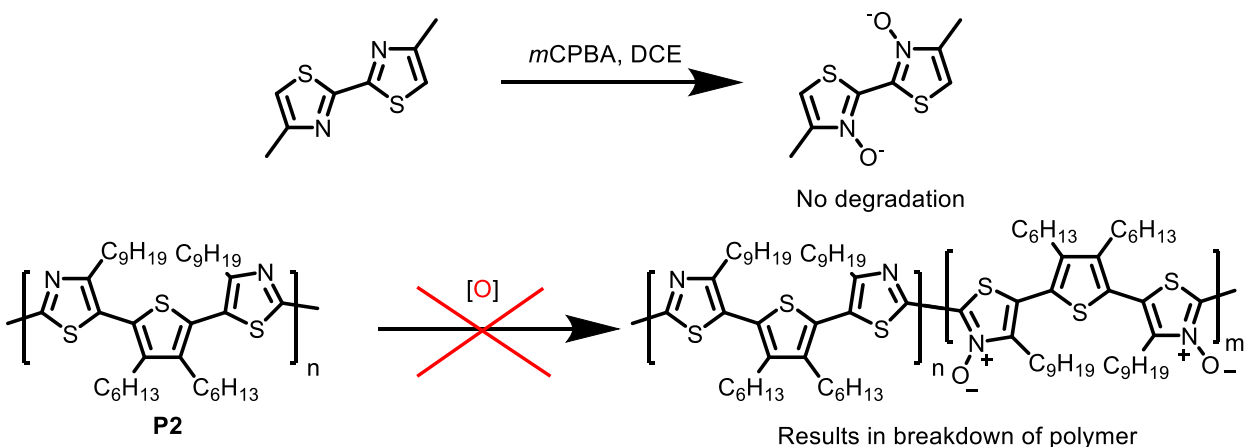
Scheme 16: Synthesis of 4,4'-dinonyl-2,2'-bithiazole containing conjugated polymers.

Table 1: Molecular weight and dispersity of polymers P2-P4.

Compound	M_n (kD)	PDI	X_n
8	29	2.2	43.3
9	32	2.2	39.6
10	52	1.9	62.3

With the thiazole-containing polymers in hand, the next and most important step in the synthesis was the oxidation of the thiazole moieties of these polymers to thiazole *N*-oxides. By oxidizing the polymers to varying degrees using different equivalents of *m*CPBA, we would hopefully observe optical and electronic changes in the UV-Vis spectra as well as voltammetry measurements as seen in the oxidation of poly(3-alkylthiophenes).¹⁷ Previous work done in the Schipper group on the oxidation of thiazole systems to thiazole *N*-oxides had been performed using *m*CPBA, so these conditions were used as a starting point for post-polymerization oxidation. Unfortunately, upon attempted oxidation of the conjugated polymers with *m*CPBA, the polymers degraded to < 4 kD (M_n) (Scheme 17). The same unfortunate phenomenon occurred when trying

to use an alternate peroxyacid magnesium monoperoxyphthalate (MMPP). Previously reported work from the Schipper lab and other reactions performed in this work have shown that small molecule bithiazole derivatives do not degrade when subjected to these oxidation conditions (Scheme 17). While the oxidation yields are often below 30%, both the mono and di-*N*-oxide materials have been synthesized and characterized. In determining if the materials were acid-sensitive, polymers synthesized through dehydration conditions containing two *N*-oxide moieties per repeating unit were subjected to trifluoroacetic acid (TFA) and no degradation was observed. This leads us to believe that the polymers themselves are robust with respect to acidic conditions, however, the reaction conditions are causing degradation of the polymer species.



Scheme 17: Oxidations of thiazole-containing small molecules proceed without degradation of the starting material. Attempted oxidations of the various polymers all resulted in degradation of the polymers to an M_n below 4 kD.

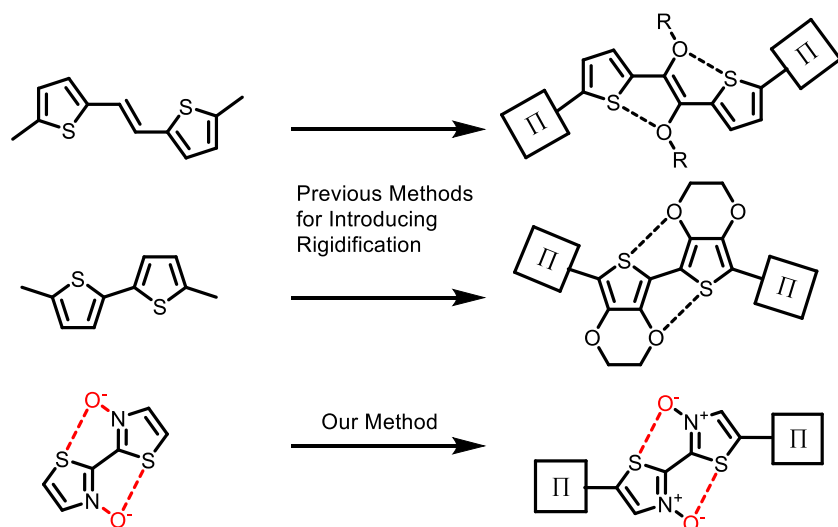
Naturally, the next step was to attempt the oxidation of the polymers under non-acidic conditions. Urea hydrogen peroxide (UHP) as well as catalytic methyltrioxorhenium (MTO)⁴⁹ with hydrogen peroxide have been shown to oxidize sp^2 nitrogens to the respective *N*-oxides in the literature, however, while the polymers no longer degraded under these conditions, both of

these methods also failed to oxidize the thiazole-containing polymers. At this time, we are unsure as to why this is and this may take further research in order to solve this issue.

2.3 Properties of Thiazole-*N*-Oxide-Containing Materials

2.3.1 Optical Electronic Effects on Small Molecules

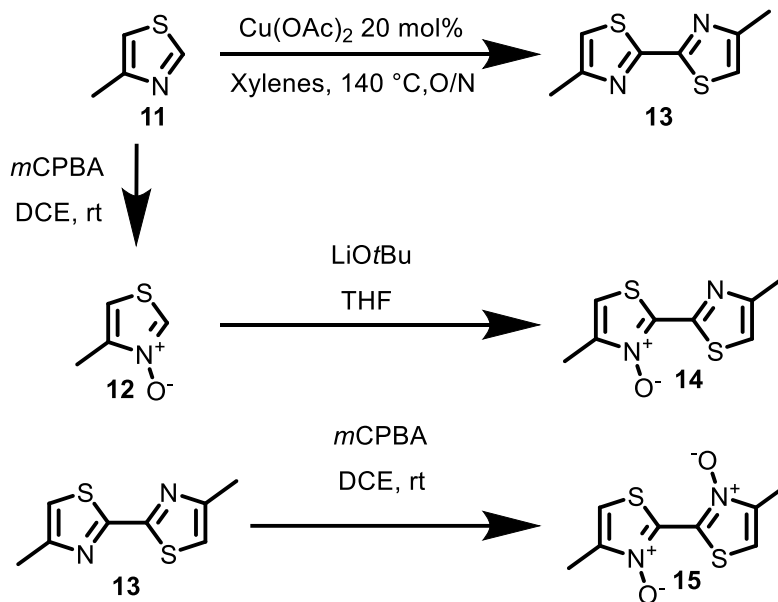
After failing to oxidize the thiazole-containing conjugated polymers post-polymerization, a new approach for testing the effect of *N*-oxide moieties in these systems was devised. As opposed to oxidizing post-polymerization, monomers with *N*-oxide moieties were to be synthesized and used accordingly to produce polymers with varying degrees of oxidation (Scheme 18). While this method does not have the same appeal as post polymerization alterations, it would still provide insight into the optical electronic effects of the successive thiazole oxidations.



Scheme 18: Conceptual scheme of utilizing non-covalent interactions for rigidification of conjugated systems.

While the ultimate goal of this project was to observe the effect of oxidation on thiazole-containing conjugated polymers, it was determined that the effect should be tested on small molecules prior to constructing the polymers. To begin our preliminary investigations, we envisioned synthesizing several thiazole-containing small molecules with various levels of oxidation, these being bithiazole derivatives containing 0, 1 and 2 *N*-oxide moieties. Oxidative coupling of 4-methylthiazole with catalytic Cu(OAc)₂ in xylenes under reflux for 14 h produced the non-oxidized bithiazole product: 4-4'-dimethyl-2,2'-bithiazole (**13**) in 85% yield (Scheme 19).⁵⁰

Next, to produce the singly oxidized bithiazole product, 4-methylthiazole was oxidized with *m*CPBA to the corresponding *N*-oxide and was subsequently subjected *N*-oxide dehydration conditions to afford product (**14**) (Scheme 19). While the methyl group in the 4 position is not ideal, as it causes steric hindrance in an extended chain and therefore a deviation from planarity, it is known from previous work in the Schipper group that an alkyl group is needed in the 4-position to facilitate the *N*-oxidation and is therefore required in this model. This is likely to cause an increase in the HOMO-LUMO gap of the system, which may not be desirable for some applications.



Scheme 19: Synthesis of bithiazole small molecules.

The bithiazole product (**13**) was subjected to oxidation conditions to afford the di-*N*-oxide product (**15**) to complete the series of bithiazole small molecules. To observe the effects of these subsequent oxidations on the thiazole units, UV-Vis spectra of all products (**13-15**), as well as 4-methylthiazole (**11**) and 4-methylthiazole *N*-oxide (**12**) were obtained (Figures 15-16).

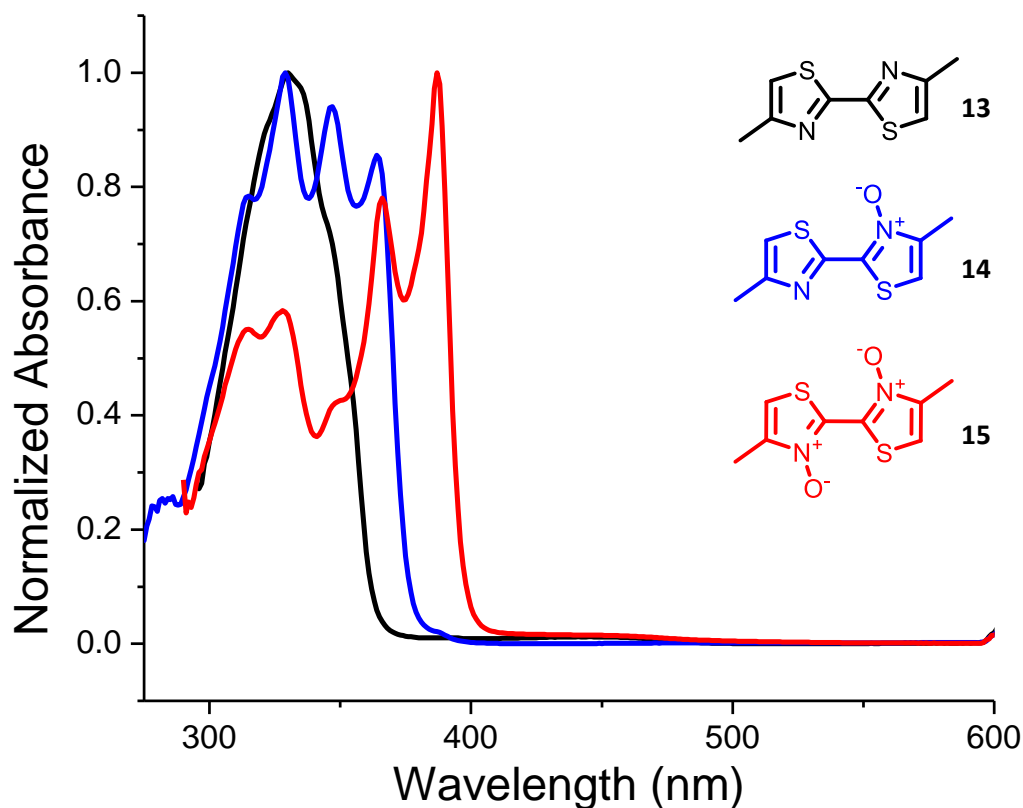


Figure 15: UV-Vis spectra of the 4-4'-dimethyl-2,2'-bithiazole compounds (**13**, **14** and **15**).

From the UV-Vis spectra of bithiazole compounds **13-15** we can see a significant bathochromic (or red) shift in the absorbance that correlates to the increasing oxidation. This redshift corresponds to a decrease of the optical HOMO-LUMO gap, as the oxidized molecules are absorbing radiation of lower energy. A redshift was also observed upon oxidation in the UV-Vis spectra of 4-methylthiazole (**11**) and the corresponding N-oxide (**12**) (Figure 16), which has no ability to stabilize through a non-covalent interaction. It was thus impossible to determine whether the shift was purely due to the oxidation, rigidification or a combination of both without additional data.

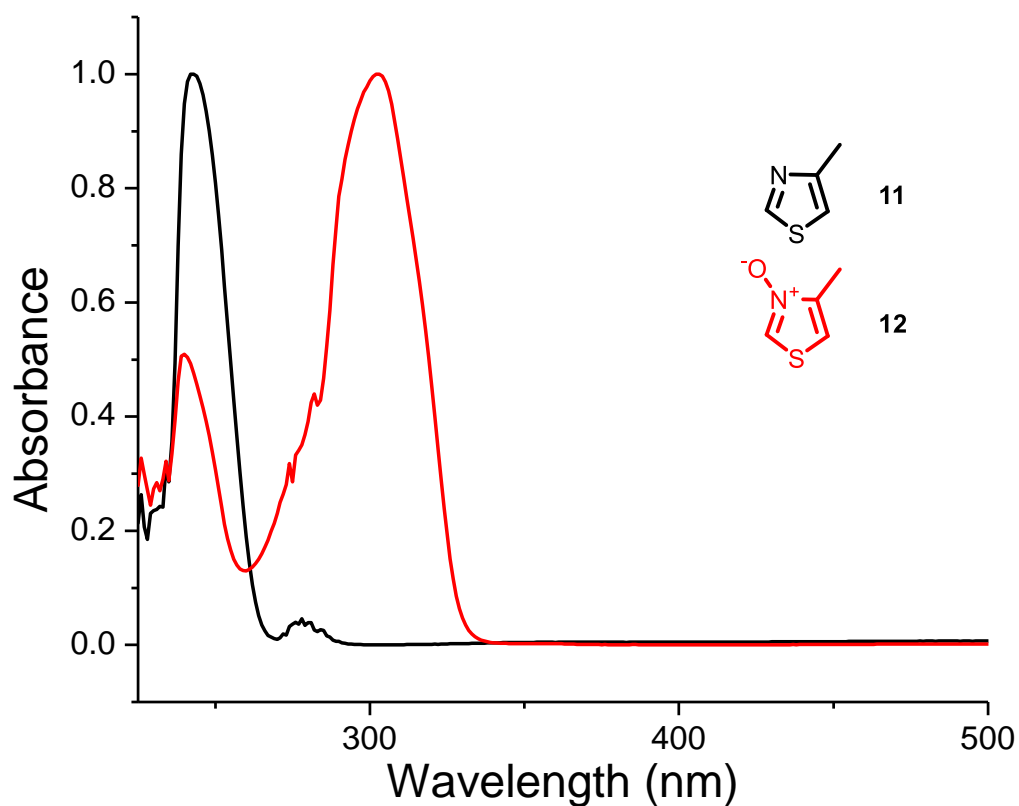
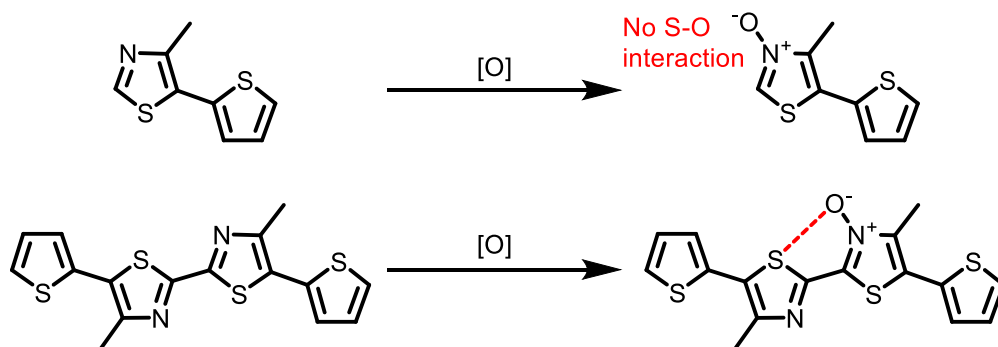


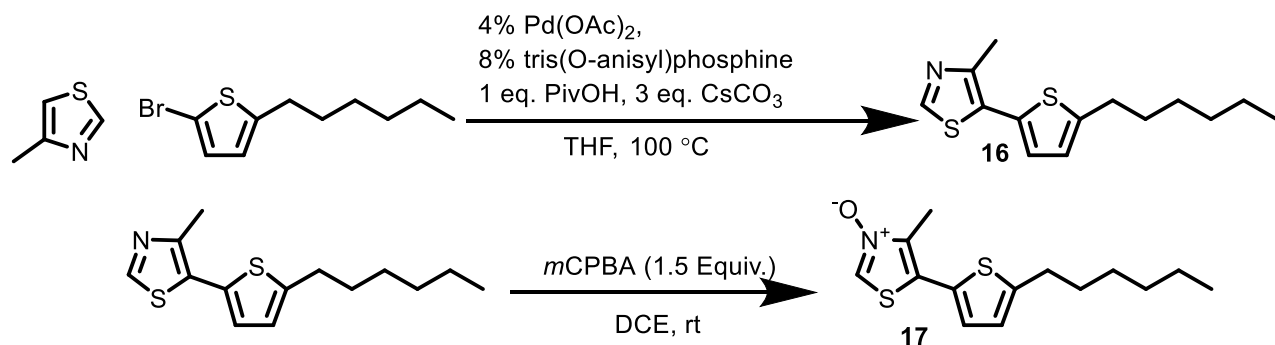
Figure 16: UV-Vis spectra of 4-methylthiazole (**3a**) and 4-methylthiazole-*N*-oxide (**12**).

To determine the cause of the reduction in band gap, a system that is unable to participate in S-O bonding was required (Scheme 20). Looking at the optical changes in



Scheme 20: The difference in systems where there can be no S-O interactions upon oxidation (top) versus a system that contains at least one S-O interaction (bottom).

the oxidation of such a molecule in comparison to that of a bithiazole system, where there are S-O interactions, would show if this interaction has a large effect on the optical properties, or if it is in fact just an electronic effect from the oxidation itself. To study this hypothesis, 5-(5-hexylthieno)-4-methylthiazole (**15**) and the corresponding *N*-oxide (**17**) were synthesized by direct arylation of 4-methylthiazole and bromothiophene (Scheme 21). The UV-Vis spectra (Figure 17) of these compounds (**16** and **17**) appeared to be largely the same, with the exception of a small change in the onset wavelength. Since compound **17** is unable to undergo chalcogen bonding, this evidence indicates that the oxidation itself does not have a major effect on the HOMO-LUMO gap. This seems contradictory to the data obtained from Figure 16, where oxidation of **11** to **12** resulted in a dramatic redshift in the UV-vis spectrum. This is most likely due to the fact that in the small thiazole system (**12**) the *N*-oxide moiety dominates the HOMO/LUMO energies, whereas in the thienylthiophene systems (**16**, **17**), the addition of 5-hexylthiophene drastically changes the electronics of the system and results in a greatly reduced influence from the *N*-oxide. This indicates that it is rather likely that there is a planarization caused by a non-covalent S-O interaction that is causing the decrease in the HOMO-LUMO gap.



Scheme 21: Synthesis of 5-(5-hexylthieno)-4-methylthiazole (**16**) and corresponding *N*-oxide (**17**).

To further support that the redshift observed with the increasing oxidation of the bithiazole systems (**13-15**, Figure 15) is due to a planarization effect, a very apparent introduction of fine structure in the UV-Vis spectra (Figure 15) of the oxidized systems is also visible. This is a characteristic feature of planar systems, as there are fewer rotational transitions when a molecule is rigid, resulting in more defined, sharper peaks that correspond to the vibrational transitions that underlie the overall electronic transition.⁵¹

This fine structure is clearly not observed in the UV-Vis spectra for compounds **11** and **12** (Figure 16), as well as **16** and **17** (Figure 17), where there are no non-covalent interactions available to planarize the system. There do appear to be some irregularities < 300 nm, but these are artifacts rather than well-defined vibrational transitions. This once again provides evidence that it is in fact non-covalent rigidification of the bithiazole system and not an electronic effect of the added oxygen that is causing the changes in optical properties.

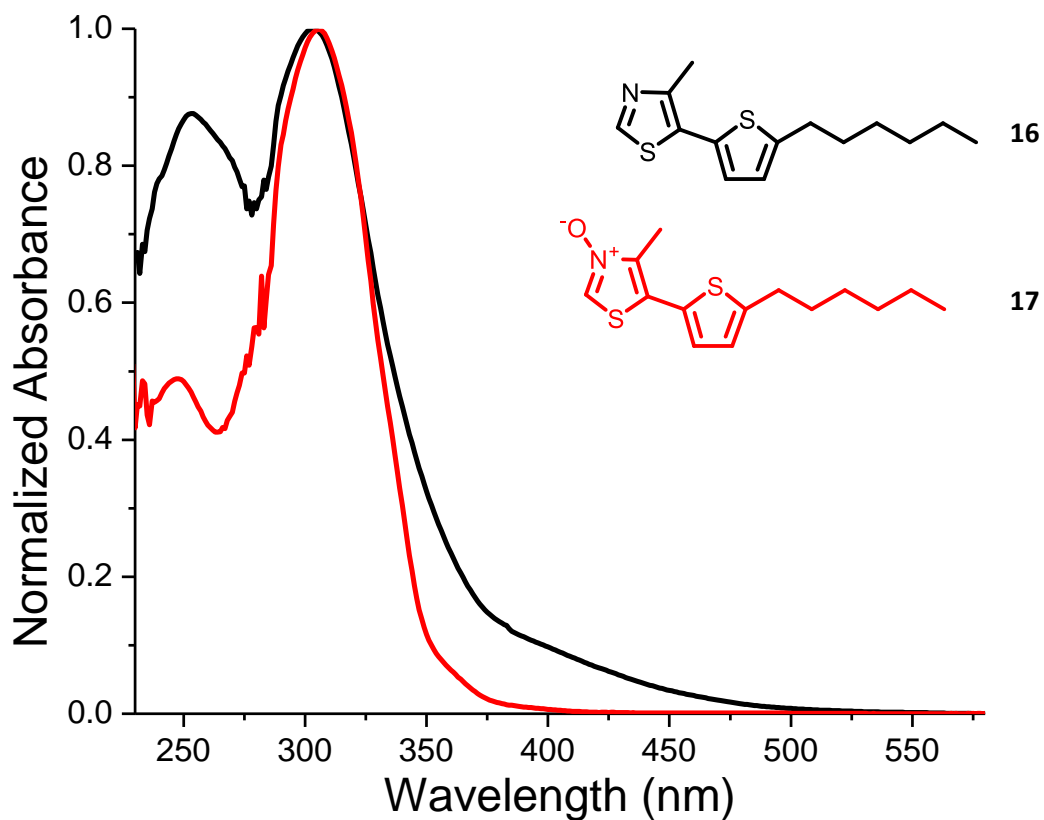


Figure 17: UV-Vis spectra of the two 5-(5-hexylthiényl)-4-methylthiazole-*N*-oxide compounds.

2.3.2 Computational Studies

To further expand our understanding of the S-O non-covalent interaction, computational studies using Gaussian 09 were performed on 2,2'-bithiazole (**18**) and respective mono (**19**) and di-*N*-oxides (**20**) (Figure 18). The first study was to probe the rotational barrier about the N-C-C-N dihedral angle to observe the difference in energy holding the ring systems in a planar conformation. This was performed by first optimizing the geometry (Figure 19) and then

calculating the single point energies of each system with CCSD(T) (coupled cluster) theory while locked in conformations from 90-180°, in 10° increments.

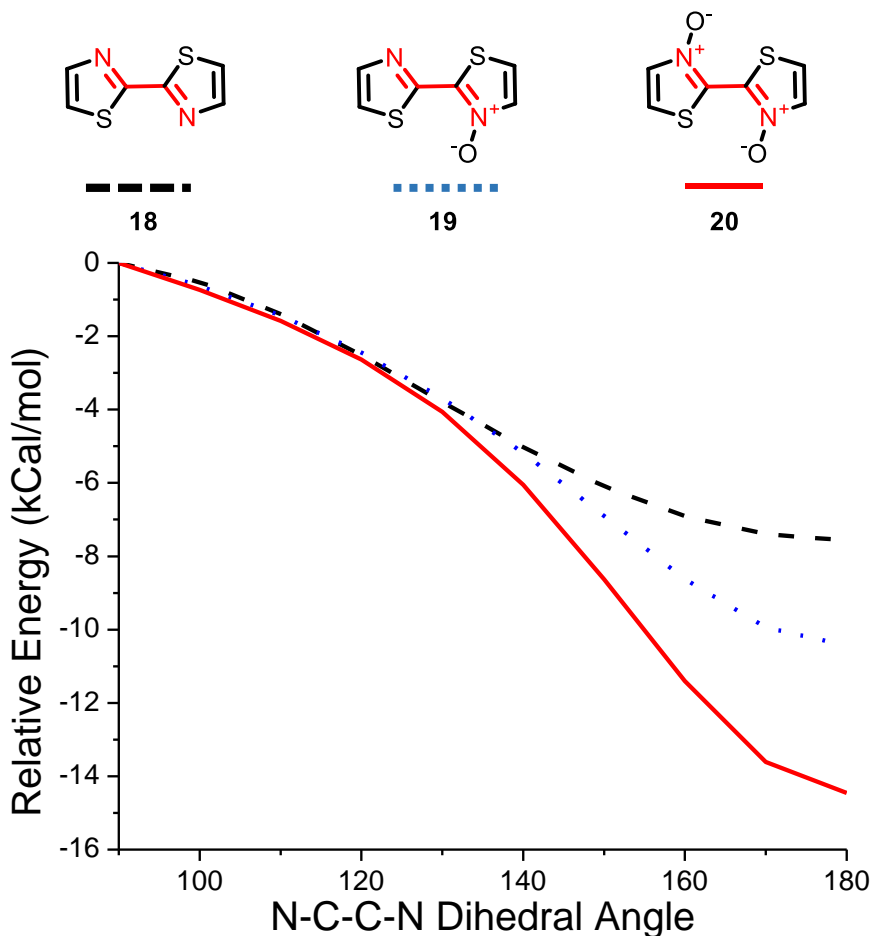


Figure 18: Single point energies of bithiazole and bithiazole-*N*-Oxides for conformations from 90-180° (N-C-C-N bond) in 10° intervals. Shows the rotational barrier, about the N-C-C-N dihedral angle, of each compound. Structures were optimized using DFT level of theory and the single point energies were calculated using CCSD(T) 6-311++g(d,p) level of theory using Gaussian 09.

As expected, with increasing oxidation a greater amount of energy is required to twist the molecule out of planarity. It can be seen in Figure 18 that when one *N*-oxide bond is incorporated, the rotational barrier about that dihedral angle (from 180°-90°) increases from 7.5 kcal/mol to 10.5 kcal/mol. Likewise, when the bithiazole molecule contains two *N*-oxide moieties (2,2'-bithiazole-3,3'-dioxide) as opposed to only 1 (2,2'-bithiazole-3-oxide) there is an increase in

the rotational barrier of 4 kcal/mol over the mono-*N*-oxide example (from 10.5 kcal/mol to 14.5 kcal/mol). It was expected that addition of the *N*-oxide groups would increase steric hindrance when the thiazole-thiazole bond was subjected to rotation. However, the calculations do not show as dramatic as an increase in slope that would be expected from a large steric repulsion. This clearly shows a greater propensity for the more oxidized systems to be in a planar conformation due to the addition of intramolecular S-O interactions.

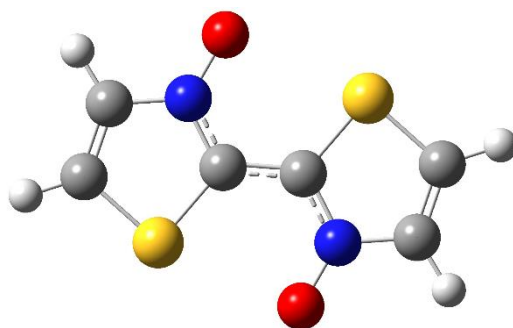


Figure 19: Optimized geometry of 2,2'-bithiazole-*N,N'*-dioxide from Gaussian DFT calculation.

There are many examples in literature of conjugated materials utilizing these intramolecular interactions as a tool for rigidification. As such, the rotational barrier of many of these materials has been reported through the use of computational calculations. These interactions have been used more frequently in thiophene-based conjugated systems. As such, S-O interactions in thienyl-vinylene systems (Figure 20:A) lead to an energy of 8.3 kcal/mol.⁵² This can be compared to 2,2'-bithiophene which has a rotational barrier of 5 kcal/mol (Figure 20:B).⁵³ When the molecules become more complex and steric hindrance becomes more of a factor (Figure 20:C), the rotational barrier can reach energies in excess of 20 kcal/mol.²⁴ Our di-*N*-oxide system has one of the largest rotational barriers seen in these types of material despite the lack of contribution from steric interactions.^{18, 19, 20, 24, 25, 52, 53}

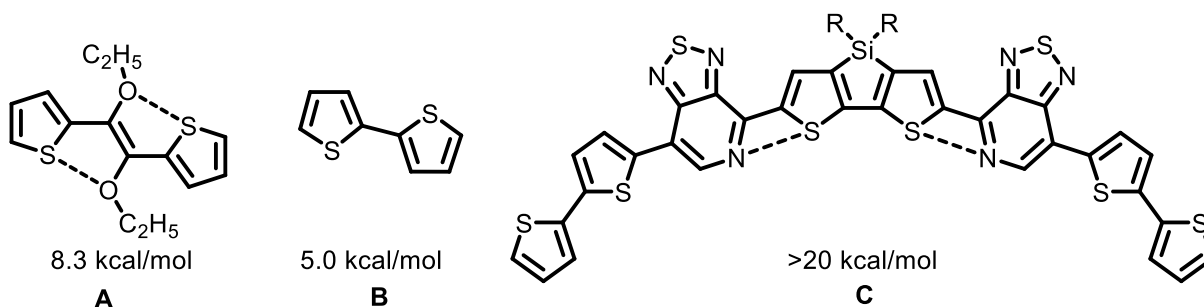


Figure 20: Rotation energy barriers of conjugated materials in literature.

To expand upon the calculations determining the bonding energy associated with the S-O interactions, an additional computational study was performed that would hopefully give additional insight into the S-O bonding. In this study the natural bond orbital (NBO) function was used in conjunction with a DFT B3LYP 6-311g (d,p)++ optimization calculation in order to determine the interaction between the sulfur in the thiazole rings with the adjacent *N*-oxide oxygen atom (Figure 18). In addition to the S-O interaction, an NBO calculation was also performed on non-oxidized bithiazole, which showed no prior interaction between the nitrogen lone pairs to the sulfur atom of the opposite thiazole ring. In the study of the theoretical orbital interactions of the *N*-oxide compounds, it was found that the mono-*N*-oxide (**19**) has 4.20 kcal/mol of stabilization energy resulting from the S-O interaction (Figure 21). In the di-*N*-oxide species (**20**), it was found that there was an average of 4.67 kcal/mol per S-O interaction. This increase in stabilization energy can possibly be explained by the fact that as an oxygen atom is added, electron density is pulled away from the sulfur, effectively making it more electrophilic so it can interact more strongly with the negatively charged oxygen from the *N*-oxide moiety.

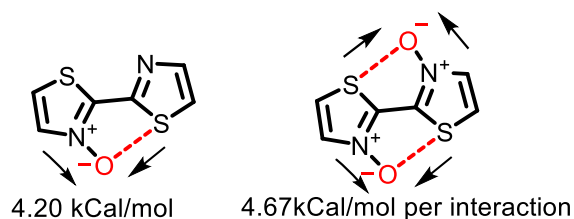


Figure 21. S-O interactions as determined through Gaussian NBO calculations.

In addition to the strength of the S-O interaction observed in the bithiazole systems, it was also possible to determine the distance between the oxygen and sulfur atoms from the DFT optimized structures. The S-O distance determined by these calculations in the mono-*N*-Oxide (**19**) is 2.76 Å, which is in good agreement with the bond length of 2.74 Å determined by single X-ray crystallography (4,4',5,5'-tetramethyl-2,2'-bithiazole), which ultimately adds validity to the calculations performed (Figure 22). The S-O distances in the di-*N*-oxide (**20**) were both determined to be 2.74 Å, lower than that of the single *N*-oxide compound. Considering that the sum of the van der Waals radii for these atoms (S + O) is 3.25 Å, we can conclude that there is a significant interaction between the sulfur and oxygen atoms of these oxidized bithiazole systems.

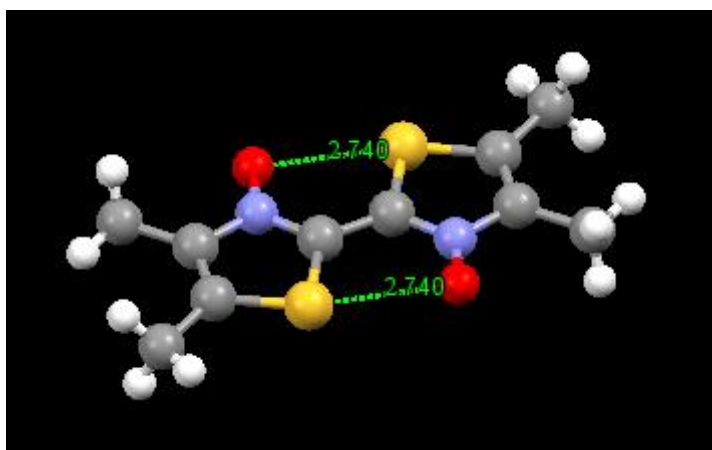
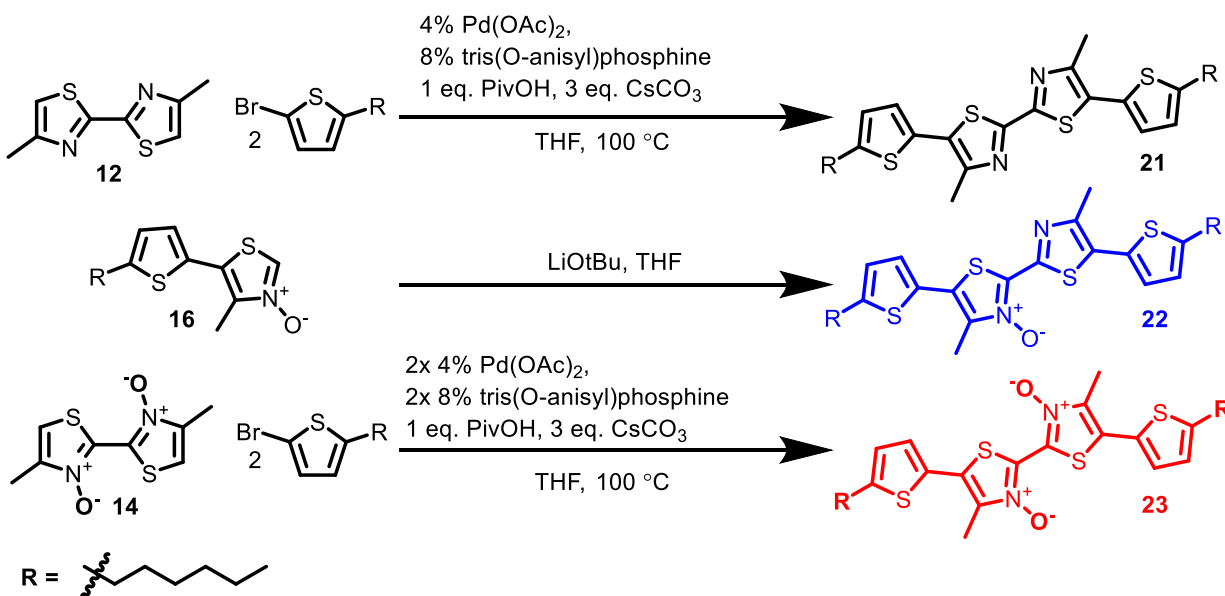


Figure 22. Molecular geometry obtained for 4,4',5,5'-tetramethyl-2,2'-bithiazole-3,3'-bis(olate) through single crystal X-ray crystallography.

2.3.3 Longer Chain Small Molecules

While the results determined in the computational experiments were encouraging, the system being tested was quite small so additional molecules with extended conjugation were needed to determine if the trend would hold at larger conjugation lengths. To test this, the 4-4'-dimethyl-2,2'-bithiazole derivatives were capped on each side with 5-hexylthiophene units (Scheme 22). Compound **21**, containing no oxidized thiazole rings, and di-*N*-oxide **23** were prepared through general direct arylation conditions with 5-bromo-2-hexylthiophene and bithiazoles **13** and **15**, respectively. The mono-*N*-oxide compound **22** was prepared through dehydration of the previously synthesized *N*-oxide compound **17**.



Scheme 22: Synthesis of the 5,5'-(5-hexylthienyl)-4-4'-dimethyl-2,2'-bithiazole compounds.

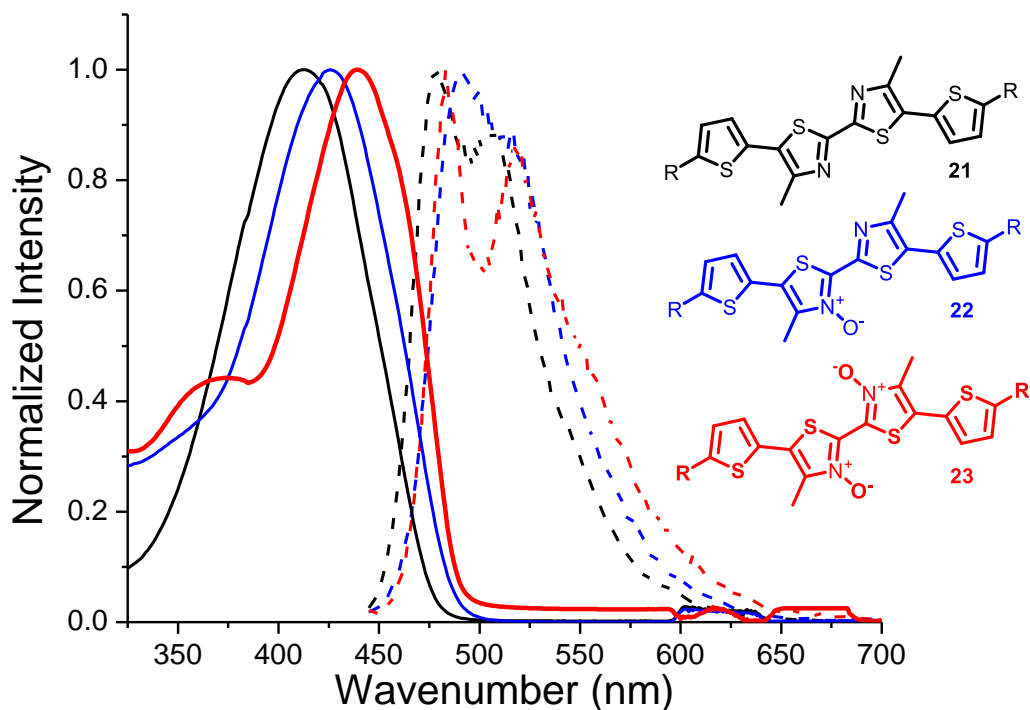


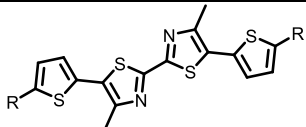

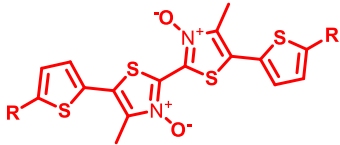
Figure 23: UV-vis (solid) and fluorescence (dash) spectra for the 5,5'-(5-hexylthienyl)-4-4'-dimethyl-2,2'-bithiazole compounds.

When analyzing the UV-Vis spectra of the three extended small molecules (Figure 23), once again a redshift associated with increasing oxidation is apparent although not quite as dramatic as observed in the bithiazoles **13-15**. This can be attributed to the fact that the rigidification of the system due to the S-O interactions is not as drastic as in the small bithiazole compounds. Nevertheless, there is still a clear trend of decreasing HOMO-LUMO gap with increasing oxidation.

Another useful handle for determining planarity in a conjugated system is to explore the changes in the Stokes shift. The Stokes shift is the difference in the maxima of the absorbance and emission spectra. A decrease in Stokes shift of a conjugated system is characteristic of a

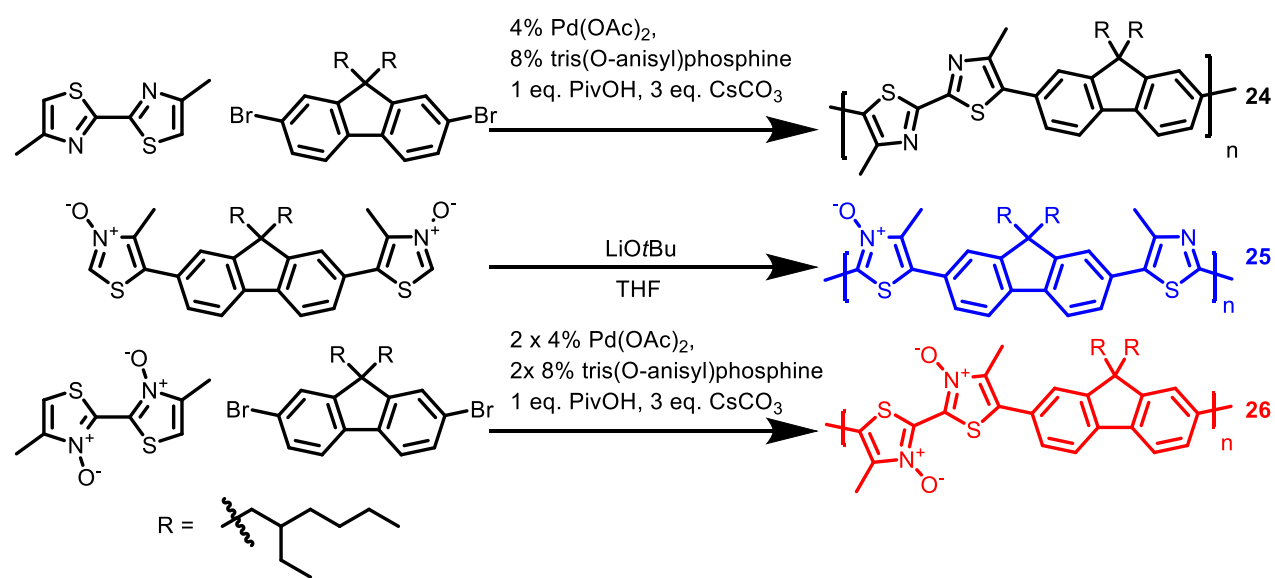
planarization effect, as there are fewer vibrational transitions that take place before the excited electron returns to the ground state.⁵⁴ For these compounds that were capped with hexylthiophene units the fluorescence spectra were also obtained. Also interesting to note, is that the Stokes shift also decreases with increasing oxidation from 67 nm (**21**), to 65 nm for (**22**) and finally to 44 nm for the di-*N*-oxide (**23**). This is additional evidence that points to a planarization of the system with increasing oxidation.

Table 2: Stokes shift of small molecules with extended conjugation.

Compound	Structure	Stokes Shift (nm)
21		67
22		65
23		44

2.3.4 Thiazole-Containing Conjugated Polymers

The next step of the project was to transition from conjugated small molecules to conjugated polymers in order to determine if the same trend is observed with successive oxidations. The first series of polymers that were envisioned would contain the bithiazole derivatives with a fluorene spacer and possessing two 2-ethylhexyl solubilizing chains (Scheme 23).



Scheme 23: Synthesis of the fluorene polymer series.

Polymer (**24**) was prepared through a direct arylation polymerization to afford the non-oxidized example of the series. The mono-*N*-oxide polymer of this series (**25**) was once again formed through dehydration of the di-*N*-oxide monomer and once again the di-*N*-oxide polymer (**26**) in the series was formed through direct arylation conditions of the di-*N*-oxide and dibromofluorene monomers. In addition to this series, a series of polymers (**27-29**) were also synthesized that contained 3,4-dihexylthiophene as the conjugated spacer since thiophene derivatives have shown good performance and are widely used in the area of organic electronic

materials (Figure 24). This series was prepared in the same fashion as the fluorene-containing polymer series.

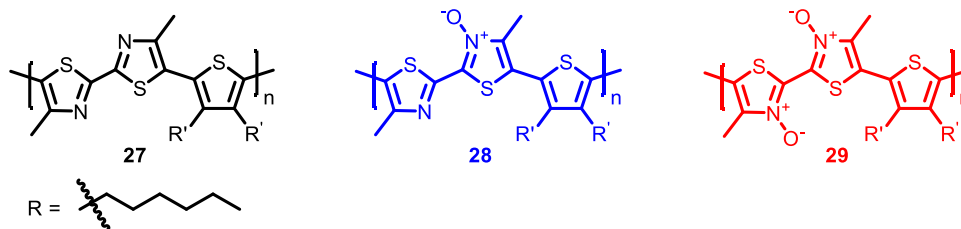


Figure 24: Thiophene series of thiazole containing polymers.

These polymers were all synthesized with respectable molecular weights in terms of conjugated materials. However, the di-N-oxide polymer (**29**) suffered from a low molecular weight of approximately 6 kD which can be attributed to the low solubility of the polymer. As the polymer reached ~ 6 kD it would start to precipitate out of the reaction mixture. Once again these values are calculated using a polystyrene standard and are overestimated due to the rigid structure of these polymers. The polydispersity index (PDI) of the samples was fairly good, ranging from 2.1 to 2.7 (Table 3). Obviously, having a low PDI is important, as high PDI values can result in less desirable optical and electronic properties. Large PDI values can result in processing difficulties and/or undesirable film morphology effects.² Conjugated polymers synthesized through direct arylation conditions tend to have PDI values above 2 but can range from $\sim 1.5 - 10+$ depending upon the monomers and conditions used. This means the values obtained from our polymers synthesized in the same manner are quite respectable.⁴⁰

In comparing the degree of polymerization (X_n) of the polymers presented here to previous fluorene and thiazole containing polymers made for organic electronic applications (synthesized through any method), the results are varied. **25** and **27** have quite high values of

62.0 and 46.1 respectively, whereas **24**, **26** and **28** fall into a more average range with X_n values of 31.3, 22.8 and 36.7 respectively. Finally, due to the highly polar nature of **29**, the degree of polymerization for this polymer was substantially lower at 12.7, though still comparable to many conjugated polymers seen in electronic applications.⁴⁰ Due to the overestimated molecular weight, the calculated X_n is also inflated and is therefore not an absolute value. However, these values still provide some evidence that the polymers are composed of a significant number of monomers.

Table 3: Molecular weights of the fluorene and thiophene polymer series.

Compound	M_n (kD)	PDI	X_n
24	18.2	2.3	31.3
25	37.1	2.2	62.0
26	14.0	2.3	22.8
27	20.6	2.2	46.1
28	17.0	2.7	36.7
290	6.1	2.1	12.7

UV-Vis and fluorescence data were collected for each of the fluorene-linker polymers (**24-26**) (Figure 25) and thiophene-linked polymers (**27-29**) (Figure 26). Once again, both polymer series display a definitive redshift in the UV-Vis corresponding to a reduction of the band gap. In addition, in the fluorene polymer series there is a clear trend in the Stokes shifts (Table 4), showing a decrease with increasing oxidation of the system. This indicates that the bithiazole system is in fact remaining planar in the polymer system as well. In the thiophene series, however, there appears to be a break in the trend where the Stokes shift of the mono-*N*-oxide polymer (**28**) is in fact larger than that of the non-oxidized polymer (**27**). Despite this discontinuity, the di-*N*-oxide polymer in the series does show a significant lowering of the Stokes shift from both the non- and mono-*N*-oxide polymers.

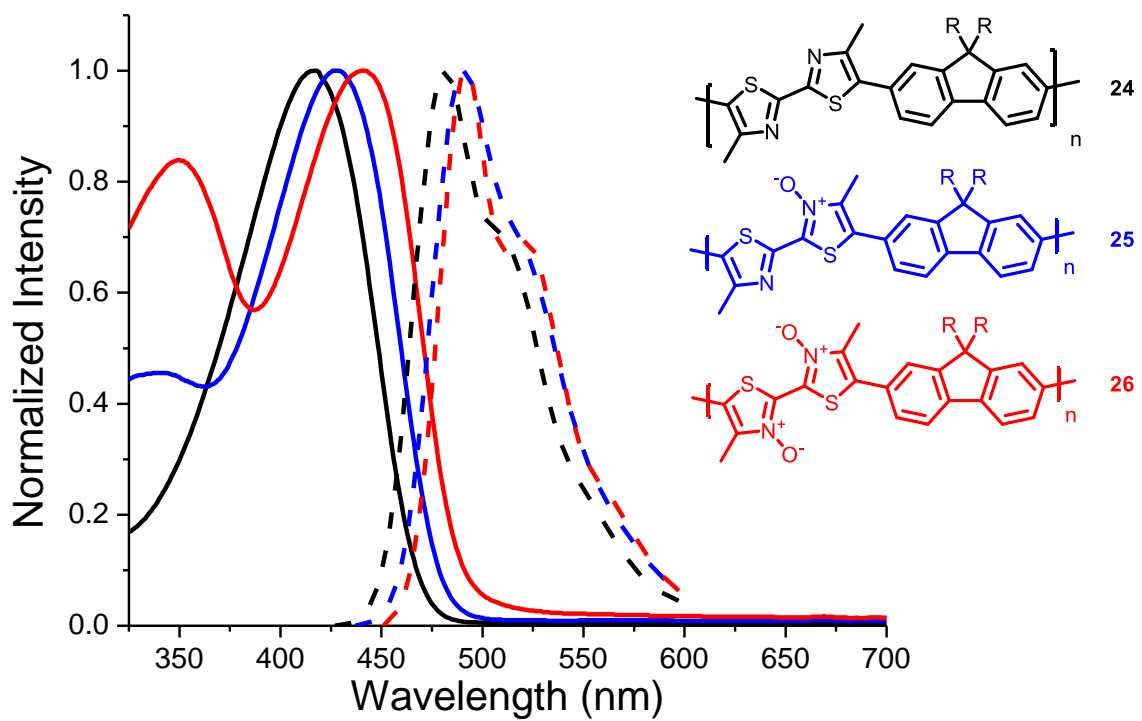


Figure 25: UV-Vis (solid) and fluorescence (dash) spectra of the fluorene polymer series.

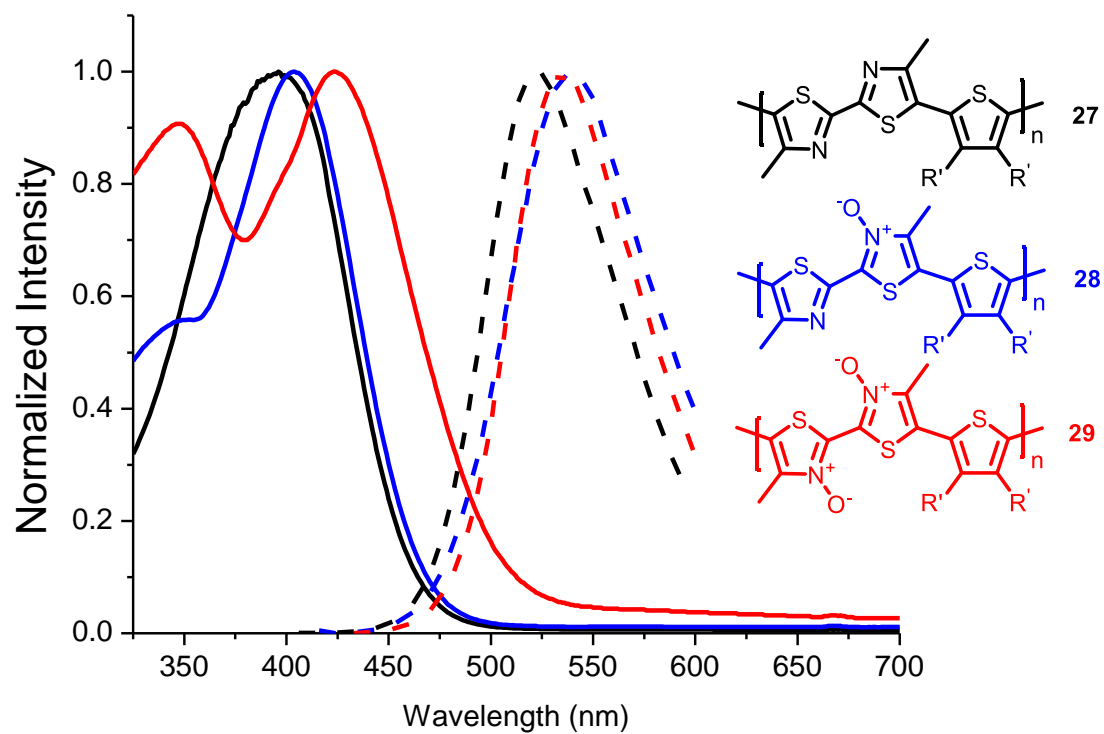
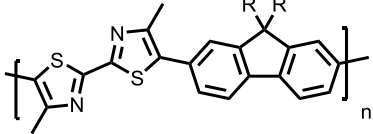
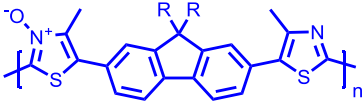
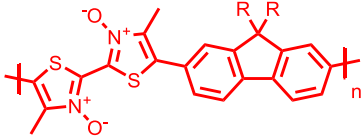
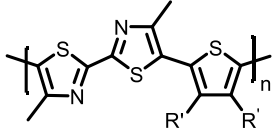
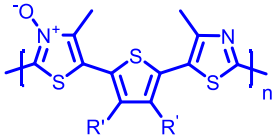
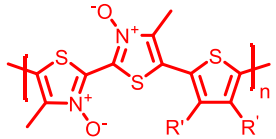


Figure 26: UV-Vis (solid) and fluorescence (dash) spectra of the thiophene polymer series.

Table 4. Stokes shifts for the fluorene and thiophene polymer series.

Compound	Structure	Stokes Shift (nm)
24		65
25		63
26		50
27		127
28		136
29		110

In addition to obtaining an estimation of the HOMO-LUMO gaps from the UV-Vis absorbance spectra, an estimate through electrochemical means can also be obtained. This method is found to be in general more accurate as it does not generate strongly bound electron-hole pairs, which does occur when a molecule is excited with light.⁵⁵ As such, the next experiments that were performed were cyclic and linear sweep voltammetry. The setup used for these experiments consists of working, reference and counter electrodes made of platinum. The electrolyte and solvent used were tetrabutylammonium hexafluorophosphate and acetonitrile, respectively, and the samples were drop cast as thin films onto the working electrode. Unfortunately, it was observed that the electrical current would burn through the polymer thin film before a cycle could be completed. Therefore, in order to more clearly see the oxidation and reduction peaks of the conjugated polymers, linear sweep voltammetry was used, in which a new sample would be drop cast on the electrode prior to every sweep.

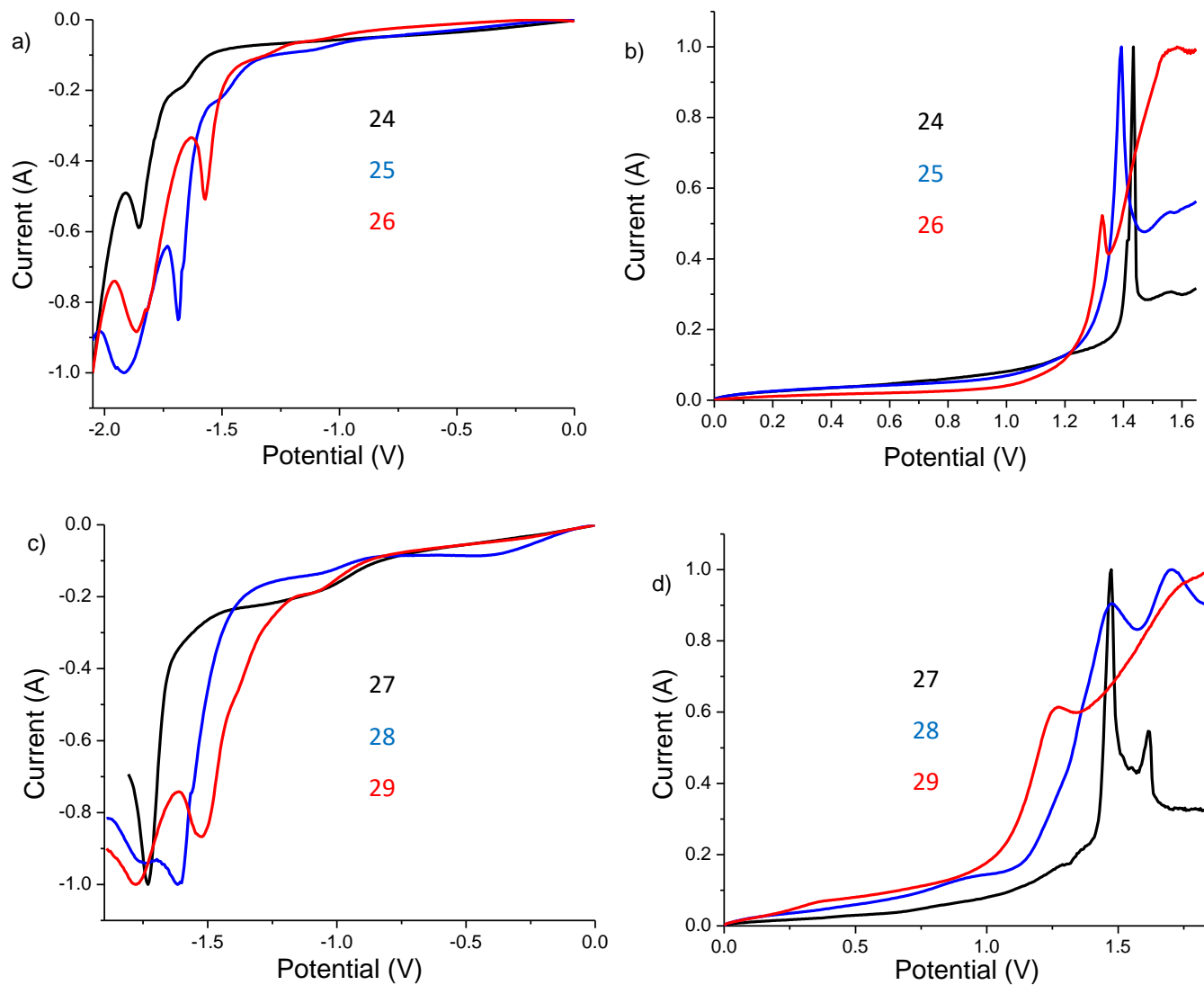


Figure 27: Linear sweep voltammograms of a) reduction (**24-26**) b) oxidation (**24-26**) and, c) reduction (**27-29**) d) oxidation (**27-29**).

Figure 27 shows the linear sweep voltammograms for both sets of polymers, **24-26** and **27-29**. For the fluorene series of polymers, as the potential is swept from negative to zero (Figure 27a, **24-26**), the reduction potential decreases with increasing oxidation. It can also be seen that sweeping from zero to positive potential (Figure 27b) also results in a decreasing of the oxidation potential with increasing oxidation in the fluorene polymer series. This trend of decreasing reduction and oxidation potentials with increasing oxidation is also observed for the thiophene polymer series (Figure 27c-d, **27-29**). While this is expected for the reduction potential, as when we oxidize the system to a greater extent, the system should become easier to reduce. It is, however, quite counterintuitive that as the polymers are oxidized they also become easier to electrochemically oxidize. The reason behind this effect is in fact quite simple. As the effective conjugation of the polymer is extended the polymeric cation becomes increasingly stabilized as it is delocalized to a greater extent throughout the system. This reduction in HOMO-LUMO gap due to an increase of the HOMO energy and decrease of the LUMO energy can be seen in other examples where the effective conjugation length is increased.⁵⁶

The fluorene polymer system saw a decrease in reduction potential from the non-oxidized (**24**) to mono (**25**) to di-*N*-oxide (**26**) of 0.06 and 0.04 eV respectively. This was combined with a decrease in the oxidation potentials being 0.06 and 0.09 eV respectively. These values led to calculated electrochemical HOMO-LUMO gap values of 2.95, 2.83 and 2.70 eV for (**24**), (**25**) and (**26**) respectively (Table 5, Entry 1-3). The thiophene series of polymers behaved very similarly, although there was a more drastic decrease in the oxidation and reduction potential between the non-oxidized (**27**) and mono- (**28**) and mono- and di-*N*-oxide polymers, with values of 0.10

eV and 0.25 eV respectively. This resulted in calculated electrochemical HOMO-LUMO gaps of 2.96, 2.61 and 2.51 for **(27)**, **(28)** and **(29)** respectively (Table 5, Entry 4-6).

Table 5: Optical and electronic data for both polymer series.

Entry	Compound	UV-Vis onset (nm)	$E_{g(op)}$ (eV)	HOMO (eV)	LUMO (eV)	$E_{g(ec)}$ (eV)
1	24	480	2.58	-5.75	-2.8	2.95
2	25	496	2.50	-5.69	-2.86	2.83
3	26	510	2.43	-5.65	-2.95	2.70
4	27	483	2.57	-5.67	-2.71	2.96
5	28	487	2.55	-5.57	-2.96	2.61
6	29	520	2.38	-5.53	-3.02	2.51

It has been shown that the band gap of these thiazole-containing polymers can be successfully tuned through the use of three successive levels of oxidation. In the fluorene series there was a range of 0.25 eV, from 2.95 to 2.70 eV (Figure 28). The thiophene series showed more promise in terms of the extent to which the band gap can be tuned, as the range of that system is 0.35 eV, from 2.96-2.51 eV (Figure 29). In addition to a greater degree of tuning seen in the thiophene series, the di-*N*-oxide polymer **(29)** also possesses a lower HOMO-LUMO gap than its fluorene polymer counterpart. Although these HOMO-LUMO gaps are fairly high, it is not the only factor that determines overall device performance. In spite of the optimum band gap for materials used in photovoltaic devices being ~1-1.5 eV with a broad absorbance spectrum, there are examples of materials possessing optical band gaps approaching or in excess of 2 eV that have competitive power conversion efficiencies of 8.0 % or greater.⁵² In spite of this, polymers **24-29** may have energy gaps that are too large to function as efficient photo-acceptors but could still potentially possess high electron or hole mobility due to the planar character of

the polymers. It has been shown that conjugated polymers with optical band gaps of 2.2 eV or greater can have high hole mobilities in excess of $0.1 \text{ (cm}^2 \text{ V}^{-1} \text{ s}^{-1}\text{)}$.³ The usefulness of these conjugated systems in organic electronics cannot be determined until they are tested in a functional device. Of the polymers synthesized **26**, **28** and **29** have the greatest probability of producing successful or positive results due to the HOMO-LUMO gaps as well as increased planarity.

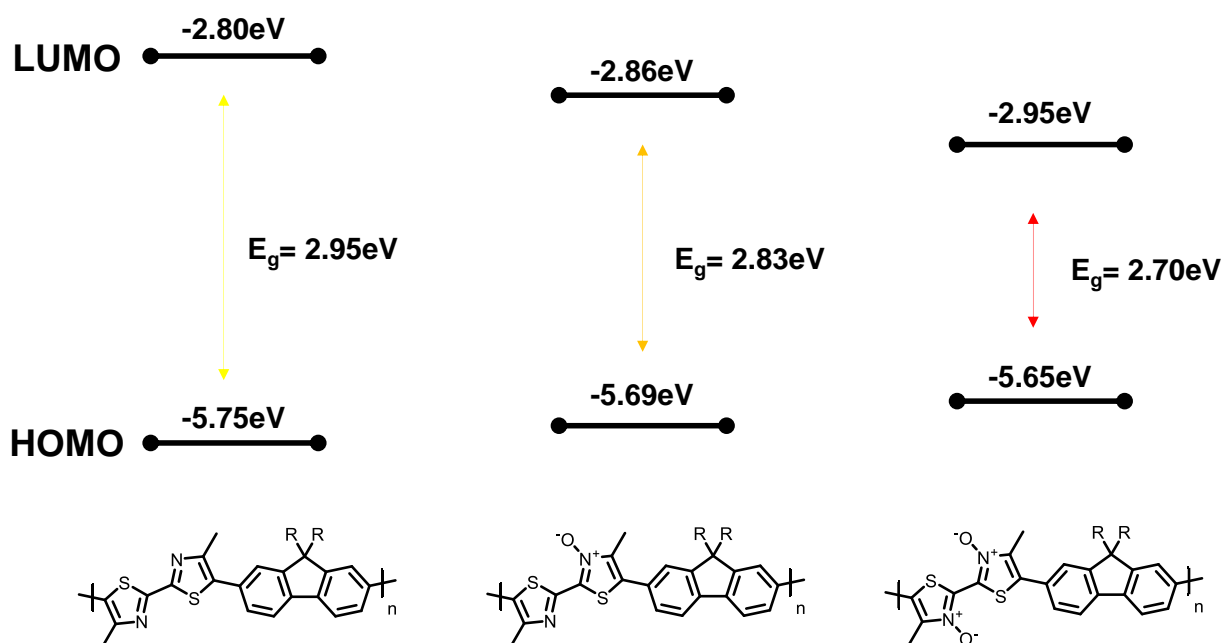


Figure 28: Frontier orbital energies and electrochemical HOMO-LUMO gaps of the fluorine series of polymers.

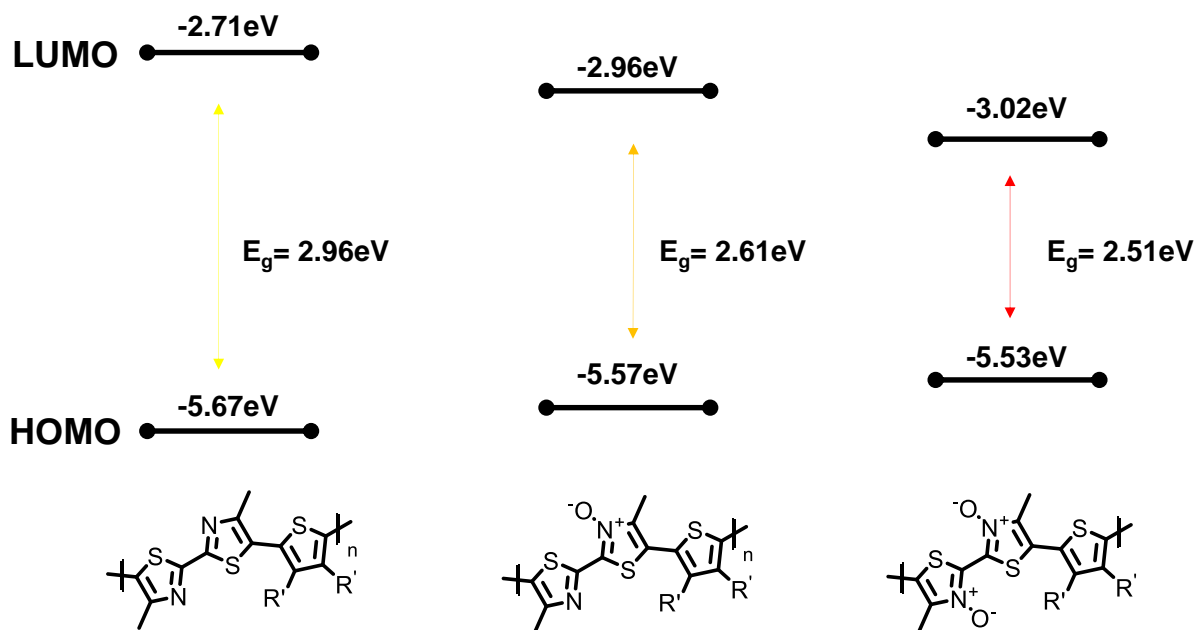


Figure 29: Frontier orbital energies and electrochemical HOMO-LUMO gaps of the thiophene series of polymers.

Due to the di-*N*-oxide polymers being fairly polar in nature, there was a question of whether there would be changes in the HOMO-LUMO gap with changes in solvent polarity. This phenomenon is known as solvatochromism and occurs due to the fact that the ground state and excited states of a molecule have different polarities. Therefore, if the polarity of the solvent is changed, it has the potential to stabilize the excited states differently than another solvent. This stabilization affects the energies of the frontier orbitals and therefore the HOMO-LUMO gap associated with them.

In the fluorene polymer system, there is no trend in the UV-Vis absorbance when compared to the polarity of the solvent. The absorption maxima were plotted against different methods for recording solvent polarity (dielectric constant, polarity index) and there was no clear

or even slight trend observed, although the absorbance maxima does change slightly while dissolved in different solvents. It is possible that solvatochromism may be observed in the fluorescence spectra, but those experiments still have to be performed in order to come to a conclusion.

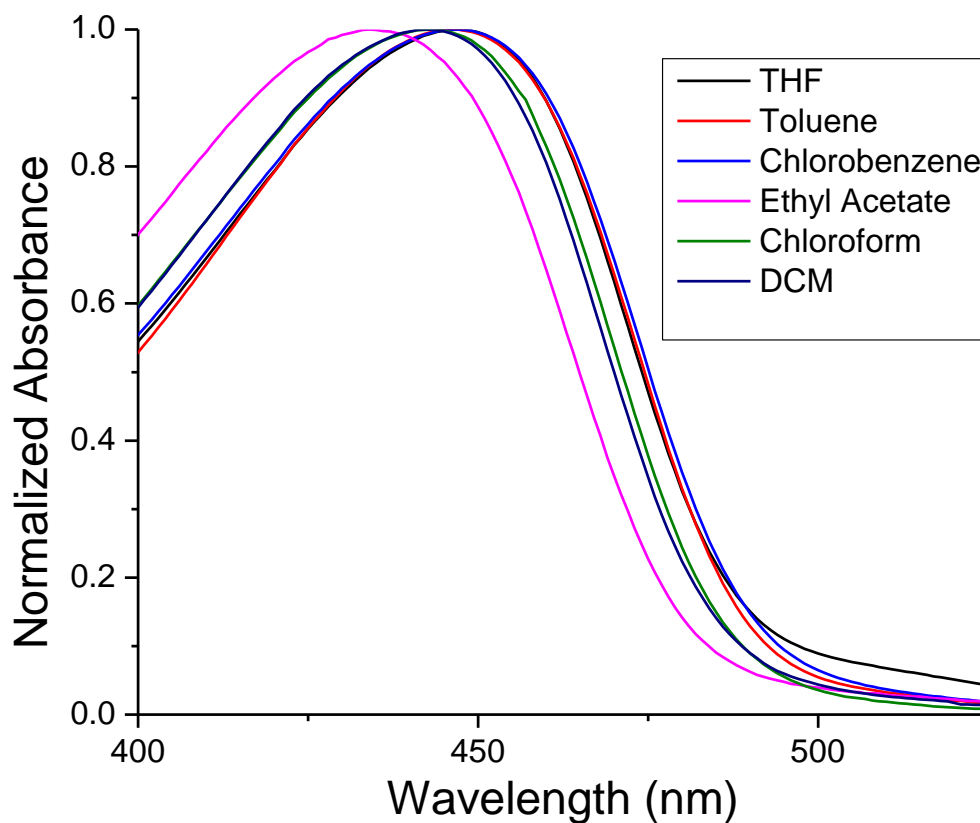


Figure 30: Solvatochromism study for the di-*N*-oxide fluorene series polymer.

Table 6. Solvent polarity.

Solvent	Dielectric Constant	λ_{\max} (nm)
THF	7.5	447
Toluene	2.4	446
Chloroform	4.4	443
DCM	9.0	442
Ethyl Acetate	6.0	434

2.4 Device Testing

Although the HOMO-LUMO gaps of the synthesized polymers were too large to be used in photovoltaic device applications, there is a very clear tuning effect seen in the HOMO-LUMO gap with increasing oxidation of the conjugated system. This effect was observed clearly in both the absorbance spectra and voltammetry measurements, and there is ample evidence showing that there is in fact a planarization effect due to the non-covalent S—O interactions. Naturally, we wanted to determine if a positive effect on device performance could be seen with increasing oxidation as well. Since the HOMO-LUMO gap of our polymers were not sufficient for any photovoltaic devices, they were tested as organic thin film transistors (OTFT's). Upon testing, the compounds were unfortunately found to have no activity in terms of charge mobility. This may be partially due to the lack of solubility of the polymers, such that they were not deposited very well as thin films on the devices. Purifying the polymers to a greater extent, with a palladium scavenger or additional Soxhlet extraction, as well as alternative deposition techniques (annealing, vapour deposition) could also have a positive effect on device performance.

Another possible method for inducing a lower HOMO-LUMO gap and better device performance is the elimination of the requisite methyl group in the 4 position of the thiazole.

This could cause a steric effect between the planar thiazole core and the adjacent conjugated spacer resulting in a twisted conformation about those bonds. Current members of the Schipper group are pursuing methods in order to make this possible.

Conclusions

Our first attempt at a controlled oxidation of thiazole-containing conjugated materials did not proceed as planned, as the polymers appeared to be acid-sensitive under the oxidation conditions and completely degraded upon addition of a peracid oxidizing agent. In order to still investigate the effects of thiazole oxidation on the conjugated materials, a new method for synthesizing small molecules and polymers through the use of *N*-oxide containing monomers was devised and executed. Through this method we were able to synthesize small molecules with 0, 1 and 2 *N*-oxide moieties per bithiazole unit (**13-15**). In the small molecule example, we determined that the redshift seen in the UV-Vis spectra, which we have hypothesized to correspond to a planarization of the system, occurs through establishing intramolecular non-covalent S—O interactions. The addition of the negatively charged oxygen itself appears to have a very minute effect on the electronics of the system which was quite unexpected. Further evidence for this theory of rigidification was observed when systems with no possible S—O interactions were possible (**16,17**). The absorption spectra were quite consistent for the thienylthiazole and corresponding *N*-oxide compound and unlike what was seen from **13-15**.

Proceeding to larger conjugated systems, such as the 5-alkylthiophene-capped bithiazole derivatives (**21-23**), the trend was still observed in the UV-Vis spectra and also seen in

voltammetry measurements. In addition to the redshift of the system, there was also a discernable decrease in the Stokes shift with increasing oxidation of these small molecules, once again providing evidence that this system is effectively being planarized. Finally, this idea of increasing the oxidation level of the system was applied to conjugated polymers to determine if the planarization effect would hold on polymers (**24-29**). Two polymer series containing the bithiazole motif were synthesized with quite respectable molecular weights (6-37 kD M_n) and dispersities (2.1-2.7). It was found that in both polymer series, the trend did in fact stay consistent with the results observed for small molecules. In both UV-Vis and voltammetry there was a clear redshift with increasing oxidation, corresponding to a decrease of the HOMO-LUMO gap. In the fluorene polymer series (**24-26**) it was seen that the Stokes shift trend agrees well with the small molecules, however in the thiophene polymer series (**27-29**) the trend is not as consistent, although the di-*N*-oxide polymer still has the lowest Stokes shift. It has been shown that the addition of *N*-oxides to bithiazole systems effectively rigidifies small molecules as well as polymers, and through this rigidification the ability to tune the HOMO-LUMO gap was obtained, from 2.95-2.70 eV in the fluorene polymer series and 2.96-2.51 eV in the thiophene polymer series. This method can be used as a model for non-covalent interaction in further conjugated material research, with the hope that these conjugated materials will ultimately show good performance in organic electronic devices.

In spite of the success in the tuning of the optical and electronic properties, the properties of these polymers synthesized in this project do not appear to be sufficient for use in devices such as in OTFT's. It was also observed that when there were no solubilizing chains on the spacing thiophene, the non-oxidized system had a fairly low HOMO-LUMO gap of 2.27eV, lower than the

lowest HOMO-LUMO gap polymer synthesized (**29**) being 2.50 eV. Since it has been proven that adding *N*-oxide moieties effectively rigidifies bithiazole-containing conjugated systems, one would assume that this would hold true if the solubilizing chains found on the spacer were absent, although this would provide a new challenge with reduced solubility and processability. This would allow for the development of a series of polymers with more ideal band gaps for use in organic electronic devices.

Supporting Information

Materials/Instrumentation

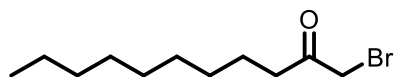
Unless otherwise specified all reactions were run without regard to exclusion of ambient air or moisture. All starting materials were purchased from Aldrich. ¹H NMR spectra were recorded in CDCl₃ solutions on a Bruker AVANCE 300 or 500 MHz spectrometer using deuterated chloroform as a reference. The chemical shift data is reported in units of δ (ppm) relative to residual solvent. UV-Vis data was collected on a Perkin Elmer Lambda 35 UV/VIS spectrometer. High resolution mass spectrometry (HRMS) was performed on a Thermo Q-Exactive, ESI. Fluorescence data was collected on a Horiba Jobin Yvon Fluorolog with a 400W xenon arc lamp. Cyclic voltammetry was performed on a Pine Wavenow. Number-average (M_n) and weight-average (M_w) molecular weights were determined by size exclusion chromatography using a Viscotek GPC MAX VE 2001 at 35 °C equipped with a VE 3580 RI detector and two PAS-104 Styrene-Divinylbenzene gel columns. The flow rate was fixed at 1.0 mL/min using tetrahydrofuran (THF) as the eluent. All GPC samples were prepared nominally at 2 mg/ml in THF and filtered through a 0.22 μ M PTFE filter into a 1 mL chromatography vial. Molecular weights and degree of polymerization values recovered

are relative to polystyrene standards. Compound **14** and **22** were received from Luke Vanderzwet and used without any chemical modification.

Computational Methods

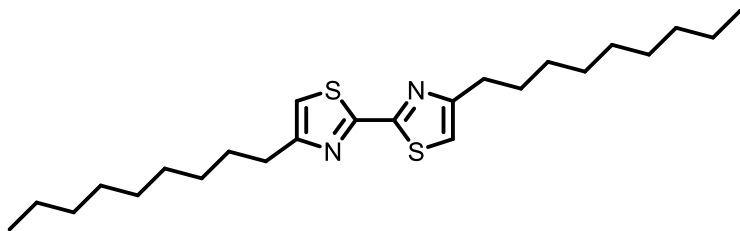
Geometry optimization and frequency calculations were performed using DFT B3LYP with a 6-311**g(d,p) basis set. The rotation barrier calculations were performed by calculating single point energies using a CCSD(t) level of theory and 6-311**g(d,p) basis set, and the rotational barrier was probed by holding the dihedral of interest at 10° intervals. NBO calculations were also performed using DFT B3LYP with a 6-311**g(d,p) basis set.

Preparation of 1-bromo-2-undecanone (**5**)



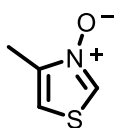
To a round bottom flask was added 2-undecanone (12.1 mL, 6 mmol, 1 equiv.) and methanol (50 mL). The flask was cooled to -10 °C, at which point liquid bromine (3.0 mL, 6 mmol, 1 equiv) was added drop-wise to the flask. After the addition, the reaction mixture was warmed to 0 °C and stirred in an ice bath for 1 hour, and then an additional 30 minutes at room temperature. At this point deionized water (10 mL) and sulphuric acid (17 mL) were added slowly to the reaction mixture on an ice bath at which point white crystals began precipitating out of solution. The mixture was stirred at room temperature for 14 hours. The white crystals were filtered with a Buchner funnel and recrystallized with a minimal amount of boiling methanol to yield **5** (8.95 g, 61%) and exhibited identical data to previously reported.⁵⁷ ¹H-NMR(CDCl₃): δ 3.88 (s, 2H), 2.64 (t, *J* = 7.4 Hz, 2H), 1.64-1.57 (m, 2H), 1.26(m, 12H), 0.88 (t, *J* = 6.9 Hz, 3H).

Preparation of 4,4'-dinonyl-2,2'-bithiazole (6)



A round bottom flask was charged with **1** (1.5 g, 6 mmol, 2.2 equiv) and ethanol (15 mL). Dithiooxamide (330 mg, 2.7 mmol, 1 equiv) was slowly added to the solution while on ice and then the reaction mixture was stirred at reflux for 14 h. After cooling to RT the reaction mixture was poured onto 100 mL of ice. This mixture was added to a separatory funnel and extracted with 3 x CH₂Cl₂ (100 mL). The organic layer was collected and dried with rotary evaporation. The material was dissolved in a minimal amount of ethyl acetate, to which silica gel was added. The solvent from the resultant slurry was then removed via reduced pressure. The product was then purified by flash chromatography (0 - 20% EtOAc in hexanes) to yield **6** as a yellow oil (905 mg, 79 %) and exhibited identical data to previously reported.⁵⁸ **¹H-NMR (CDCl₃):** δ 6.94 (s, 2H), 2.81-2.77 (t, 4H), 1.76-1.68 (m, 4H), 1.33-1.25 (m, 24H), 0.88 (t, 6H).

Preparation of 4-methylthiazole-3-oxide (12)

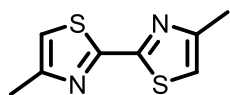


To a microwave vial was added **1** (250 mg, 2.5 mmol, 1 equiv) DCE (0.3 M, 8.3 mL) and stirred until fully dissolved. *m*CPBA (77% purity, 802 mg, 3.8 mmol, 1.5 eq.) was slowly added followed by the sealing of the reaction vessel. The reaction was stirred at room temperature for 3 h until *m*CPBA precipitates out of solution. Product was filtered, dried via vacuum and then dissolved in a minimal amount of methanol, to which silica gel was added. The solvent from the resultant slurry was then removed via reduced pressure. Through column chromatography (0 - 10% MeOH in EtOAc) product **12** was collected as a red/brown oil

(146 mg, 50 %). $^1\text{H-NMR}$ (CDCl_3): δ 8.20 (d, J = 3.1 Hz, 1H), 7.05 (d, J = 2.1 Hz, 1H), 2.38 (s, 3H).

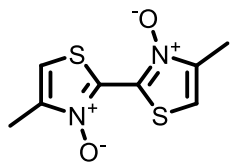
Characterization data was identical to previously reported literature.⁵⁹

Preparation of 4,4'-dimethyl-2,2'-bithiazole (13)



The preparation of bithiazoles followed the procedures reported by Li et al.⁴⁹ A round bottom flask containing xylenes (33 mL) was charged with $\text{Cu}(\text{OAc})_2$ (405 mg, 2 mmol, 0.2 equiv) and 4-methylthiazole (1) (0.92 mL, 10.1 mmol, 1 equiv). The reaction mixture was stirred at reflux (140 °C) for 14 h. The reaction mixture was cooled to room temperature, followed by the addition of silica gel (~2 g). The solvent from the resultant slurry was then removed via reduced pressure. Purification by column chromatography (0 – 20 % EtOAc in hexanes) yields product **13** as white crystals (660 mg, 67%) and exhibited identical data to previously reported.⁵⁰ $^1\text{H-NMR}$ (CDCl_3): δ 6.94 (s, 2H), 2.49 (s, 6H).

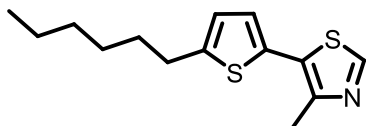
Preparation of 4,4'-dimethyl-(2,2'-bithiazole)-3,3'-dioxide (15)



To a microwave vial was added **13** (50 mg, 0.284 mmol, 1 equiv) with DCE (0.5 mL) and stirred until fully dissolved. *m*CPBA (77% purity, 162 mg, 0.937 mmol, 3 equiv) was slowly added, followed by the sealing of the reaction vessel. Reaction stirred until *m*CPBA and corresponding acid precipitate out of solution. Methanol (~0.2 mL) was added until reaction mixture becomes transparent. Second addition of *m*CPBA (77% purity, 162 mg, 0.937 mmol, 3 equiv) was performed and the reaction mixture is once again sealed and stirred until acid precipitates. Product was filtered, dried via vacuum and then dissolved in a minimal

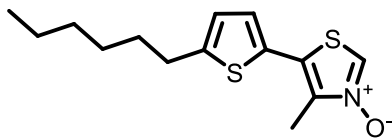
amount of ethyl acetate/methanol, to which silica gel was added. The solvent from the resultant slurry was then removed via reduced pressure. Purification performed by column chromatography (0 - 15% MeOH in EtOAc) to yield **15** as an orange solid (42 mg, 65%). **¹H-NMR (CDCl₃):** δ 7.15 (s, 2H), 2.46 (s, 6H). **¹³C NMR (CDCl₃):** δ 206.63, 143.94, 113.50, 11.96. **HRMS (ESI) m/z:** HRMS calculated for C₈H₉N₂O₂S₂ (M + H⁺): 229.0100 Found: 229.0101. rf = 0.36 (9:1 EtOAc:MeOH).

Preparation of 5-(hexylthiophen-2-yl)-4-methylthiazole (**16**)



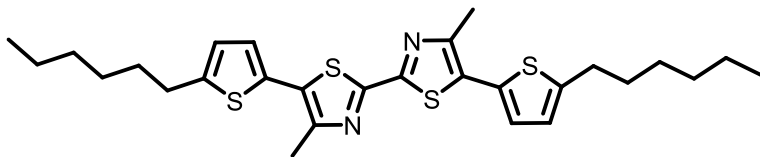
Reaction vessel charged with all solids: **11** (50 μL, 0.55 mmol, 1.1 equiv) , pivalic acid (52 mg, 0.5 mmol, 1 equiv) , Cs₂CO₃ (492 mg, 1.5 mmol, 3 equiv) , Pd(OAc)₂ (4.5 mg, 0.02 mmol, 0.04 equiv) and tris(*O*-methoxytriphenyl)phosphine (14 mg, 0.04 mmol, 0.08 equiv). The reaction vessel was purged with argon, followed by the addition of THF (1.8 mL) and then 5-bromo-2-hexylthiophene (101 μL, 0.5 mmol, 1 equiv). The reaction was stirred for 3 h at 90 °C. After 3 hours the reaction mixture was diluted with 15 mL of ethyl acetate and added to separatory funnel. The organic layer was washed with 3 x 15 mL deionized water and 1 x 15 mL brine. The organic layer was removed and dried with MgSO₄ and then reduced to ~5 mL using rotary evaporator, to which silica gel was added. The solvent from the resultant slurry was then removed via reduced pressure. Product purified by flash chromatography to yield **16** (70 mg, 53%). **¹H-NMR (CDCl₃):** δ 8.51 (s, 1H), 6.90 (d, *J* = 3.3 Hz, 1H), 6.69 (d, *J* = 2.9 Hz, 1H), 2.77 (t, *J* = 7.6 Hz, 2H), 2.56 (s, 3H), 1.75-1.56 (m, 2H), 1.44-1.20 (m, 6H), 0.86 (t, *J* = 6.3 Hz, 3H). Characterization data was identical to previously reported literature.⁴²

Preparation of 5-(5-hexylthiophen-2-yl)-4-methylthiazole-3-oxide (17)



Compound **12** (50 mg, 0.28 mmol, 1 equiv) (**2a**) added to a vial with DCE (2 mL) and stirred until fully dissolved. *m*CPBA (162 mg, 77% purity, 0.937 mmol, 3 equiv) was slowly added followed by sealing of the reaction vessel. The reaction was stirred until *m*CPBA and corresponding acid precipitated out of solution. Methanol was added dropwise until reaction mixture became transparent. A second addition of *m*CPBA (77% purity, 0.937 mmol, 3 equiv) was performed and reaction mixture was once again sealed and stirred until acid precipitated. Material was filtered by suction filtration and then dissolved in a minimal amount of ethyl acetate, to which silica gel was added. The solvent from the resultant slurry was then removed via reduced pressure. Purification performed by column chromatography with a gradient (0 -10% MeOH in EtOAc) to yield product **17** (22.9 mg, 29%). ¹H-NMR (CDCl₃): 8.21 (s, 1H), 7.04 (d, *J* = 3.6 Hz, 1H), 6.78 (d, *J* = 3.6 Hz, 1H), 2.82 (t, *J* = 7.7 Hz, 2H), 2.513(s, 3H), 1.68(tt, *J* = 7.6, 7.1 Hz, 2H), 1.32(m, 6H), 0.88 (t, *J* = 6.7 Hz, 3H). Characterization data was identical to previously reported literature.⁴²

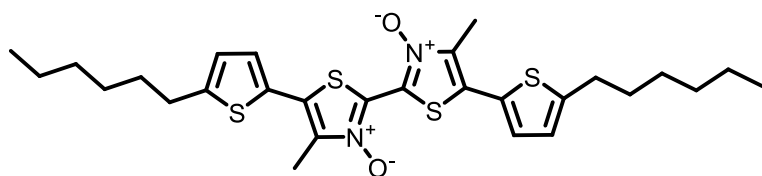
Preparation of 5,5'-bis(5-hexylthiophen-2-yl)-4,4'-dimethyl-2,2'-bithiazole (21)



Reaction vessel charged with all solids: **13** (50 mg, 0.255 mmol, 1 equiv) , pivalic acid (26 mg, 0.255 mmol, 1 equiv), Cs₂CO₃ (108 mg, 0.785 mmol, 3 equiv), Pd(OAc)₂ (5 mg, 0.02 mmol, 0.04 equiv) and tris(*O*-methoxytriphenyl)phosphine (14.4 mg, 0.0408 mmol, 0.08 equiv). The reaction vessel was purged with argon followed by the addition of THF (0.85 mL) and then 5-bromo-2-hexylthiophene (107 μL, 0.536 mmol, 2.1 equiv). Reaction stirred for 3 h at 90 °C. After 3 hours the reaction mixture was diluted with 15 mL of ethyl acetate and added to separatory funnel. The organic layer was washed with 3 x 15 mL

deionized water and 1 x 15 mL brine. The organic layer was removed and dried with MgSO_4 and then reduced to ~5 mL using rotary evaporator, to which silica gel was added. The solvent from the resultant slurry was then removed via reduced pressure. Purification by flash chromatography (0-20% EtOAc in hexanes) yielded **21** (7 mg, 6%). $^1\text{H-NMR}$ (CDCl_3): δ 6.99 (d, 2H), 6.75 (d, 2H), 2.81 (t, 4H), 2.60 (s, 6H), 1.69 (m, 4H), 1.32 (m, 12H), 0.88 (s, 6H). $^{13}\text{C NMR}$ (CDCl_3): 156.5, 148.7, 147.4, 130.4, 128.4, 126.8, 124.7, 31.4, 30.0, 28.6, 22.4, 16.7, 13.9. HRMS calculated for $\text{C}_{28}\text{H}_{37}\text{N}_2\text{S}_4$ ($\text{M} + \text{H}^+$): 529.18341 Found: 529.1833. rf = 0.80 (4:1 Hexanes:EtOAc).

Preparation of 5,5'-bis(5-hexylthiophen-2-yl)-4,4'-dimethyl-2,2'-bithiazole-3-3'-dioxide (**23**)



Reaction vessel charged with all solids: **17** (100 mg, 0.44 mmol, 1 equiv), pivalic acid (45 mg, 0.44 mmol, 1 equiv), Cs_2CO_3 (429.9 mg, 1.3 mmol, 3 equiv), $\text{Pd}(\text{OAc})_2$ (4 mg, 0.018 mmol, 0.04 equiv) and tris(*O*-methoxytriphenyl)phosphine (12.4 mg, 0.035 mmol, 0.08 equiv). The reaction vessel was purged with argon, followed by the addition of THF (1.5 mL) and then 5-bromo-2-hexylthiophene (165 μL , 0.88 mmol, 2.1 equiv). The reaction was stirred for 3 h at 90 $^\circ\text{C}$. A second addition of $\text{Pd}(\text{OAc})_2$ (4 mg, 0.018 mmol, 0.04 equiv) was added after 3 h. Reaction stirred overnight at 90 $^\circ\text{C}$ and then a third addition of $\text{Pd}(\text{OAc})_2$ (3.95 mg, 0.018 mmol, 0.04 equiv) was performed and stirred for an additional 3 h at 90 $^\circ\text{C}$. After 3 hours the reaction mixture was diluted with 15 mL of ethyl acetate and added to separatory funnel. The organic layer was washed with 3 x 15 mL deionized water and 1 x 15 mL brine. The organic layer was removed and dried with MgSO_4 and then reduced to ~5 mL using rotary evaporator, to which silica gel was added. The solvent from the resultant slurry was then removed via reduced pressure. Flash chromatography was performed (30-60% EtOAc in hexanes) to yield product **23** (11 mg, 4%). $^1\text{H-NMR}$ (CDCl_3): δ 7.17 (d, 2H), 6.84 (d, 2H), 2.86 (t, 4H), 2.64 (s, 6H), 1.74 (m, 4H), 1.34 (m, 12H), 0.90 (s, 6H). $^{13}\text{C NMR}$ (CDCl_3): 149.4,

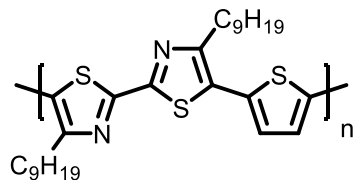
138.9, 132.0, 129.4, 127.4, 125.3, 31.5, 30.2, 29.7, 28.8, 22.6, 14.1, 11.6. **HRMS** calculated for $C_{28}H_{37}N_2O_2S_4$ ($M + H^+$): 561.17324 Found: 561.17338. RF = 0.50 (1:1 hexanes:EtOAc).

Direct Arylation Polymerization (DAP) General Procedure

A 2 mL vial was charged with all solids: pivalic acid (0.15 mmol, 1 equiv), cesium carbonate (0.45 mmol, 3 equiv), $Pd(OAc)_2$ (0.006 mmol, 0.04 equiv) and tris(*O*-methoxytriphenyl)phosphine (0.012 mmol, 0.08 equiv). For solid starting materials, the bithiazole (0.15 mmol, 1 equiv) and the aryl halide (0.15 mmol, 1 equiv) were added at this point. The vessel was then purged with an argon balloon. Dry solvent (0.24 M) was then added to reaction mixture. For liquid starting materials the bithiazole and aryl halide were added at this point. The reaction was sealed and stirred for 3 h at 90 °C. The polymer was purified by precipitation in methanol (20 mL) and then filtered to yield the DAP product.

Di-*N*-oxide polymers required a second addition (after 3 h) and third addition (after an additional 3 h) of $Pd(OAc)_2$ (0.04 mmol) and then subjected to a Soxhlet extraction with acetone to yield the final product.

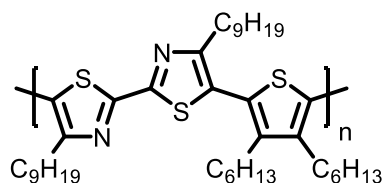
Preparation of Poly(4,4'-diononyl-5-thienyl-2,2'-bithiazole) (7)



A 2 mL vial was charged with all solids: **(2)** (100 mg, 0.238 mmol, 1 equiv), pivalic acid (24.3 mg, 0.238 mmol, 1 equiv), cesium carbonate (232.2 mg, 0.713 mmol, 3 equiv), $Pd(OAc)_2$ (2.13 mg, 0.0095 mmol, 0.04 equiv) and tris(*O*-methoxytriphenyl)phosphine (6.70 mg, 0.019 mmol, 0.08 equiv). The vessel was then

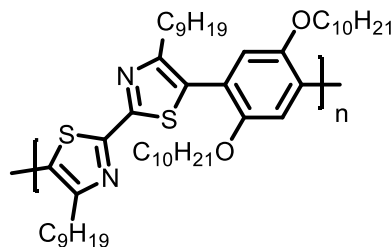
purged with an argon balloon. Dry toluene (0.8 mL, 0.3 M) was then added to reaction mixture followed by 2,5-dibromothiophene (26.8 μ L, 0.238 mmol, 1 equiv). The reaction was sealed and stirred for 3 h at 90 $^{\circ}$ C. The reaction mixture was then added drop-wise to stirring methanol (20 mL) to precipitate the polymer, which was then collected through suction filtration to yield the DArP product **7** in quantitative yield, $M_n < 5$ kD. $^1\text{H-NMR}(\text{CDCl}_3)$: δ 7.16 (s, 1H). 6.98 (s, 1H), 2.98 (br, 2H), 2.82 (m, 2H), 1.79 (br, 4H), 1.27 (br, 22H), 0.88 (br, 6H).

Preparation of Poly(4,4'-dinonyl-5-(3,4-dihexylthienyl)-2,2'-bithiazole) (**8**)



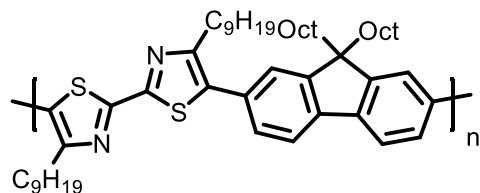
A 2 mL vial was charged with all solids: (**2**) (50.0 mg, 0.12 mmol, 1 equiv), pivalic acid (12.1 mg, 0.12 mmol, 1 equiv), cesium carbonate (116.1 mg, 0.36 mmol, 3 equiv), Pd(OAc)₂ (1.1 mg, 0.0048 mmol, 0.04 equiv) and tris(*O*-methoxytriphenyl)phosphine (3.35 mg, 0.0096 mmol, 0.08 equiv). The vessel was then purged with an argon balloon. Dry THF (0.5 mL, 0.24 M) was then added to reaction mixture followed by 2,5-dibromo-3,4-dihexylthiophene (37 μ L, 0.12 mmol, 1 equiv). The reaction was sealed and stirred for 24 h at 90 $^{\circ}$ C. The reaction mixture was then added drop-wise to stirring methanol (20 mL) to precipitate the polymer, which was then collected through suction filtration to yield the DArP product **8** in quantitative yield, $M_n = 29$ kD, $M_w = 64$ kD. $^1\text{H-NMR}(\text{CDCl}_3)$: δ 2.74 (br, 4H), 2.58 (br, 4H), 1.74 (br, 4H), 1.47/1.26 (br m, 44H), 0.86 (s, 12H).

Preparation of Poly(4,4'-dinonyl-5-(1,4decyloxybenzene)-2,2'-bithiazole) (9)



A 2 mL vial was charged with all solids: **(2)** (50.0 mg, 0.12 mmol, 1 equiv), pivalic acid (12.1 mg, 0.12 mmol, 1 equiv), cesium carbonate (116.1 mg, 0.36 mmol, 3 equiv), Pd(OAc)₂ (1.1 mg, 0.0048 mmol, 0.04 equiv) and tris(*O*-methoxytriphenyl)phosphine (3.35 mg, 0.0096 mmol, 0.08 equiv). The vessel was then purged with an argon balloon. Dry toluene (0.5 mL, 0.24 M) was then added to reaction mixture followed by 1,4-dibromo-2,5-(bis)decyloxybenzene (65.2 μL, 0.12 mmol, 1 equiv). The reaction was sealed and stirred for 24 h at 90 °C. The reaction mixture was then added drop-wise to stirring methanol (20 mL) to precipitate the polymer, which was then collected through suction filtration yield the DARp product **9** in quantitative yield, M_n =32 kD, M_w= 70 kD. ¹H-NMR (CDCl₃): δ 6.98 (s, 2H), 3.95 (br, 4H), 2.88-2.68 (br, 4H), 1.75 (br, 8H), 1.25 (br, 48H), 0.87 (m, 12H).

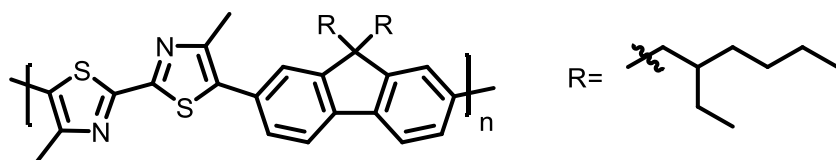
Preparation of Poly(4,4'-dinonyl-5-(9,9-dioctylfluorene)-2,2'-bithiazole) (10)



A 2 mL vial was charged with all solids: **(2)** (50.0 mg, 0.12 mmol, 1 equiv), pivalic acid (12.1 mg, 0.12 mmol, 1 equiv), cesium carbonate (116.1mg, 0.36 mmol, 3 equiv), Pd(OAc)₂ (1.1 mg, 0.0048 mmol, 0.04 equiv) and tris(*O*-methoxytriphenyl)phosphine (3.35 mg, 0.0096 mmol, 0.08 equiv). The vessel was then purged

with an argon balloon. Dry toluene (0.5 mL, 0.24 M) was then added to reaction mixture followed by 9,9-dioctyl-2,7-dibromofluorene (65.2 μ L, 0.12 mmol, 1 equiv). The reaction was sealed and stirred for 48 h at 90 $^{\circ}$ C. The reaction mixture was then added drop-wise to stirring methanol (20 mL) to precipitate the polymer, which was then collected through suction filtration to yield the DArP product **10** in quantitative yield, $M_n = 52$ kDa, $M_w = 99$ kDa. $^1\text{H-NMR}$ (CDCl_3): δ 7.87-7.73 (br, 2H), 7.49 (s, 4H), 2.99-2.79 (br, 4H), 2.14-1.91 (br, 4H), 1.47-0.97 (br, 48H), 0.92-0.77 (m, 14H).

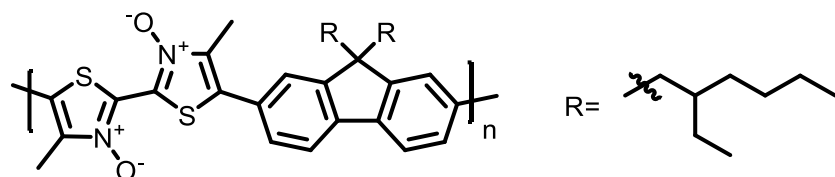
Preparation of Poly(4,4'-dinonyl-5-(9,9-di(2-ethylhexyl)fluorene)-2,2'-bithiazole) (**24**)



A 2 mL vial was charged with all solids: (**13**) (50.0 mg, 0.25 mmol, 1 equiv), 9,9-di(2'-ethylhexyl)-2,7-dibromofluorene (125 mg, 0.25 mmol, 1 equiv), pivalic acid (25.9 mg, 0.25 mmol, 1 equiv), cesium carbonate (248.3 mg, 0.76 mmol, 3 equiv), $\text{Pd}(\text{OAc})_2$ (2.3 mg, 0.01 mmol, 0.04 equiv) and tris(*O*-methoxytriphenyl)phosphine (7.2 mg, 0.02 mmol, 0.08 equiv). The vessel was then purged with an argon balloon. Dry toluene (1 mL, 0.24 M) was then added to reaction mixture. The reaction was sealed and stirred for 48 h at 90 $^{\circ}$ C. The reaction mixture was then added drop-wise to stirring methanol (20 mL) to precipitate the polymer which was then collected through suction filtration to yield the DArP product **24** in quantitative yield, $M_n = 18$ kDa, $M_w = 42$ kDa. $^1\text{H-NMR}$ (CDCl_3): δ 7.81 (s, 2H), 7.51 (s, 4H), 2.63 (s, 6H), 2.19-1.89 (br, 4H), 0.95-0.70 (br, 20H), 0.64 (s, 6H), 0.55 (s, 6H).

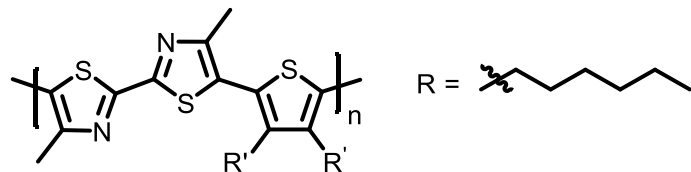
Preparation of Poly(4,4'-dinyl-5-(9,9-di(2-ethylhexyl)fluorene)-2,2'-bithiazole-3,3'-dioxide) (26)

(26)



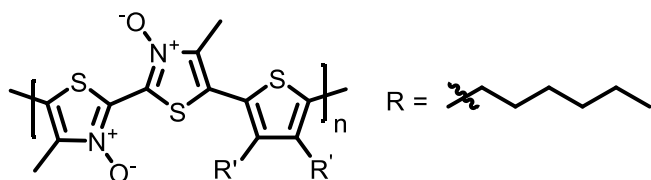
A 2 mL vial was charged with all solids: **(15)** (25 mg, 0.11 mmol, 1 equiv), 9,9-di(2'-ethylhexyl)-2,7-dibromofluorene (53.9 mg, 0.11 mmol, 1 equiv), pivalic acid (11.2 mg, 0.11 mmol, 1 equiv), cesium carbonate (107.0 mg, 0.33 mmol, 3 equiv), Pd(OAc)₂ (1 mg, 0.0045 mmol, 0.04 equiv) and tris(*O*-methoxytriphenyl)phosphine (3.2 mg, 0.009 mmol, 0.08 equiv). The vessel was then purged with an argon balloon. Dry THF (0.5 mL, 0.24 M) was then added to reaction mixture. The reaction was sealed and stirred for 3 h at 90 °C. Pd(OAc)₂ (1 mg, 0.0045 mmol, 0.04 equiv) and tris(*O*-methoxytriphenyl)phosphine (3.2 mg, 0.009 mmol, 0.08 equiv) were then added a second time to the reaction mixture and stirred for an additional 42 hours at 90 °C. The reaction mixture was then added drop-wise to stirring methanol (20 mL) to precipitate the crude polymer, which was collected through suction filtration. A Soxhlet extraction with acetone was then performed for 16 hrs to yield the DArP product **26** in 39% yield, $M_n = 14$ kDa, $M_w = 32$ kDa. ¹H-NMR (CDCl₃): δ 7.88 (br, 2H), 7.60 (br, 4H), 2.65 (s, 6H), 2.19-1.91 (br, 4H), 0.95-0.70 (m, 20H), 0.63 (s, 6H), 0.54 (s, 6H).

Preparation of Poly(5-(3,4-hexylthiophen-2-yl)-4,4'-dimethyl-2,2'-bithiazole) (27)



A 2 mL vial was charged with all solids: **(13)** (30 mg, 0.15 mmol, 1 equiv), pivalic acid (15.6 mg, 0.15 mmol, 1 equiv), cesium carbonate (149.6 mg, 0.46 mmol, 3 equiv), Pd(OAc)₂ (1.4 mg, 0.0061 mmol, 0.04 equiv) and tris(*O*-methoxytriphenyl)phosphine (4.3 mg, 0.012 mmol, 0.08 equiv). The vessel was then purged with an argon balloon. Dry THF (0.24 M) was then added to reaction mixture followed by 2,5-dibromo-3,4-dihexylthiophene (48 μL, 0.15 mmol, 1 equiv). The reaction was sealed and stirred for 24 h at 90 °C. The reaction mixture was then added drop-wise to stirring methanol (20 mL) to precipitate the polymer which was then collected through suction filtration to yield the DARP product **27** in quantitative yield, M_n= 20 kDa, M_w = 45 kDa. ¹H-NMR (CDCl₃): δ 2.57 (br, 2H), 2.47 (s, 3H), 1.46 (br, 2H), 1.24 (br, 6H), 0.85 (br, 3H).

Preparation of Poly(5-(3,4-hexylthiophen-2-yl)-4,4'-dimethyl-2,2'-bithiazole-3-3'-dioxide) (**29**)

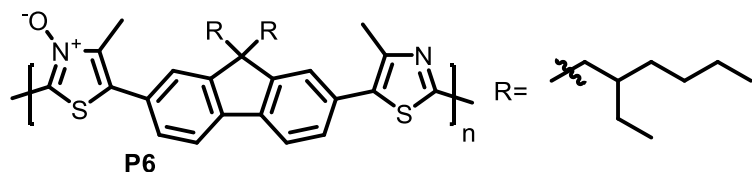


A 2 mL vial was charged with all solids: **(15)** (30 mg, 0.13 mmol, 1 equiv), pivalic acid (13.4 mg, 0.13 mmol, 1 equiv), cesium carbonate (128.1 mg, 0.39 mmol, 3 equiv), Pd(OAc)₂ (2.4 mg, 0.011 mmol, 0.08 equiv) and tris(*O*-methoxytriphenyl)phosphine (7.4 mg, 0.021 mmol, 0.16 equiv). The vessel was then purged with an argon balloon. Dry THF (0.24 M) was then added to reaction mixture followed by 2,5-dibromo-3,4-dihexylthiophene (41 μL, 0.15 mmol, 1 equiv). Pd(OAc)₂ (2.4 mg, 0.011 mmol, 0.08 equiv) and tris(*O*-methoxytriphenyl)phosphine (7.4 mg, 0.021 mmol, 0.16 equiv) were then added a second time to the reaction mixture and stirred for an additional 42 hours at 90 °C. The reaction mixture was then added drop-wise to stirring methanol (20 mL) to precipitate the crude polymer, which was collected through suction filtration. A Soxhlet extraction with acetone was then performed for 16 hrs to yield the DARP

product **29** in 74% yield (45.1 mg), $M_n = 6$ kD, $M_w = 13$ kD $^1\text{H-NMR}$ (CDCl_3): δ 2.57 (br, 4H), 2.47 (s, 4H), 1.45 (br, 4H), 1.24 (br, 10H), 0.86 (br, 6H).

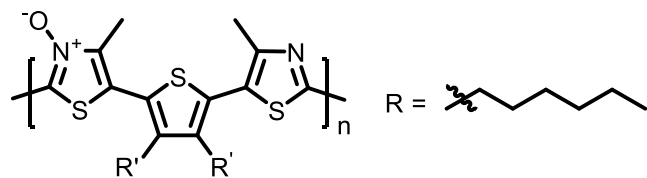
Polymers prepared through dehydration

Preparation of Poly(4,4'-dinonyl-5-(9,9-di(2-ethylhexyl)fluorene)-2,2'-bithiazole-3-oxide) (**25**)



The di-*N*-oxide monomer was dissolved in reagent grade THF (0.03 M) placed in an ice bath. To this cold solution was added 1.0 M LiOtBu in THF (1.5 eq) which usually resulted in a significant color change. The mixture was allowed to warm to room temperature and was stirred for 3 hours. The solution was then concentrated and precipitated in methanol and isolated through suction filtration to give **25** in quantitative yield, $M_n = 37$ kDa, $M_w = 80$ kDa. $^1\text{H-NMR}$ (CDCl_3): δ 7.86 (br, 2H), 7.60 (br, 2H), 7.29 (br, 2H), 2.69 (br, 3H), 2.65 (br, 3H), 2.04 (br, 2H), 1.25 (m, 12H), 0.88 (br, 8H) 0.65 (br, 6H), 0.57 (br, 6H).

Preparation of Poly(5-(3,4-hexylthiophen-2-yl)-4,4'-dimethyl-2,2'-bithiazole-3-oxide) (**28**)



The di-*N*-oxide was dissolved in reagent grade THF (0.03 M) placed in an ice bath. To this cold solution was added 1.0 M LiOtBu in THF (1.5 eq) which usually resulted in a significant color change. The mixture was allowed to warm to room temperature and was stirred for 3 hours. The solution was then concentrated and precipitated in methanol and isolated through suction filtration in to give **28** quantitative yield, $M_n = 17$ kDa, $M_w = 46$ kDa. $^1\text{H-NMR}$ (CDCl_3): δ 2.65-2.40 (br, 10H), 2.35 (s, 6H), 1.50-1.10 (m, 16H), 0.85 (br, 6H).

Optimized Molecular Geometries from DFT calculations

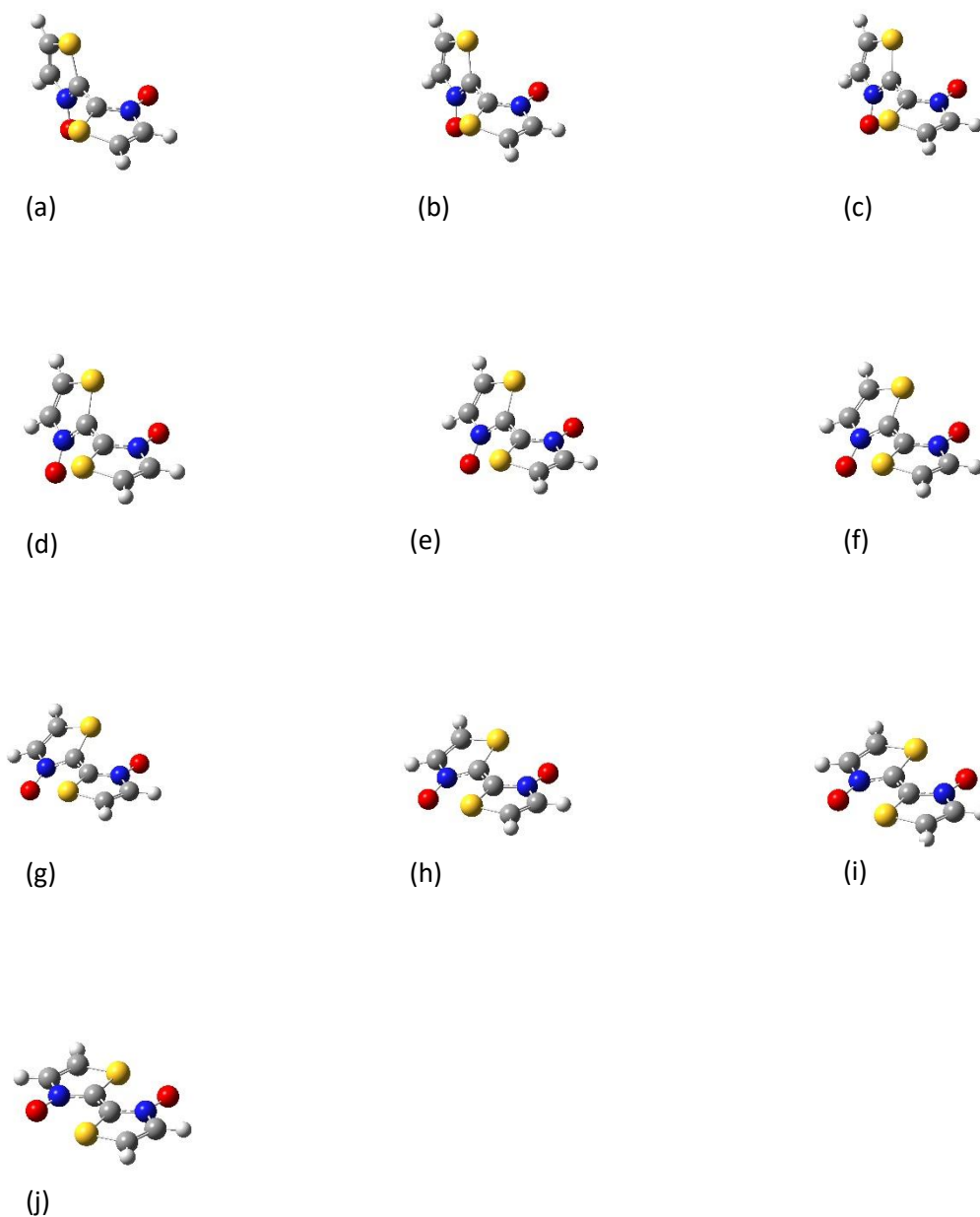


Figure S1. Optimized molecular geometries of 2,2'-bithiazole-3,3'-dioxide using DFT level theory in Gaussian 09. Optimized for N-C-C-N dihedral angles in 10° increments from 90 (a) – 180 (j).

CCSD single point energy calculations

Table S1. Single point energy calculations performed for bithiazole and the corresponding *N*-oxide and di-*N*-oxide at N-C-C-N dihedral angles from 90-180° in increments of 10°. The geometries obtained from the DFT calculations were used in CCSD (T) theory energy calculations in order to obtain the data shown above.

Total Molecular Energies (HF)			
Angle (°)	Bithiazole	Mono- <i>N</i> -oxide	Di- <i>N</i> -oxide
90	-1133.540487	-1208.328794	-1283.118228
100	-1133.541316	-1208.329786	-1283.119401
110	-1133.542695	-1208.331077	-1283.120752
120	-1133.544504	-1208.33269	-1283.122429
130	-1133.546524	-1208.334666	-1283.124697
140	-1133.548498	-1208.337054	-1283.127874
150	-1133.550204	-1208.339791	-1283.131978
160	-1133.55149	-1208.342535	-1283.136397
170	-1133.552278	-1208.344641	-1283.139914
180	-1133.552542	-1208.345438	-1283.141265

Second Perturbation Theory Interaction Energies

Table S2. Shows calculated interactions between the oxygen lone pairs with the C-S antibonding orbital of the adjacent thiazole ring. The data was obtained utilizing the NBO function with a DFT-B3LYP g(d,p)** optimized structure.

Molecule	Interaction (Donor:Acceptor)	E (kCal/mol)
2,2'-bithiazole-3-oxide	LP(O): σ^* C-S	0.64
	LP(O): σ^* C-S	2.70
	LP(O): σ^* C-S	0.86
2,2'-bithiazole-3,3'-dioxide	LP(O15): σ^* C-S	0.64
	LP(O15): σ^* C-S	0.84
	LP(O15): σ^* C-S	3.11
	LP(O16): σ^* C-S	0.65
	LP(O16): σ^* C-S	3.09
	LP(O16): σ^* C-S	1.01

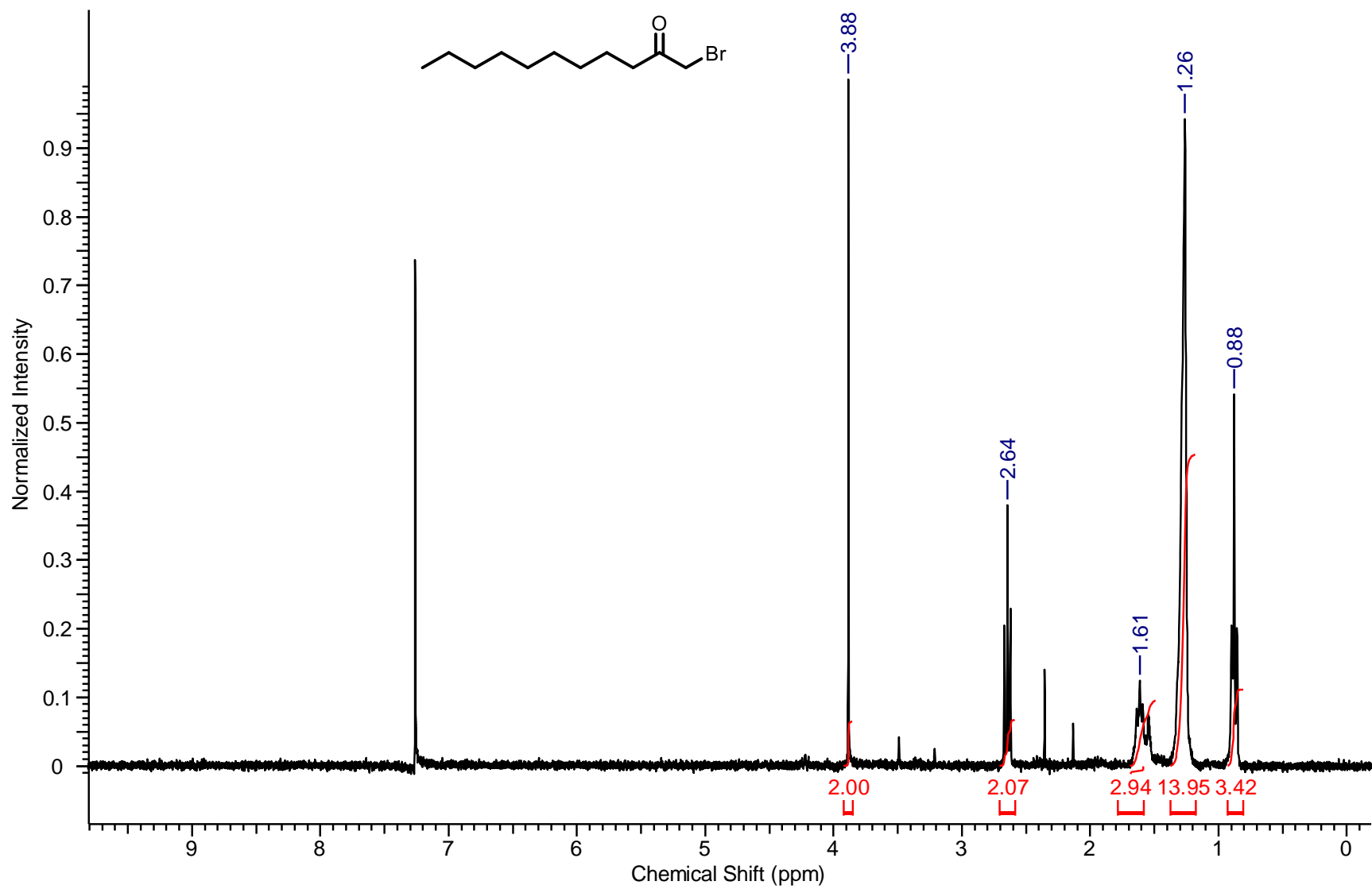


Figure S2. ¹H-NMR spectrum of 5.

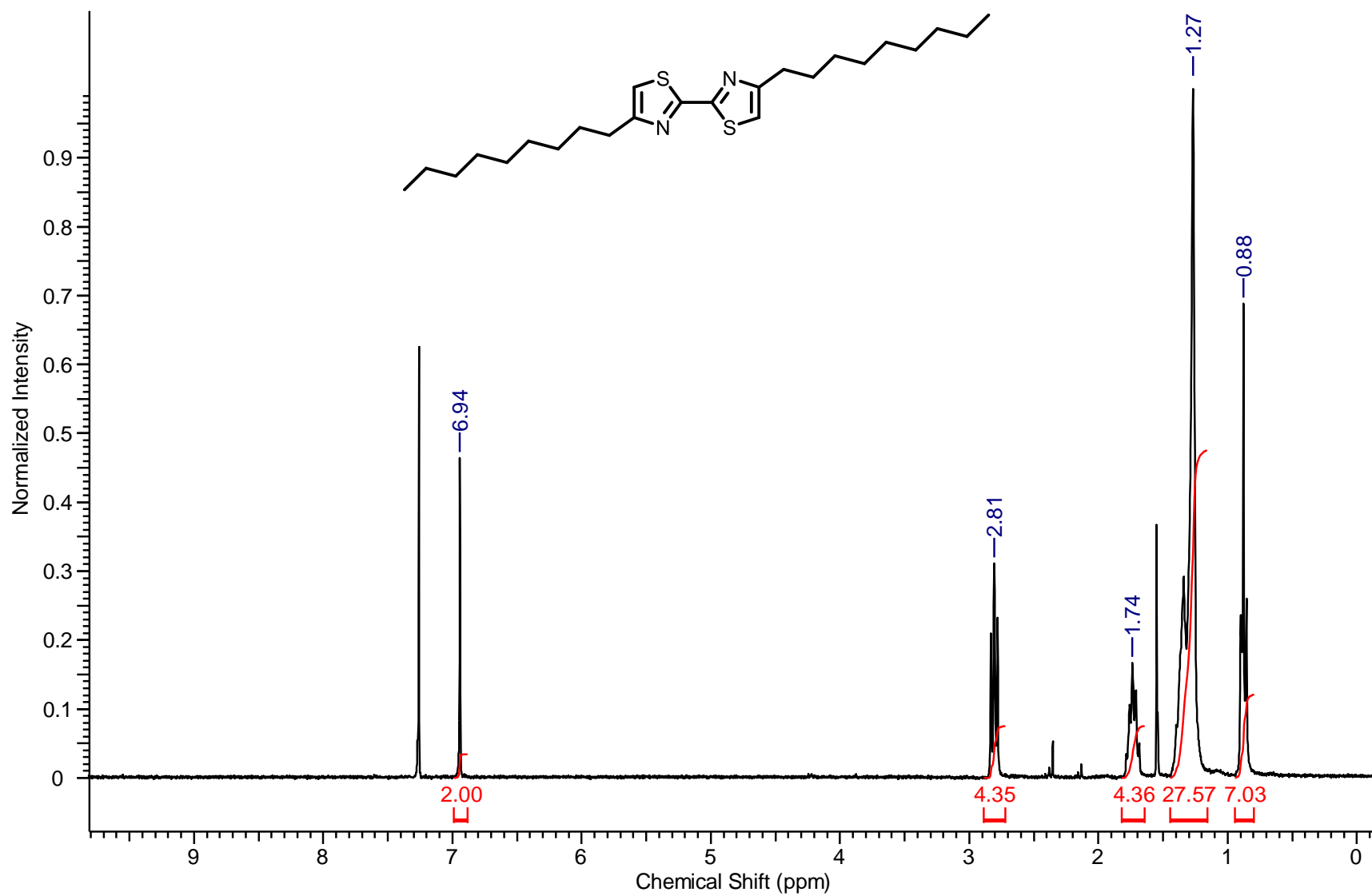


Figure S3. ¹H-NMR spectrum of **6**.

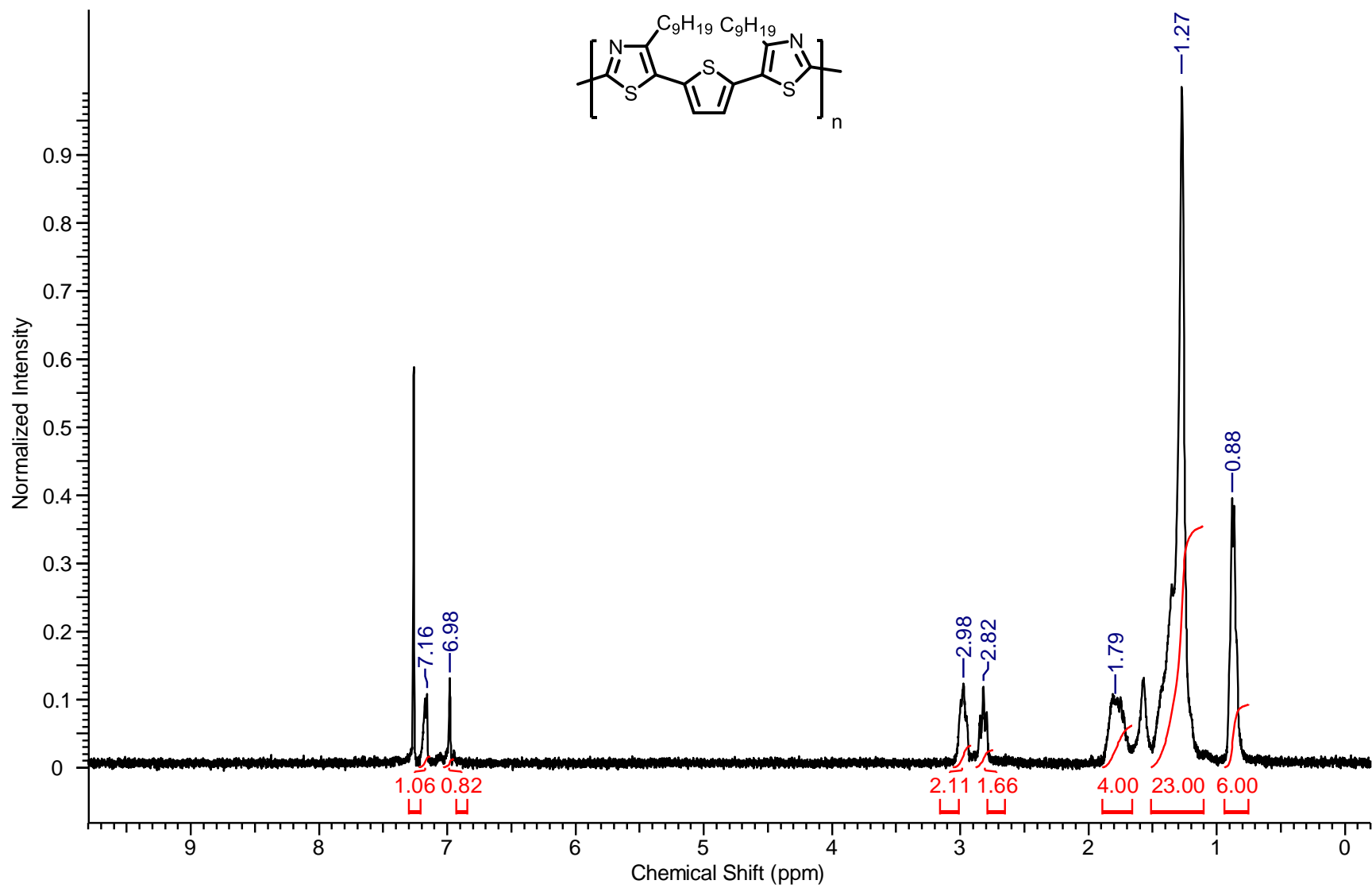


Figure S4. ¹H-NMR spectrum of 7.

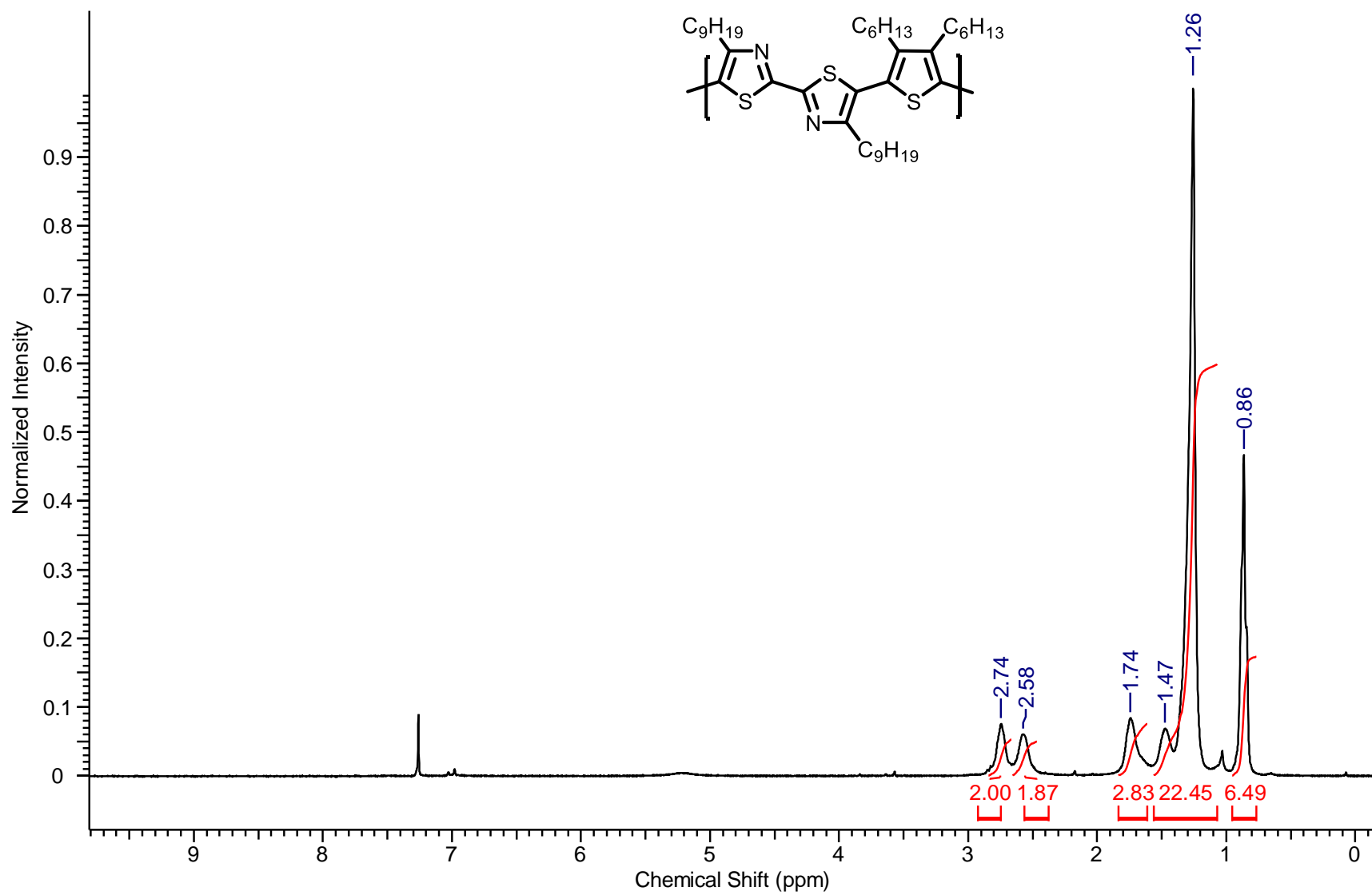


Figure S5. ¹H-NMR spectrum of **8**.

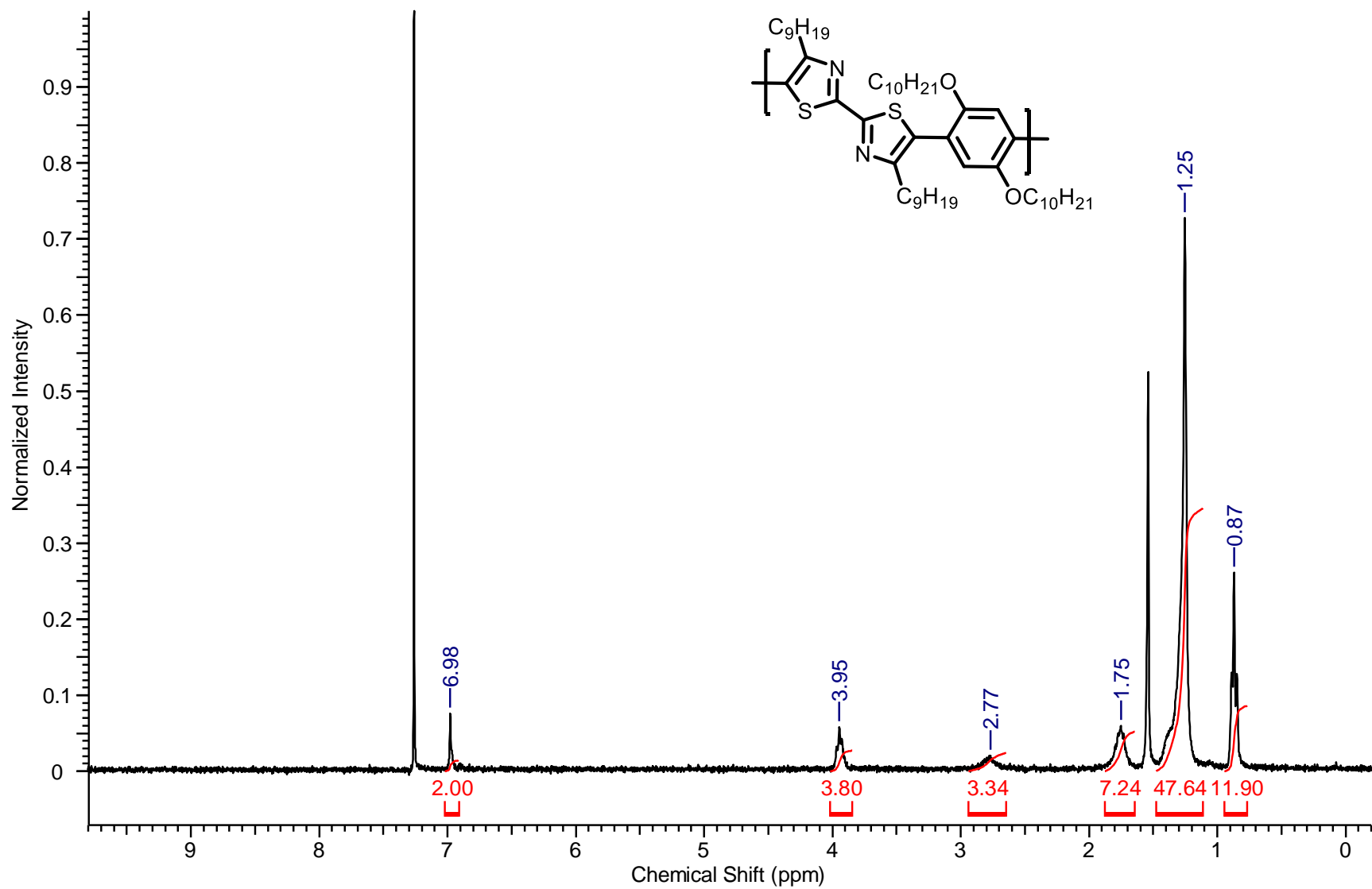


Figure S6. ¹H-NMR spectrum of 9.

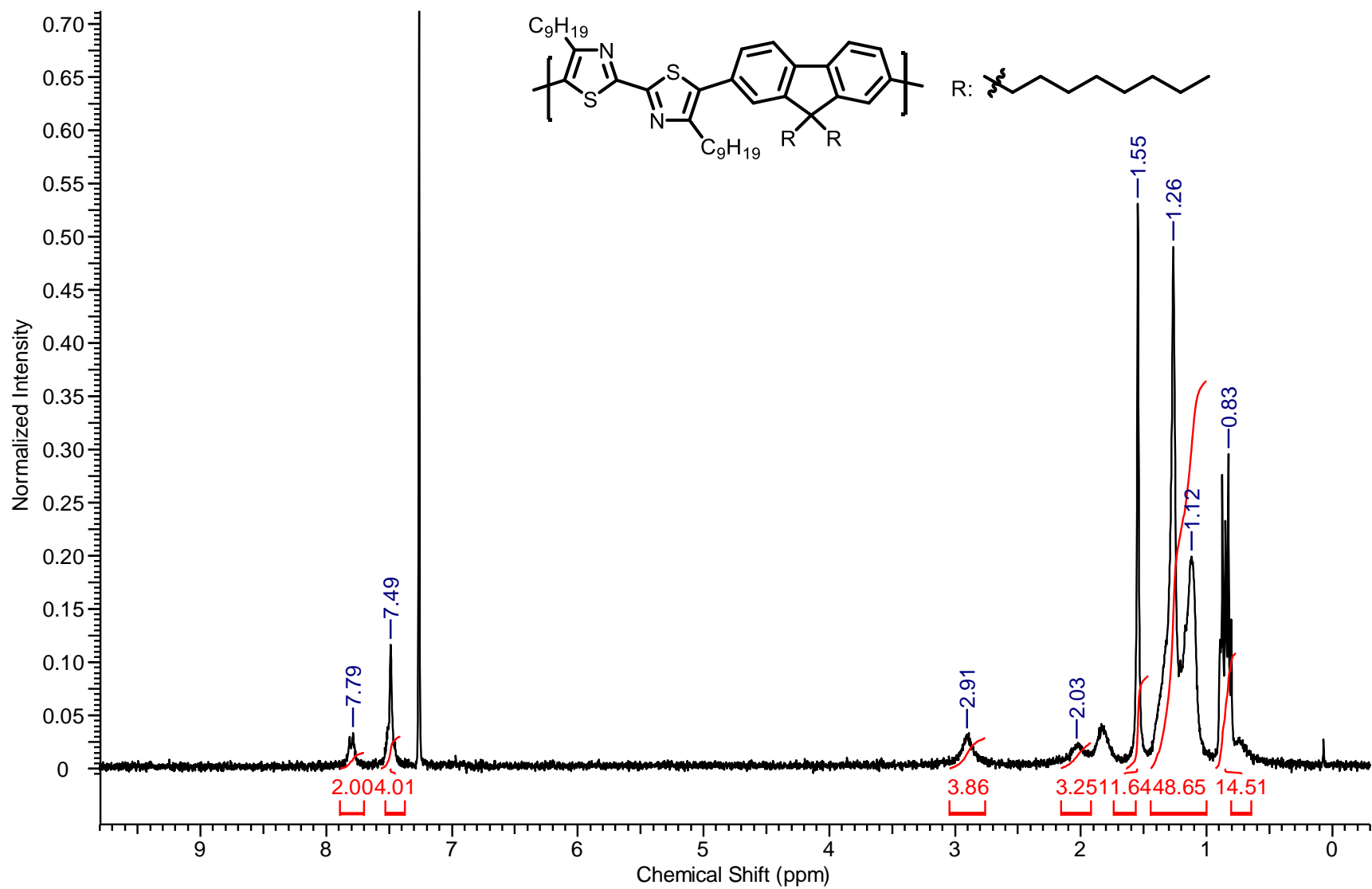
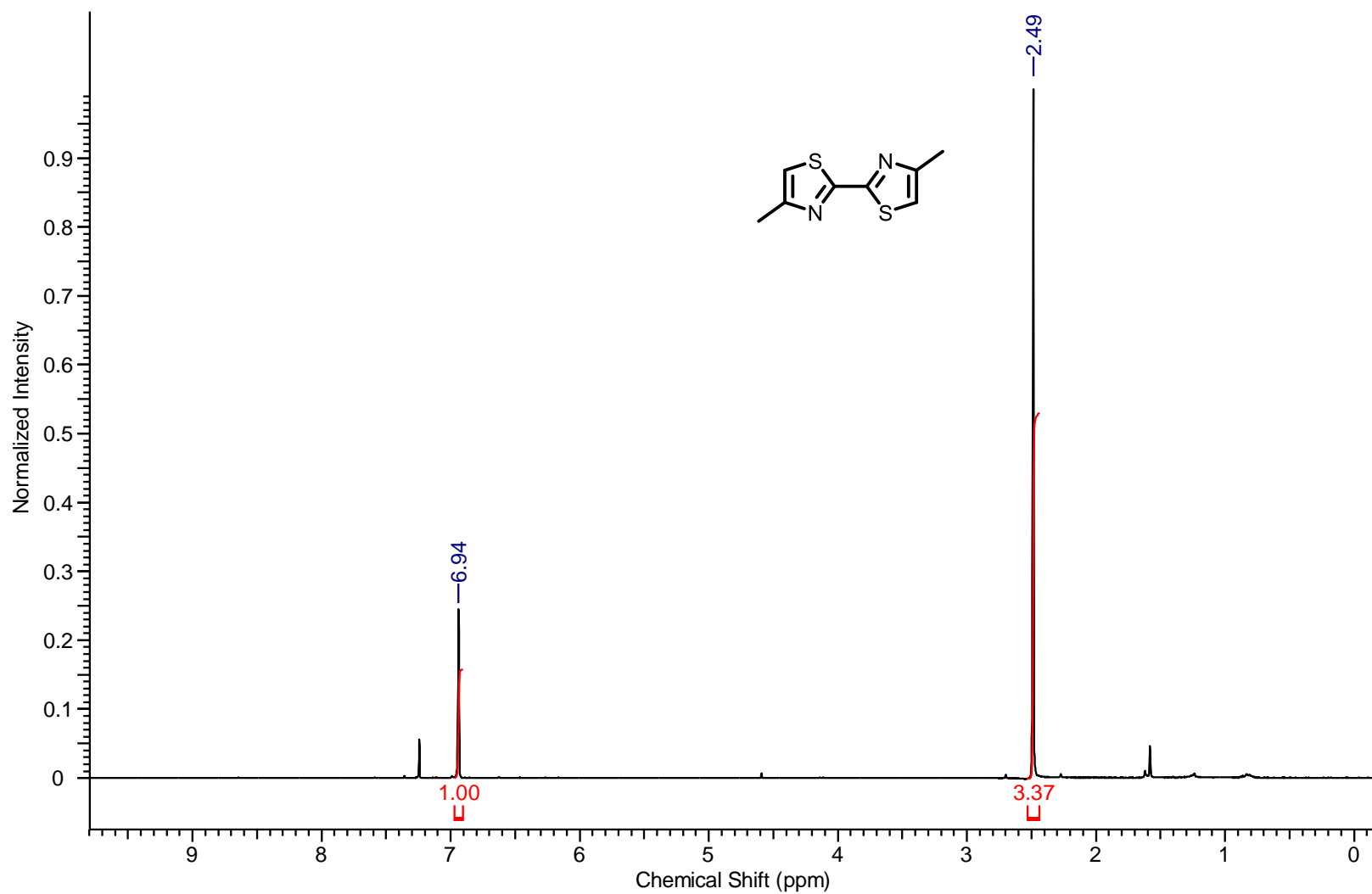


Figure S7. ¹H-NMR spectrum of **10**.



Figure

S8. $^1\text{H-NMR}$ spectrum of **13**.

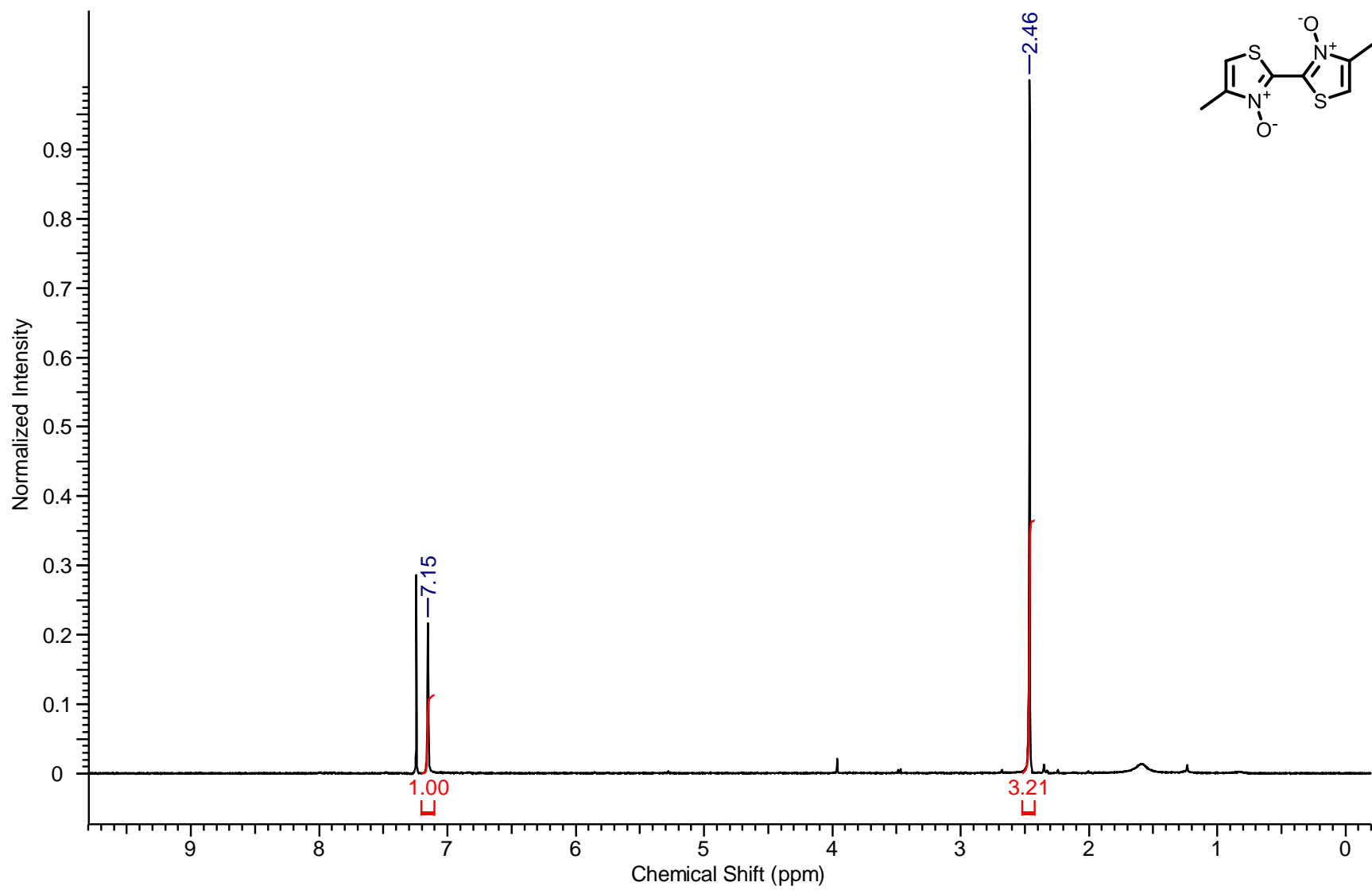


Figure S9. $^1\text{H-NMR}$ spectrum of **15**.

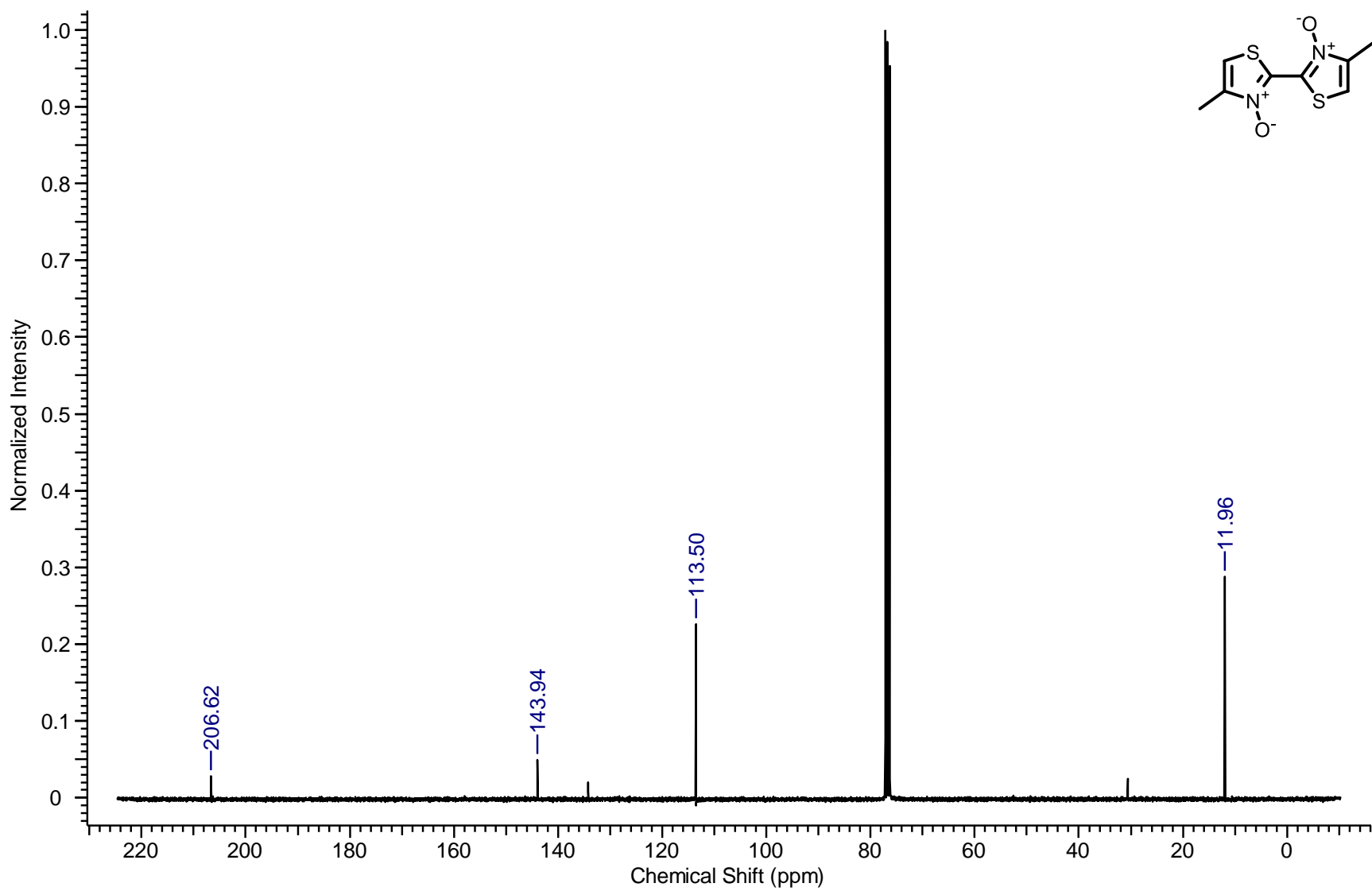


Figure S10. ^{13}C -NMR spectrum of **15**.

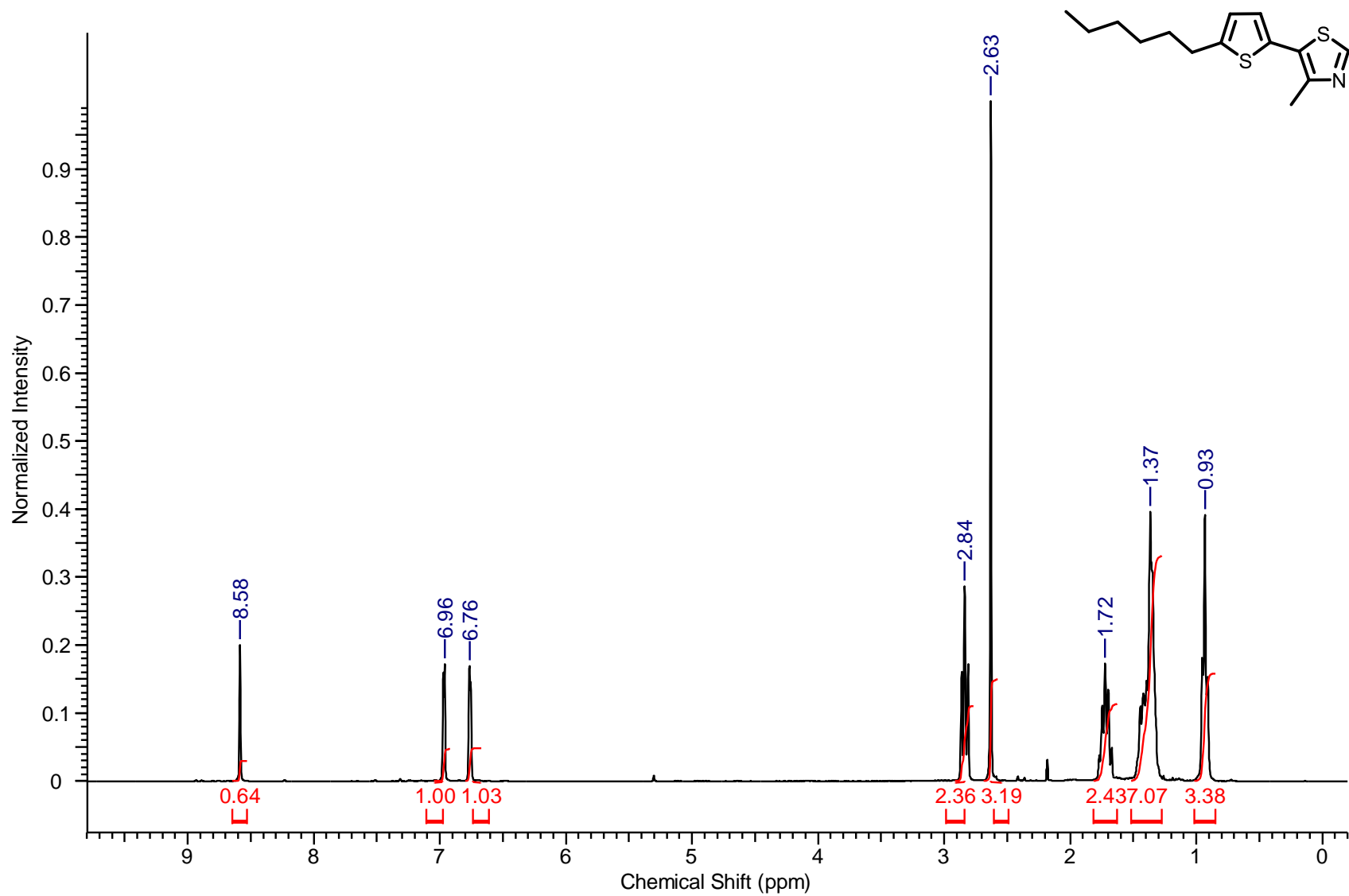


Figure S11. ¹H-NMR spectrum of **16**.

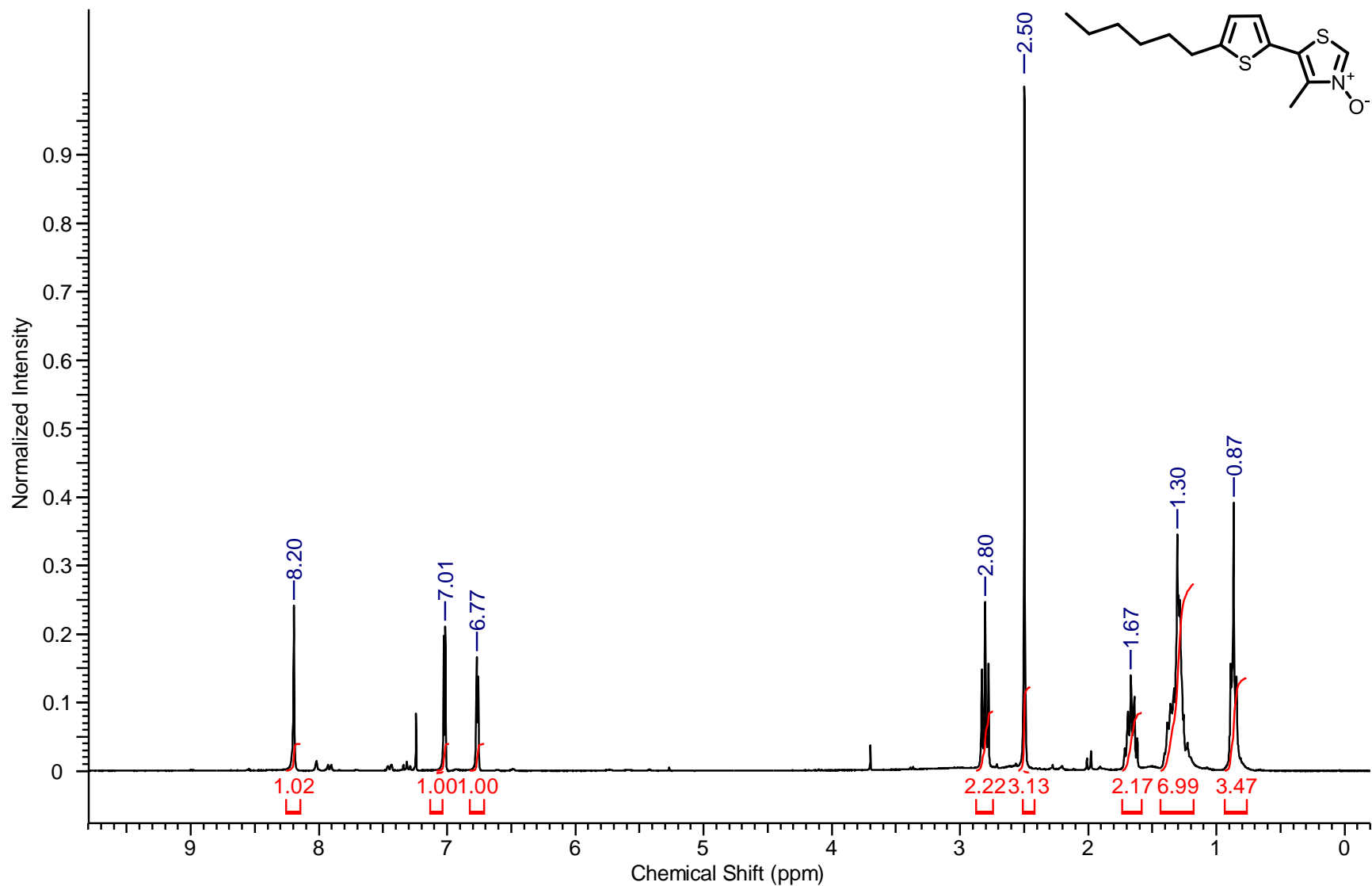


Figure S12. ¹H-NMR spectrum of 17.

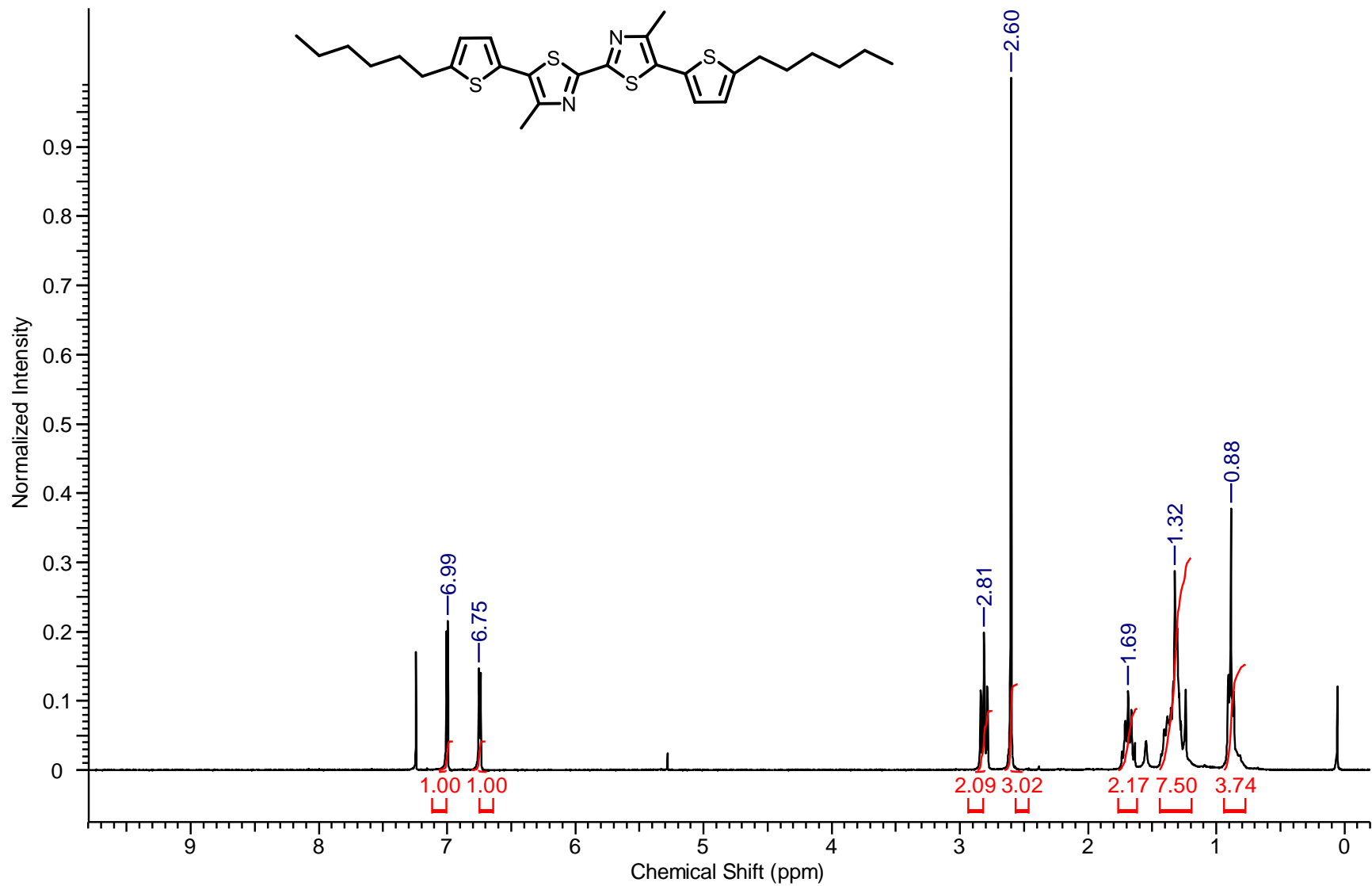


Figure S13. ¹H-NMR spectrum of **21**.

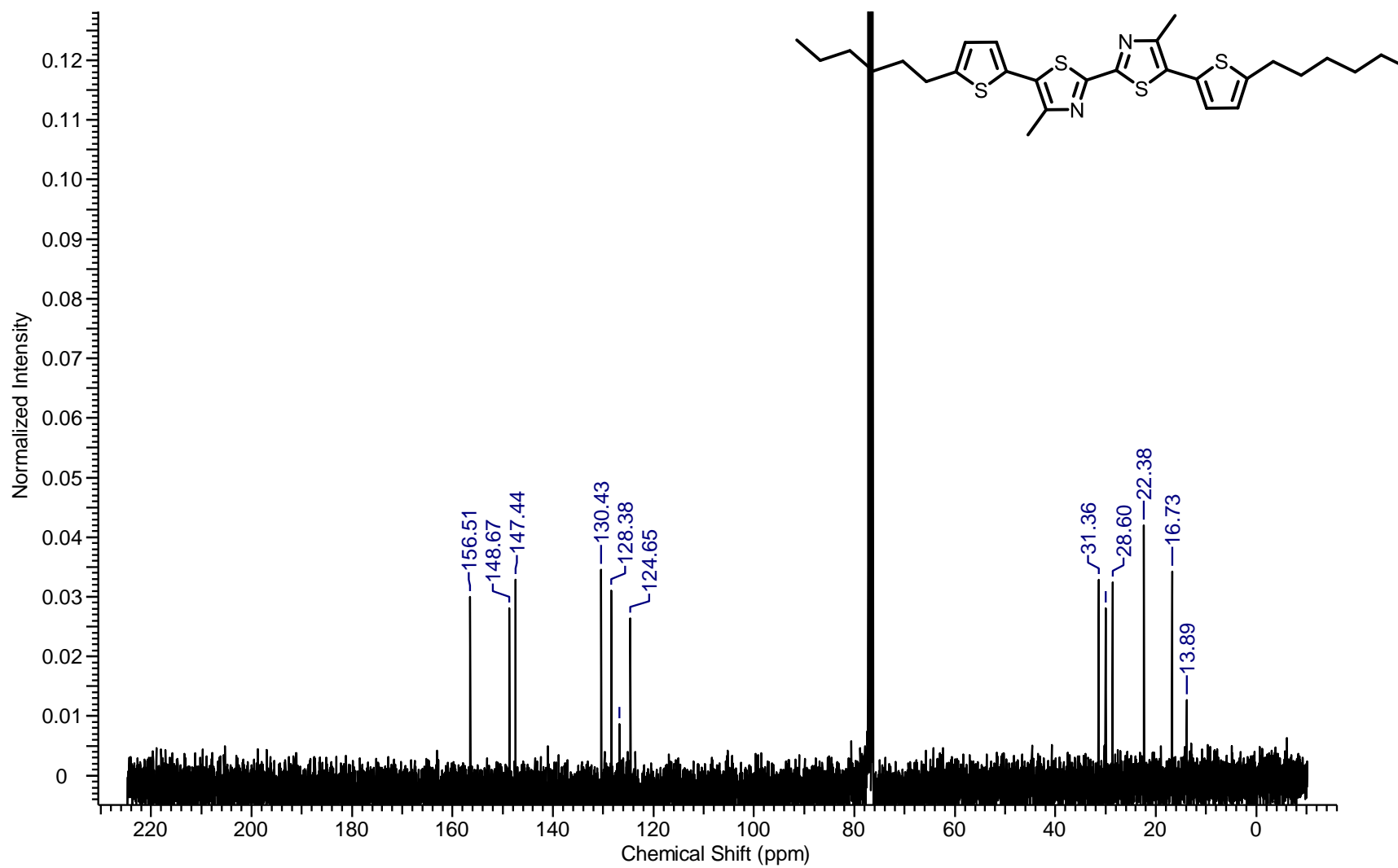


Figure S14. ¹³C-NMR spectrum of **21**.

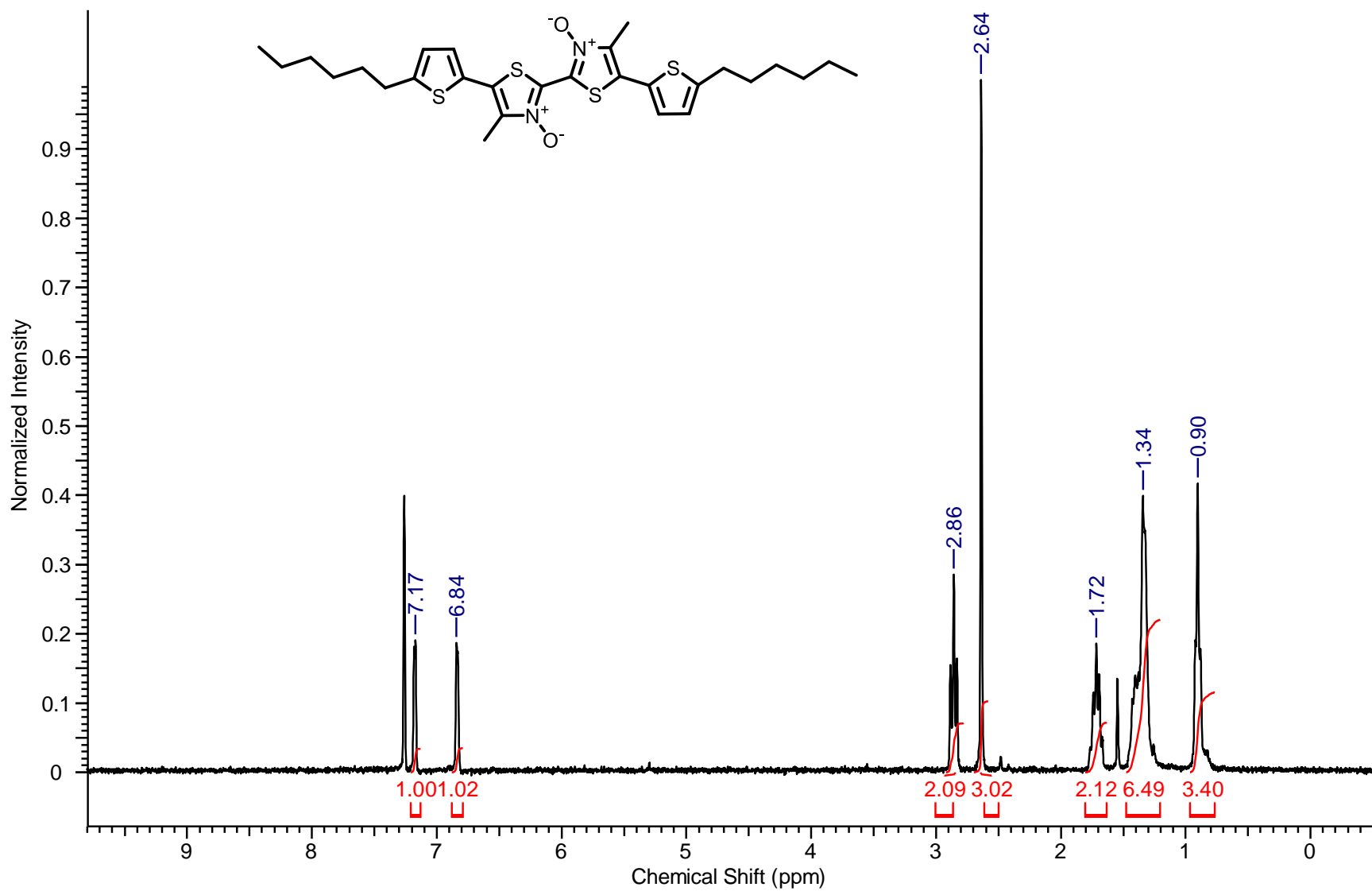


Figure S15. ¹H-NMR spectrum of **23**.

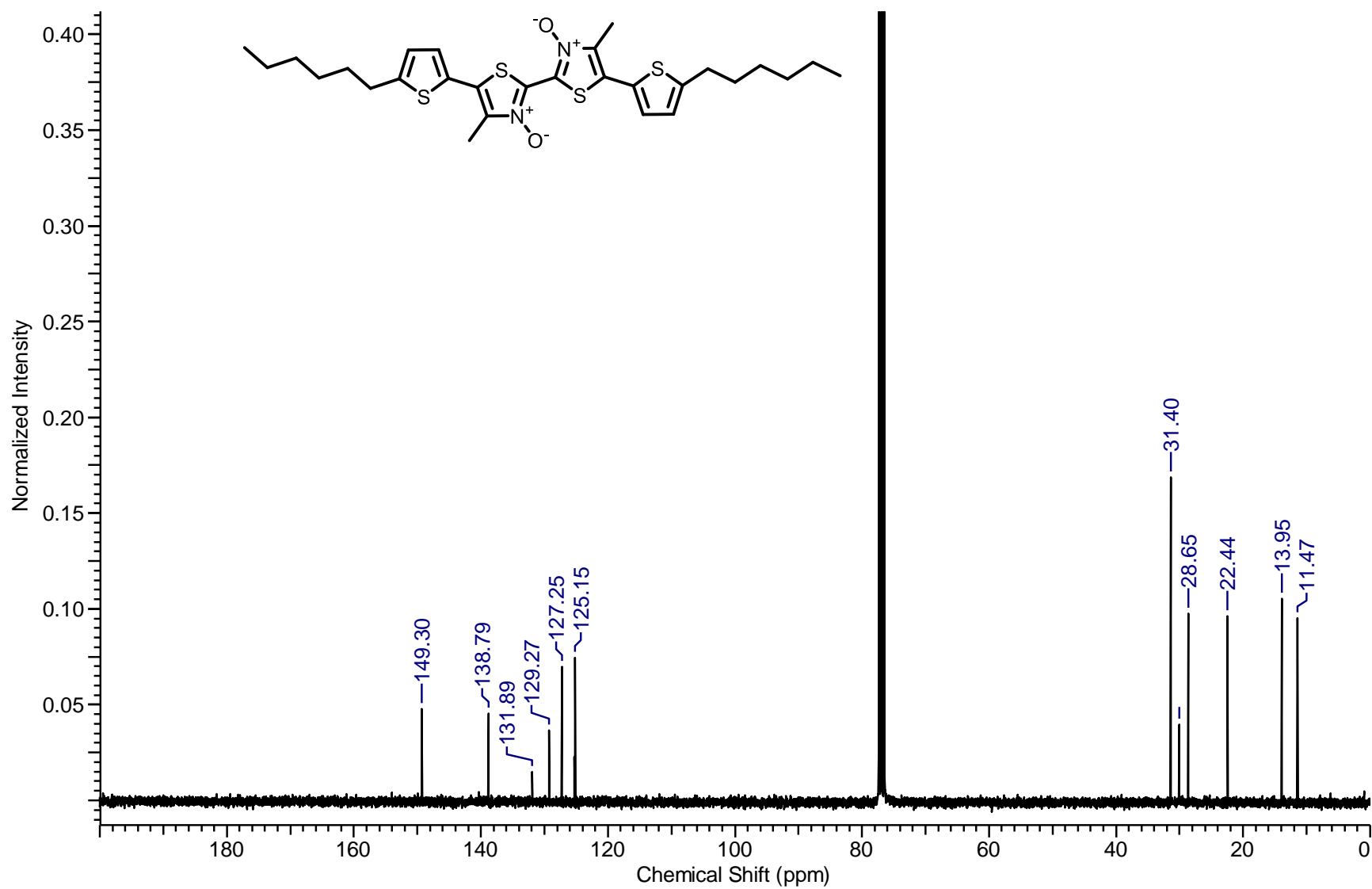


Figure S16. ¹³C-NMR spectrum of **23**.

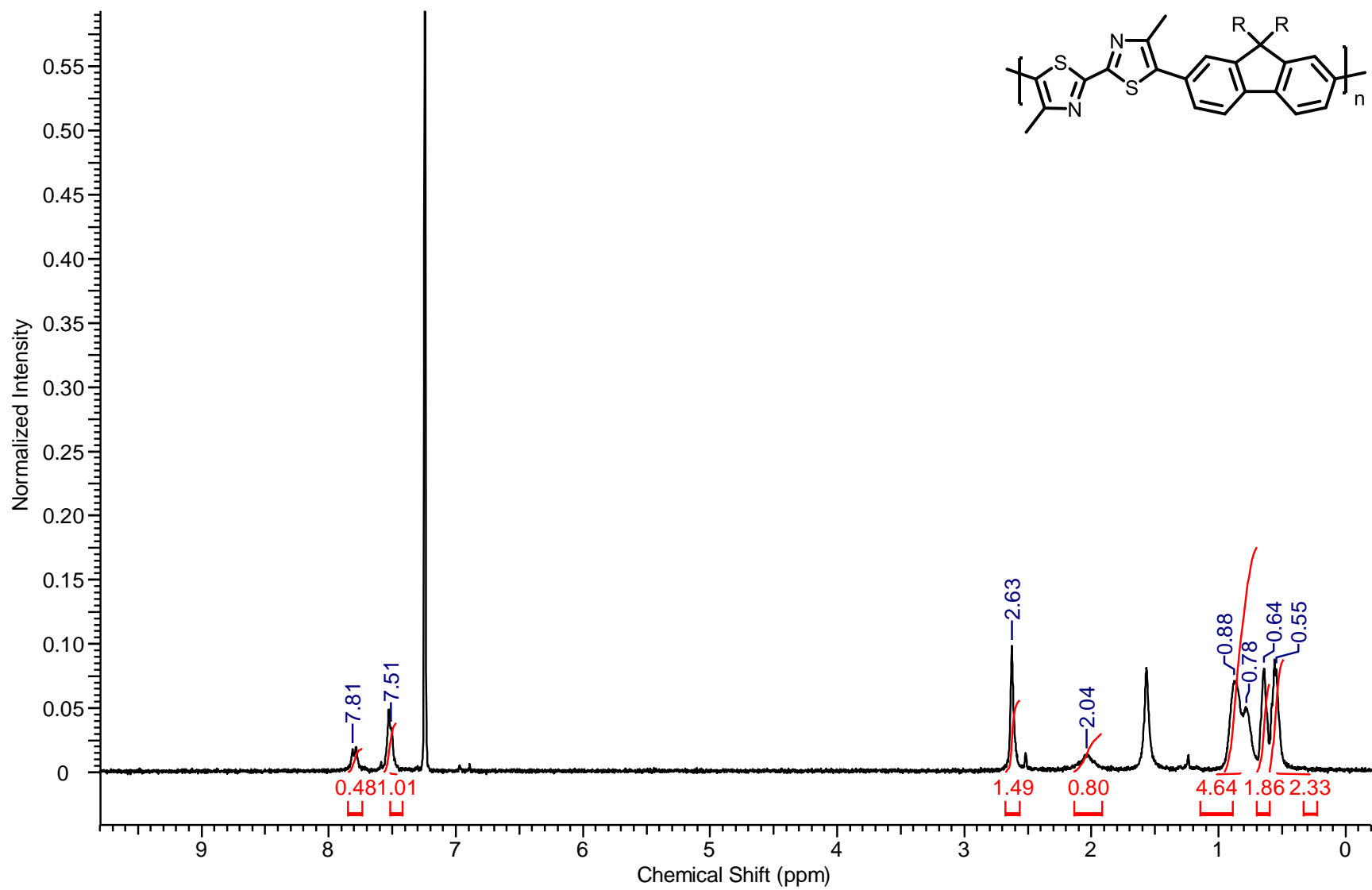


Figure S17. ¹H-NMR spectrum of 24.

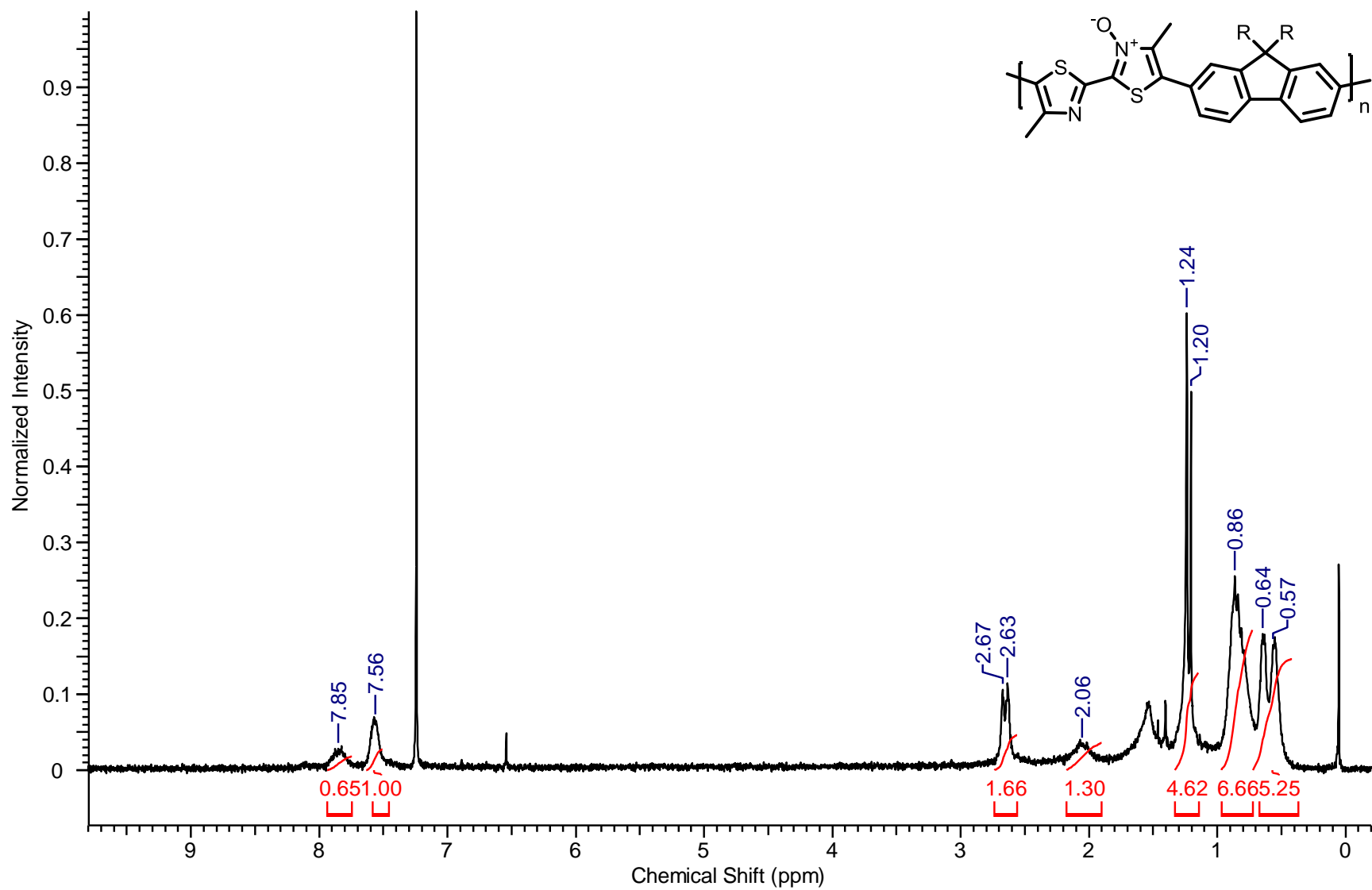


Figure S18. ¹H-NMR spectrum of 25.

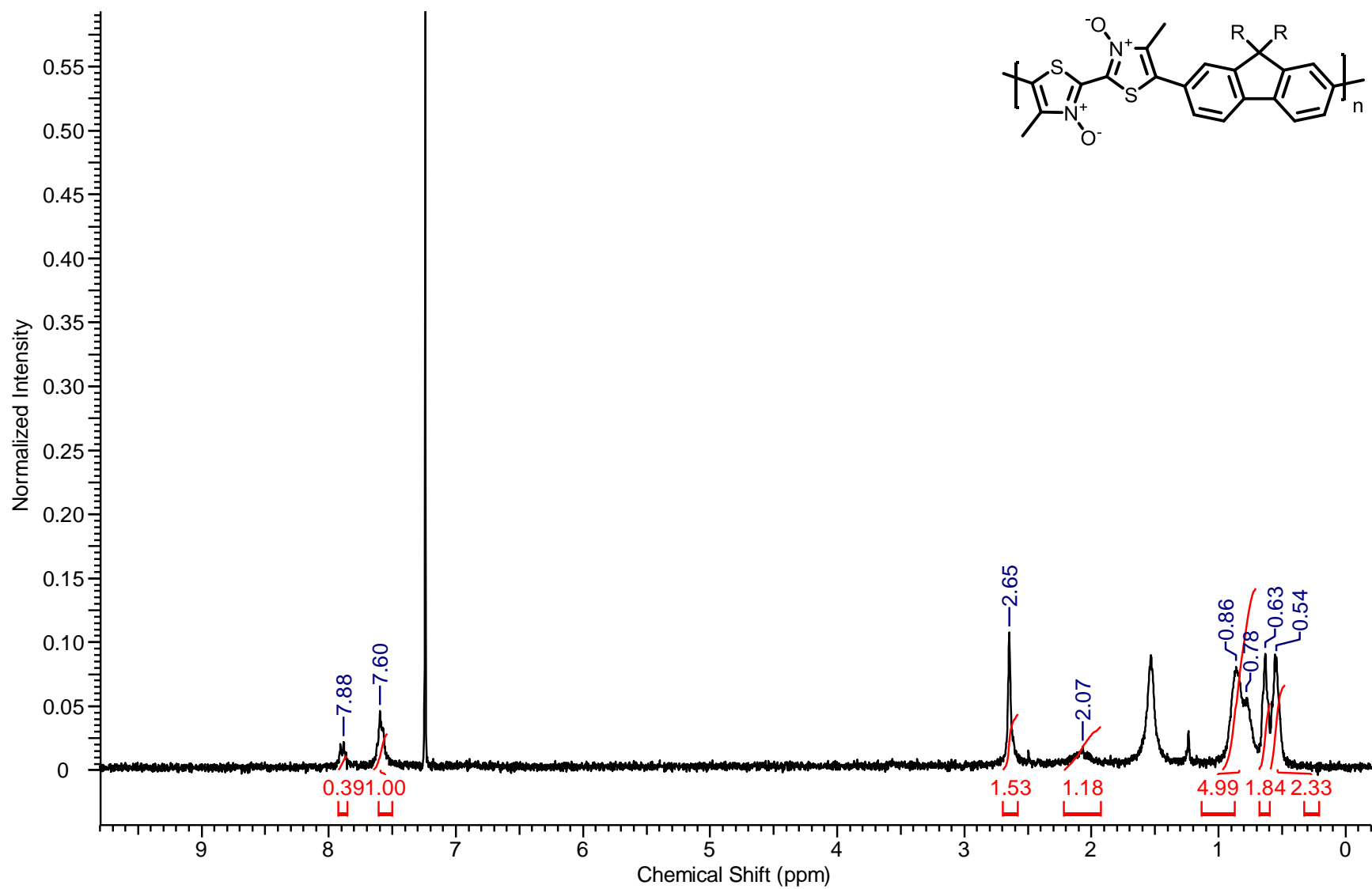


Figure S19. ¹H-NMR spectrum of **26**.

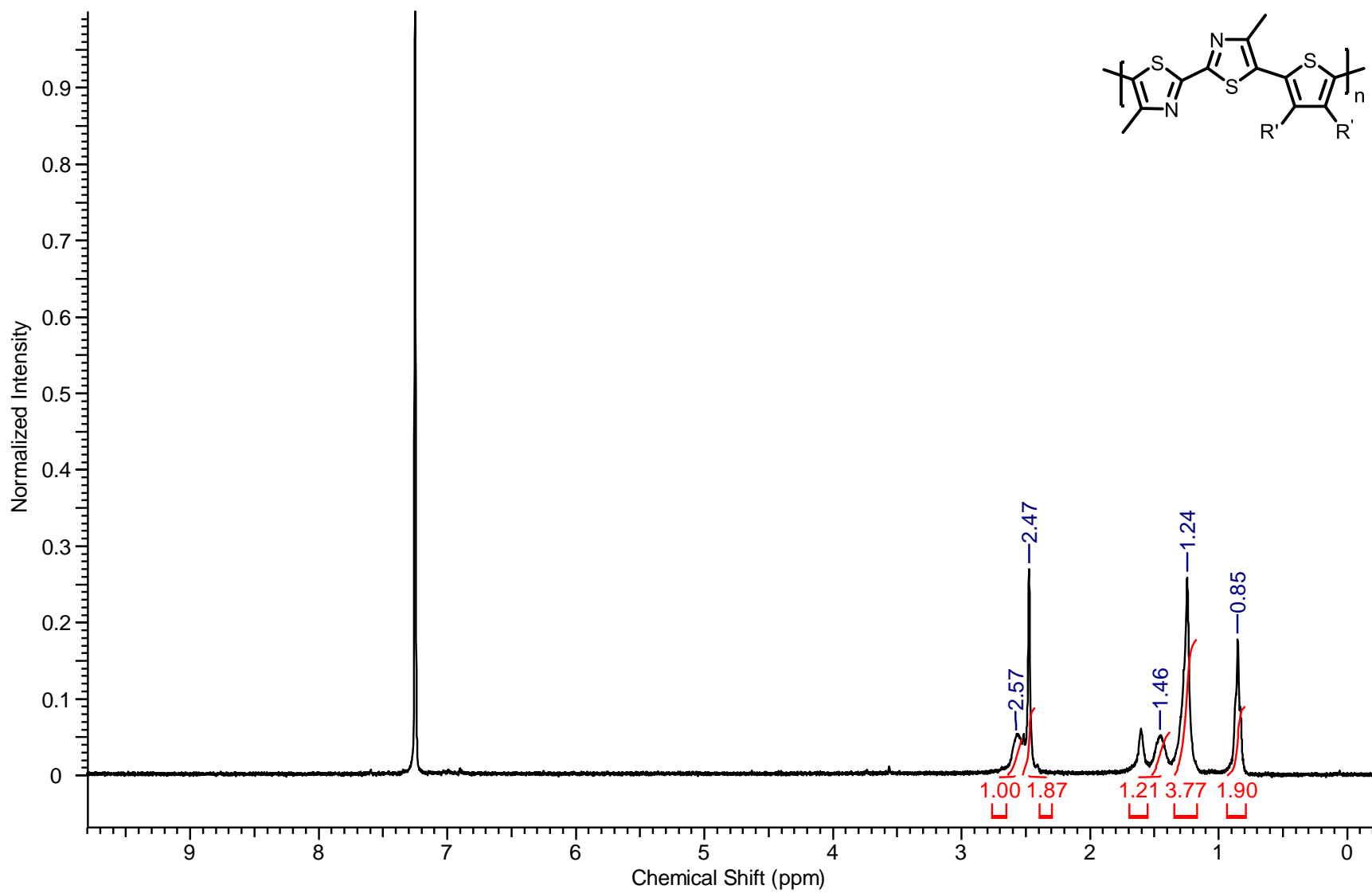


Figure S20. ¹H-NMR spectrum of 27.

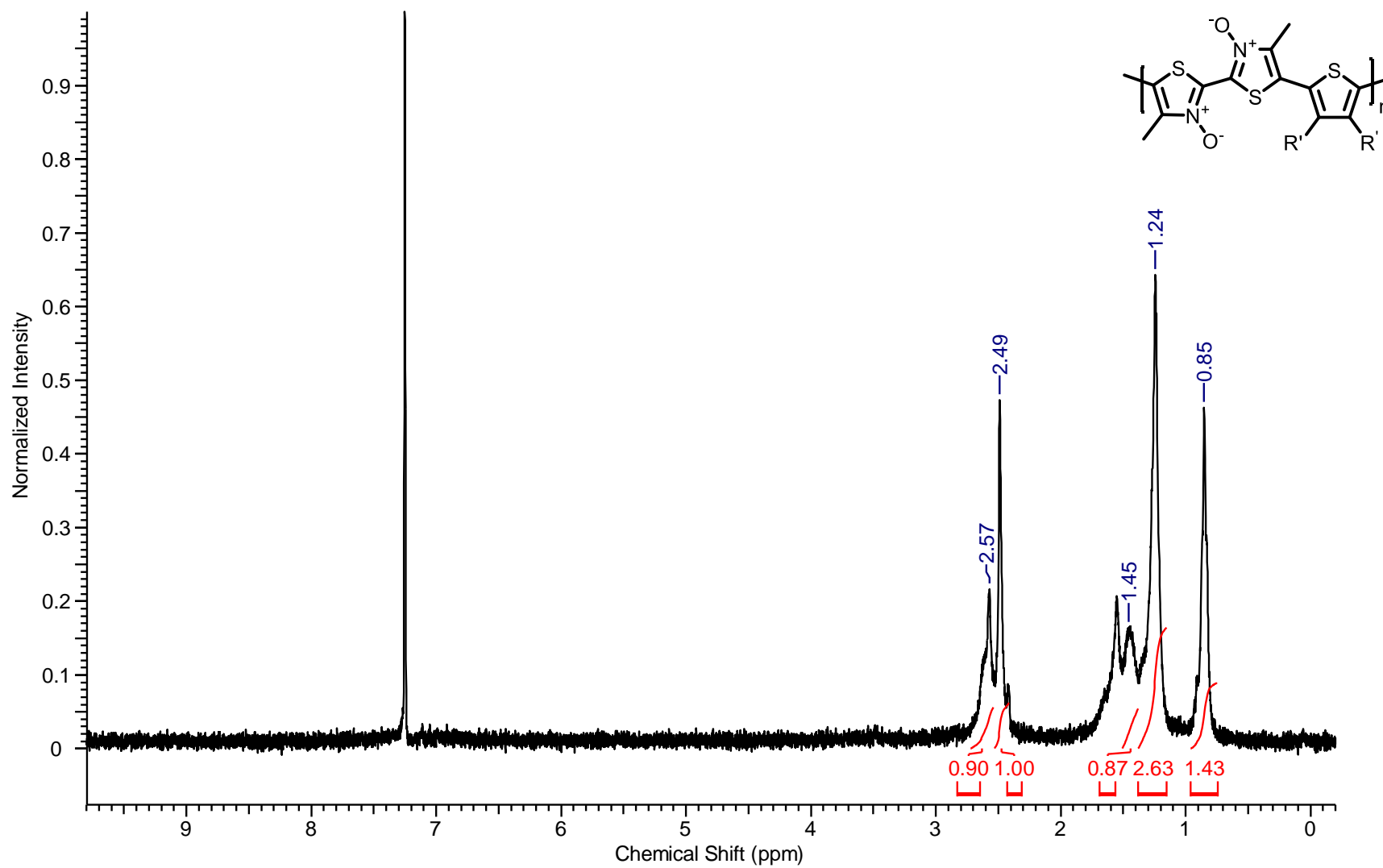


Figure S21. $^1\text{H-NMR}$ spectrum of **29**.

GPC Traces

The GPC computer had a hard drive crash, which contained traces and data for **7-9**. There was no remaining sample for these polymers so the GPC traces for these materials are not included within.

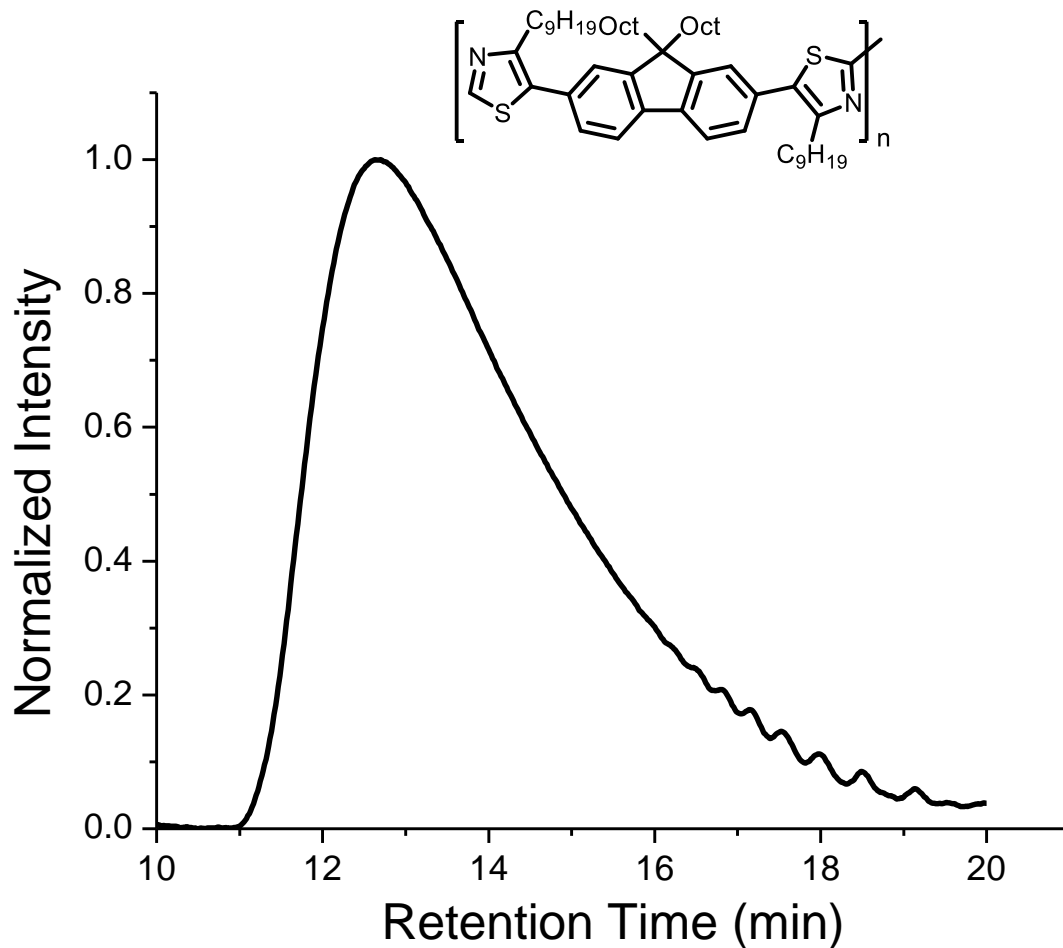


Figure S22. GPC trace of **10**.

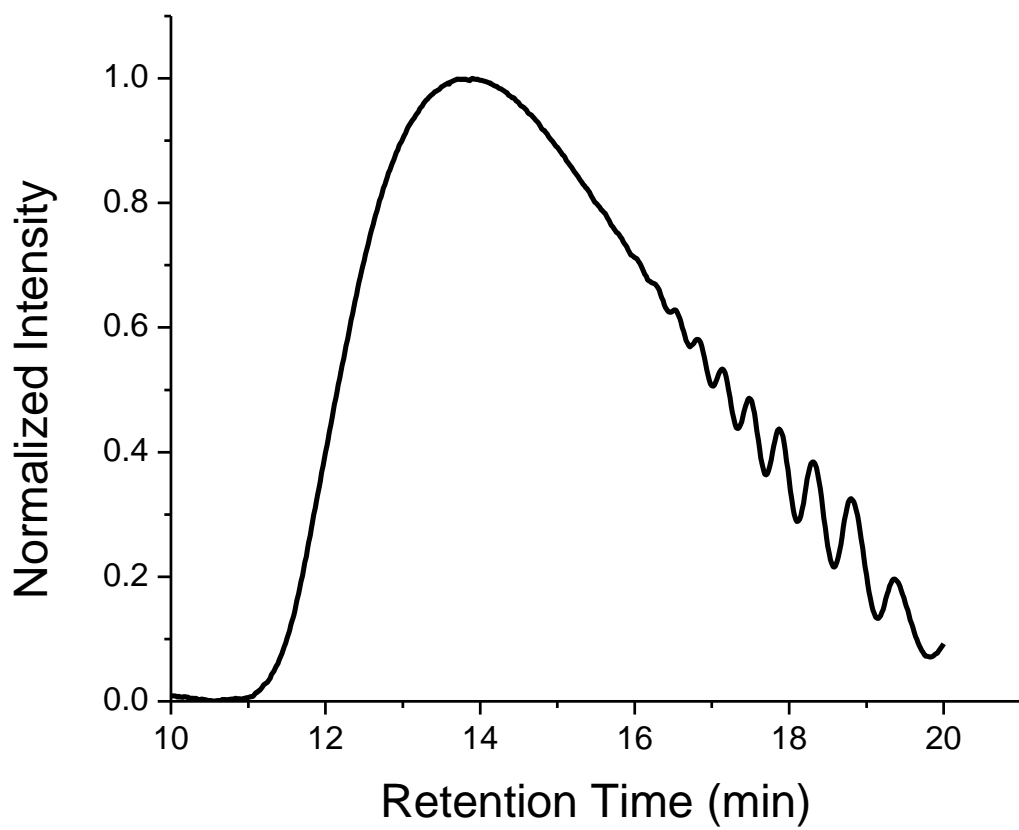
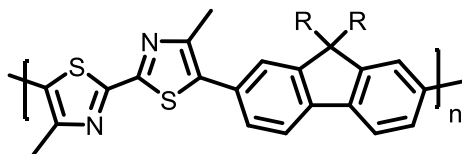


Figure S23. GPC trace of **24**.

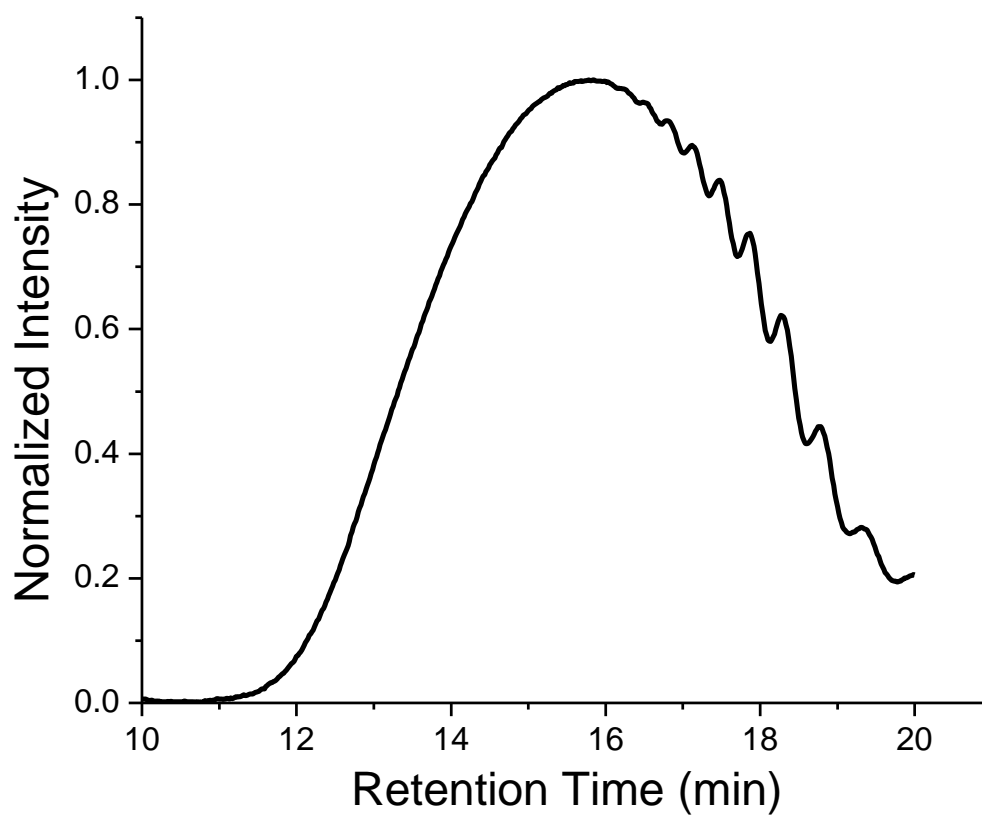
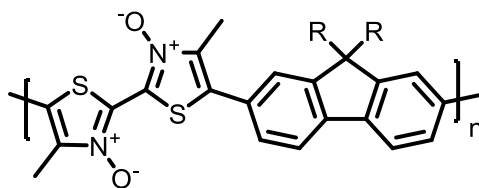


Figure S24. GPC trace of **26**.

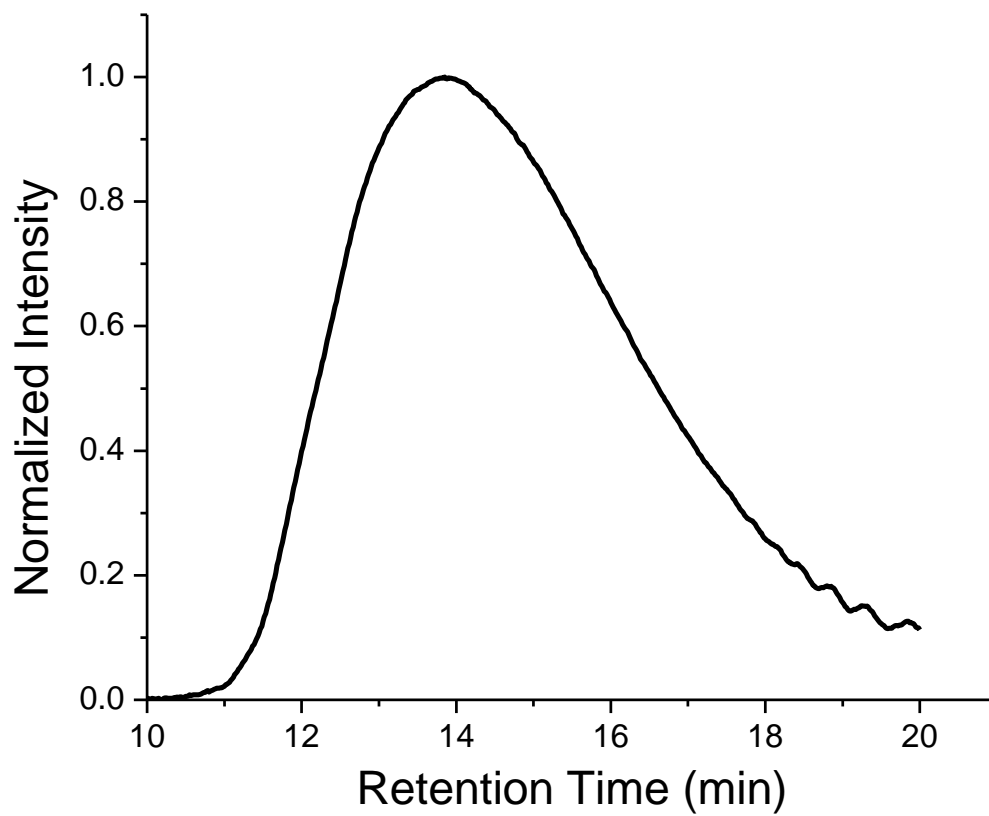
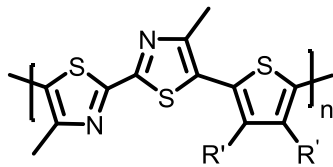


Figure S25. GPC trace of **27**.

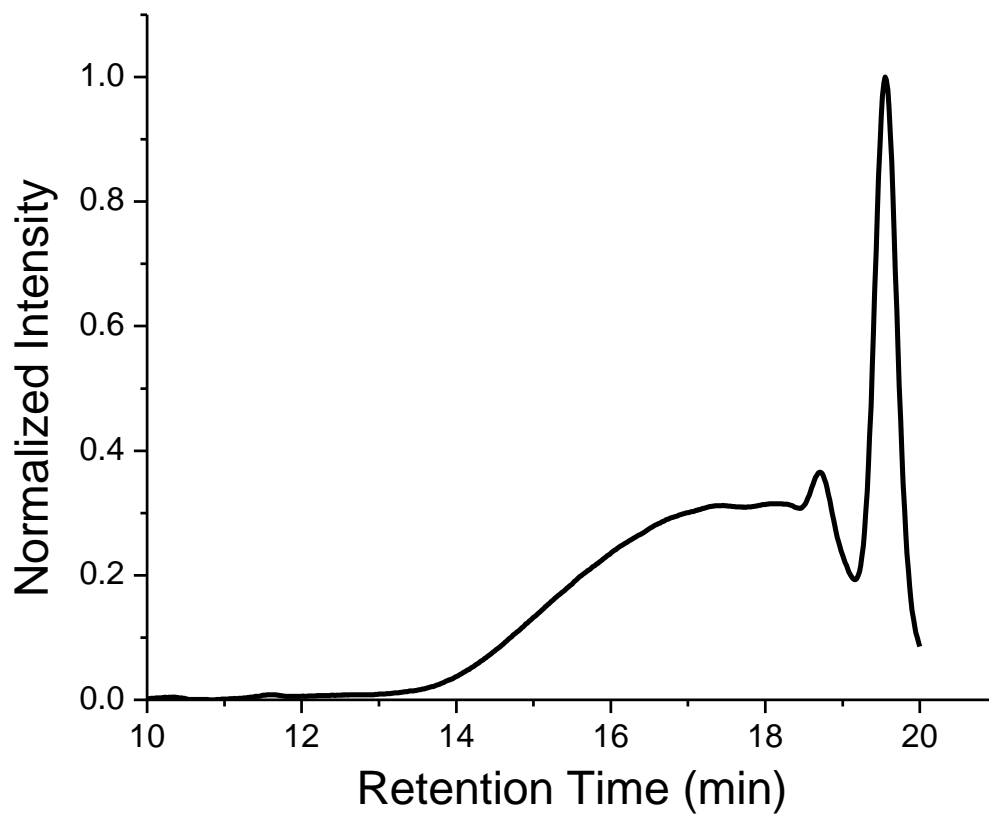
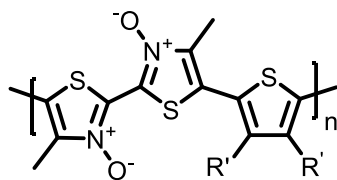


Figure S26. GPC trace of **29**.

References

- (1) Shirota, Y.; Kageyama, H. *Chem. Rev.* **2007**, *107*, 953.
- (2) Zhan, X.; Zhu, D. *Polym. Chem.* **2010**, *1*, 409.
- (3) He, Y.; Hong, W.; Li, Y. *J. Mater. Chem. C Mater. Opt. Electron. Devices* **2014**, *2*, 8651.
- (4) Lu, W.; Kuwabara, J.; Iijima, T.; Higashimura, H.; Hayashi, H.; Kanbara, T. *Macromolecules* **2012**, *45*, 4128.
- (5) Zhang, Z. G.; Wang, J. *J. Mater. Chem.* **2012**, *22*, 4178.
- (6) Jung, J. W.; Lee, J. U.; Jo, W. H. *J. Phys. Chem. C* **2010**, *114*, 633.
- (7) Giannouli, M.; Drakonakis, V. M.; Savva, A.; Eleftheriou, P.; Florides, G.; Choulis, S. A. *ChemPhysChem*, **2015**, *16*, 1134.
- (8) Cheng, Y.; Yang, S.; Hsu, C. *Chem. Rev.* **2009**, *109*, 5868.
- (9) Huang, H.; Chen, Z.; Ortiz, R. P.; Newman, C.; Usta, H.; Lou, S.; Youn, J.; Noh, Y.; Baeg, K.; Chen, L. X.; Facchetti, A.; Marks, T. *J. Am. Chem. Soc.* **2012**, *134*, 10966.
- (10) Yablonovitch, E. *J. Opt. Soc. Am. B* **1993**, *10*, 283.
- (11) Ohno, H. *Science* **1998**, *281*, 951.
- (12) Coropceanu, V.; Cornil, J.; Demetrio, A.; Filho, S.; Olivier, Y.; Silbey, R.; Jean-Luc Brédas, J. *Chem. Rev.* **2007**, *107*, 926.
- (13) Roncali, J. *Macromol. Rapid Commun.* **2007**, *28*, 1761.
- (14) Milad, R.; Aguirre, A.; Cardone, A.; Milian-Medina; B., Farinola, G. M.; Abderrabba, M. G. *J. Mater. Chem. C* **2016**, *4*, 6900.
- (15) Pei, Q.; Zuccarello, G.; Ahlsgott, M.; Ingan, O. *Polym. Papers* **1994**, *35*, 1347.
- (16) a) Kitamura, C.; Tanaka, S.; Yamashita, Y. *Chem. Mater.* **1996**, *8*, 570. b) Brocks, G.; Tol, A. *J. Phys. Chem.* **1996**, *100*, 1838.
- (17) Wei, S.; Xia, J.; Dell, E. J.; Jiang, Y.; Song, R.; Lee, H.; Rodenbough, P.; Briseno, A. L.; Campos, L. M. *Angew. Chem. Int. Ed.* **2014**, *53*, 1832.
- (18) Liu, Y.; Zhang, Z.; Feng, S.; Li, M.; Wu, L.; Hou, R.; Xu, X.; Chen, X.; Bo, Z. *J. Am. Chem. Soc.* **2017**, *139*, 3356.
- (19) Roncali, J.; Blanchard, P.; Fre, P. *J. Mater. Chem.* **2005**, *15*, 1589.
- (20) a) Huang, H.; Chen, Z.; Ortiz, R. P.; Newman, C.; Usta, H.; Lou, S.; Youn, J.; Noh, Y.; Baeg, K.; Chen, L. X.; Facchetti, A.; Marks, T. *J. Am. Chem. Soc.* **2012**, *134*, 10966. b) Takacs, C. J.; Sun, Y.; Welch, G. C.; Perez, L. A.; Liu, X.; Wen, W.; Bazan, G. C.; Heeger, A. J. *J. Am. Chem. Soc.* **2012**, *134*, 16597. c) Liu, Y.; Zhang, Z.; Feng, S.; Li, M.; Wu, L.; Hou, R.; Xu, X.; Chen, X.; Bo, Z. *J. Am. Chem. Soc.* **2017**, *139*, 3356

- (21) Pascoe, D. J.; Ling, K. B.; Cockroft, S. L. *J. Am. Chem. Soc.* **2017**, *139*, 15160.
- (22) Benz, S.; Macchione, M.; Verolet, Q.; Mareda, J.; Sakai, N.; Matile, S. *J. Am. Chem. Soc.* **2016**, *138*, 9093.
- (23) Nagao, Y.; Hirata, T.; Goto, S.; Sano, S.; Kakehi, A.; Iizuka, K.; Shiro, M. *J. Am. Chem. Soc.* **1998**, *120*, 3104.
- (24) Coughlin, J. E.; Zhugayevych, A.; Bakus, R. C.; Poll, T. S. Van Der; Welch, G. C.; Teat, S. J.; Bazan, G. C.; Tretiak, S. *J. Phys. Chem. C* **2014**, *118*, 15610.
- (25) Jackson, N. E.; Kohlstedt, K. L.; Savoie, B. M.; Olvera, M.; Cruz, D.; Schatz, G. C.; Chen, L. X.; Ratner, M. A. *J. Am. Chem. Soc.* **2015**, *137*, 6254.
- (26) (a) Meyer, V. *Chem. Ber.* **1883**, *16*, 1465. (b) Lin, J. W.P.; Dudek, L. P. *J. Polym. Sci. Part A: Polym. Chem.* **1980**, *18*, 2869.
- (27) Roncali, J. *Chem. Rev.* **1997**, *97*, 173.
- (28) McCullough, R. D.; Tristram-Nagle, S.; William, S. P.; Lowe, R. D.; Jayaraman, M. *J. Am. Chem. Soc.* **1993**, *115*, 4910.
- (29) Chen, T.A.; Wu, X.; Rieke, R. D. *J. Am. Chem. Soc.* **1995**, *117*, 233.
- (30) Koizumi T., Kanbara T. (2014) Cross-Coupling Polymerization. In: Osakada K. (eds) Organometallic Reactions and Polymerization. Lecture Notes in Chemistry, vol 85. Springer, Berlin, Heidelberg.
- (31) Chang, S.W.; Waters, H.; Kettle, J.; Kuo, Z.-R.; Li, C.-H.; Yu, C.Y.; Horie, M. *Macromol. Rapid Commun.* **2012**, *33*, 1927.
- (32) Bohra, H.; Wang, M. *J. Mater. Chem. A* **2017**, *5*, 11550.
- (33) Zhang, M.; Tsao, H. N.; Pisula, W.; Yang, C.; Mishra, A. K.; Mu, K. *J. Am. Chem. Soc.* **2007**, 3472.
- (34) Wang, E.; Wang, L.; Lan, L.; Luo, C.; Zhuang, W.; Peng, J.; Cao, Y. *Appl. Phys. Lett.* **2008**, *92*, 2006.
- (35) A) Duff, J. I.; Stoner, H. B.; Barnes, J. M. *Brit. J. Indust. Pharmacol.* **1955**, *10*, 16–25. B) Barnes, J. M.; Stoner, H. B. *Brit. J. Indust. Med.* **1958**, *15*, 15–16. C) Kimbrough, B. R. D. *Env. Heal. Perspect.* **1976**, *14*, 51.
- (36) Thompson, B. C.; Rudenko, A. E.; Khlyabich, P. P. *ACS Macro. Lett.* **2014**, *3*, 387.
- (37) *Metal-Catalyzed Cross-Coupling Reactions*, (Eds.: A. de Meijere, F. Diederich), Wiley-VCH, Weinheim, **2004**.
- (38) Schipper, D. J.; Fagnou, K. *Chem. Mater.* **2011**, *23*, 1594.

- (39) Blaszykowski, C.; Aktoudianakis, E.; Alberico, D.; Bressy, C.; Hulcoop, D. G.; Jafarpour, F.; Joushaghani, A.; Lautens, M. *J. Org. Chem.* **2008**, *73*, 1888.
- (40) Mercier, L. G.; Leclerc, M. *Acc. Chem. Res.* **2013**, *46*, 1597.
- (41) S. I. Gorelsky, D. Lapointe and K. Fagnou, *J. Am. Chem. Soc.*, **2008**, *130*, 10848.
- (42) Mirabal, R.; Vanderzwet, L.; Abuadas, S.; Emmitt, M.; Schipper, D. *J. Chem. Eur. J.* **2018**, *24*, 12231.
- (43) Su, H.; Sredojevic, D. N.; Bronstein, H.; Marks, T. J.; Schroeder, B. C.; Al-hashimi, M. *Macromol. Rapid Commun.* **2017**, *38*, 1600610.
- (44) A) Li, Z.; Ding, J. F.; Song, N. H.; Lu, J. P.; Tao, Y. *J. Am. Chem. Soc.* **2010**, *132*, 13160. B) Ying, L.; Hsu, B. B. Y.; Zhan, H. M.; Welch, G. C.; Zalar, P.; Perez, L. A.; Kramer, E. J.; Nguyen, T. Q.; Heeger, A. J.; Wong, W. Y.; Bazan, G. C. *J. Am. Chem. Soc.* **2011**, *133*, 18538. C) Cho, H. H.; Kang, T. E.; Kim, K. H.; Kang, H.; Kim, H. J.; Kim, B. J. *Macromolecules* **2012**, *45*, 6415.
- (45) Wade, J.; Wood, S.; Beatrup, D.; Hurhangee, M.; Bronstein, H.; Mcculloch, I.; Durrant, J. R.; Kim, J.; Wade, J.; Wood, S.; Beatrup, D.; Hurhangee, M.; Bronstein, H.; Mcculloch, I.; Durrant, J. R.; Kim, J. *J. Chem. Phys.* **2015**, *142*, 244904.
- (46) A) Dell, E. J.; Campos, L. M. *J. Mater. Chem.* **2012**, *22*, 12945. B) Amir, E.; Rozen, S. *Chem. Commun.* **2006**, 2262.
- (47) A) Do, H.; Daugulis, O. *J. Am. Chem. Soc.* **2009**, *131*, 17052. B) Zhu, M.; Fujita, K.; Yamaguchi, R. *Chem. Commun.* **2011**, *47*, 12876.
- (48) Guo, Q.; Jiang, R.; Wu, D.; You, J. *Macromol. Rapid Commun.* **2016**, *37*, 794.
- (49) A) Varma, R. S.; Naicker, K. P. *Org. Lett.* **1999**, *1*, 189. B) Cope, C.; Adolfsson, H.; Khuong, T. V.; Yudin, A. K.; Sharpless, K. B. *J. Org. Chem.* **1998**, *63*, 1740.
- (50) Li, Y.; Jin, J.; Qian, W.; Bao, W. *Org. Biomol. Chem.* **2010**, *8*, 326.
- (51) Brusso, J. L.; Lilliedal, M. R.; Holdcroft, S. *Polym. Chem.* **2011**, *2*, 175–180.
- (52) Huang, H.; Yang, L.; Facchetti, A.; Marks, T. J. *Chem. Rev.* **2017**, *117*, 10291.
- (53) Hernandez, V.; Lopez Navarrete J. T. *J. Chem. Phys.* **1994**, *101*, 1369.
- (54) Leriche, P.; Turbiez, M.; Monroche, V.; Frere, P.; Blanchard, P.; Skabara, P. J.; Roncali, J. *Tetrahedron Lett.* **2003**, *44*, 469.
- (55) Bakulin, A. A.; Rao, A.; Pavelyev, V. G.; van Loosdrecht, P. H. M.; Pshenichnikov, M. S.; Niedzialek, D.; Cornil, J.; Beljonne, D.; Friend, R. *Science*. **2012**, *335*, 1340.

(56) Rissler, J. *Chem. Phys. Lett.*, **2004**, 395, 92.

(57) Hai, J.; Shi, G.; Yu, J.; Zhu, E.; Bian, L.; Ma, W.; Tang, W. *New J. Chem.* **2014**, 38, 4816.

(58) Yang, M.; Peng, B.; Liu, B.; Zou, Y.; Zhou, K.; He, Y.; Pan, C.; Li, Y. *J. Phys. Chem* **2010**, 114, 17989.

(59) Lai, L.; Ho, C.; Chen, Y.; Wu, W.; Dai, F.; Chui, C.; Huang, S.; Guo, K.; Lin, J.; Tian, H.; Yang, S.; Wong, W. *Dyes Pigment.* **2013**, 96, 516.